UNIVERSITY of TASMANIA

Ocean Deoxygenation, a paleo-proxy perspective

by
Axel Durand, M.Sc

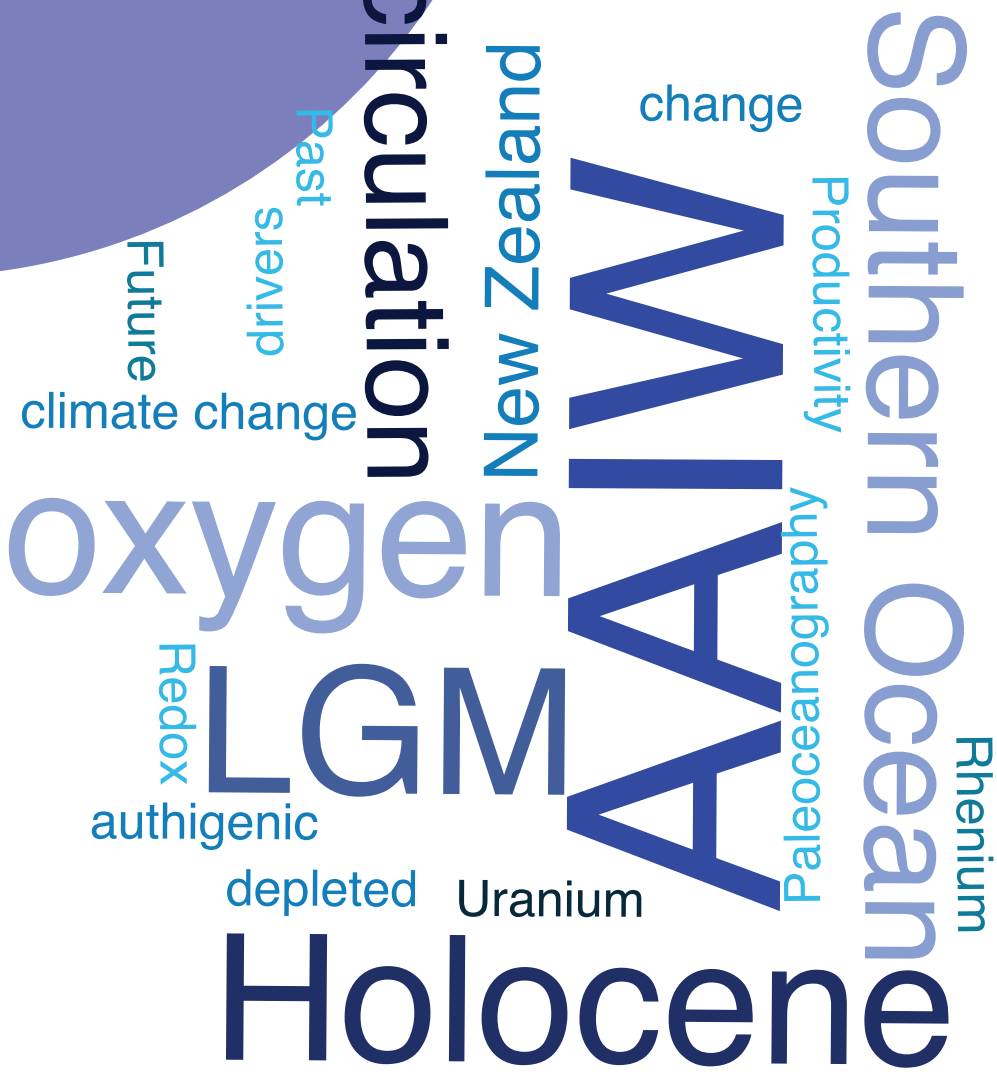

Under the supervison of ***Zanna Chase, Taryn Noble, Ashley Townsend*** *and* ***Nathan Bindoff***

Submitted in partial fulfilment of the requirements for the degree of ***Doctor of Philosophy***

Institute for Marine and Antarctic Studies (IMAS), University of Tasmania
April 2017

Ocean deoxygenation: a paleo-proxy perspective
by
Axel Durand

Abstract

The oceans are losing oxygen because of global warming and the consequences of this ocean deoxygenation are far reaching, particularly for aerobic marine organisms that depend on dissolved oxygen to live. Furthermore, in oxygen-deficient waters, ocean deoxygenation promotes global warming through the microbial production of nitrous oxide, a powerful greenhouse gas. The study of the Southern Ocean deoxygenation is particularly essential because through global circulation, it supplies dissolved oxygen to all ocean basins. Moreover, this region is particularly affected by deoxygenation and accounts for one quarter of the total oxygen losses observed since 1970. However, future oxygenation trends remain unclear.

To help forecast future Southern Ocean deoxygenation accurately, a precise knowledge of historical oxygen trends and their drivers is essential. One way to do this is to use sediments which record and preserve changes in the water column above them and offer a window on past conditions in the oceans. In this thesis a set of 12 sediment cores retrieved from the New Zealand region (Campbell Plateau, Challenger Plateau, Solander Trough) was used to investigate dissolved oxygen changes in the southwest Pacific sector of the Southern Ocean since the last glacial maximum (LGM) and the potential factors driving these changes. Moreover, because remineralisation by bacteria at depths constitutes the main oxygen sink in the ocean interior, export production (EP) changes since the LGM were also investigated directly.

Sediment composition has to be quantified in order to identify potential changes in oxygenation and EP. This requires the complete digestion (transformation of solid material to solution) of the sediments. Previous studies have shown that microwave-assisted digestion of marine sediments using a mix of hydrochloric, nitric and hydrofluoric acids provides a complete, rapid and relatively easy digestion method. However, due to the carbonate rich composition of the New Zealand sediments, all previously published methods

generated insoluble fluoride precipitate and failed to complete their digestions. **Chapter 2** addresses this problem and shows that a pre-digestion step, exposing sediments to concentrated HCl at 150 °C before microwave digestion helps eliminate precipitate formation, leading to the complete digestion of carbonate rich sediments. This method was tested on four different certified standards with a wide range of carbonate contents. Overall, around 90% recovery across 20 elements analysed was observed.

In this work, Inductively Coupled Plasma Mass Spectrometry (ICP-MS) was used as the analytical method of choice for broad screen multi-element analysis. However, for the determination of radiogenic isotopes of extremely low abundance, a special analytical methodology was introduced for the first time in our laboratories. **Chapter 3** details the isotopic dilution method employed as well as the incremental analytical developments necessary to measure precisely low abundance isotopes, such as 230-Thorium (^{230}Th), using a single collector Sector Field-ICP-MS. The importance of factors such as instrumental detector dead time on the precision of the isotopic ratio measurements was also investigated. Furthermore, the benefit of enhanced sensitivity through the activation of the instrument Platinum guard electrode in combination with a desolvating nebuliser is described. The precision of the measurements produced was assessed through intercomparison with two other techniques. Overall, measurements of 238-Uranium (^{238}U), ^{232}Th, and ^{230}Th from sediment digests were achieved with deviations of less than 5%.

In **chapter 4**, ^{230}Th-normalised opal, organic carbon, excess barium and calcium carbonate fluxes were used to investigate changes in EP in the southwest Pacific sector of the Southern Ocean since the LGM. The variations of these fluxes reveal that in Subtropical Waters (STW) and in the Subantarctic Zone (SAZ), EP largely remained unchanged since the LGM. Only one of the four sites studied shows increased EP during the deglaciation. At this site it is proposed that a shift in the position of the highly productive subtropical front to above the core site drove the increase in EP. In STW, it is suggested that nitrogen has been limiting any EP increase. In the SAZ, it is proposed that even though the increased glacial dust deposition relieved the iron (Fe)-limitation, silicic acid ($Si(OH)_4$) limited any resultant increase in EP during the LGM. This result

shows that both $Si(OH)_4$ and Fe co-limit EP in the SAZ around New Zealand, and is consistent with modern process studies. To understand the influence of iron fertilisation by dust since the LGM, lithogenic supply changes at the core sites were also investigated. At sites east of New Zealand an unusual lithogenic deposition pattern was observed, offset from other sites in the rest of the Southern Ocean. An explanation may be that this offset was driven by intense erosion and glacier melts, which increased the sediment discharged during the deglaciation.

As EP remained mostly unchanged since the LGM in the southwest Pacific sector of the Southern Ocean, other factors are likely to have driven any observed oxygen changes. In **chapter 5**, authigenic Uranium and Rhenium (aU and aRe) variations in the sediments were investigated and show that intermediate depths (800-1500 m) of the southwest Pacific sector of the Southern Ocean were deoxygenated during the LGM compared to the Holocene. Additionally, data from deeper locations ($\geq$ 1500 m) indicate higher oxygen content during the LGM compared to the Holocene. To understand the factors driving these variations all benthic foraminiferal $\delta^{13}C$ data available in the New Zealand region were compiled. These data together with aU and aRe variations are consistent with a dramatic circulation change in the Southern Ocean, which induced a shallower Antarctic Intermediate Water (AAIW)-Upper Circumpolar Deep Water (UCDW) boundary during the LGM compared to the Holocene over the Campbell Plateau. It is proposed that this shoaling can be explained by either a decrease in the AAIW production or a northward shift of the AAIW formation region. However, aU and aRe also show that AAIW contained less oxygen during the LGM compared to the Holocene. These results are in contrast with the enhanced AAIW ventilation inferred during the LGM in the southeast Pacific sector of the Southern Ocean, and therefore highlight an asymmetry in AAIW response to climatic forcing during the LGM in the Pacific.

The insights presented in this thesis improve our understanding of how circulation and EP influence the ventilation of the ocean interior on glacial-interglacial timescales. **Chapter 6** details the importance of these findings for future research and also highlights the remaining gaps.

Declaration and statements

Declaration of originality

This thesis contains no material which has been accepted for a degree or diploma by the University or any other institution, except by way of background information and duly acknowledged in the thesis, and to the best of my knowledge and belief no material previously published or written by another person except where due acknowledgement is made in the text of the thesis, nor does the thesis contain any material that infringes copyright.

Authority of access and statement regarding published work contained in the thesis

The publishers of the papers comprising Chapter 2 and Chapter 4 hold the copyright for that content, and access to the material should be sought from the respective journal. The remaining non published content of the thesis may be made available for loan and limited copying and communication in accordance with the Copyright Act 1968.

Signed:

Axel Durand
PhD candidate
Date: 22/04/2017

Statement of co-authorship

The following people and institutions contributed to the publication of work undertaken as part of this thesis:
(1) Axel Durand (candidate) — Institute for Marine and Antarctic Studies (IMAS), University of Tasmania, Hobart (TAS), Australia.
(2) Zanna Chase — Institute for Marine and Antarctic Studies (IMAS), University of Tasmania, Hobart (TAS), Australia.
(3) Taryn L. Noble — Institute for Marine and Antarctic Studies (IMAS), University of Tasmania, Hobart (TAS), Australia.
(4) Ashley T. Townsend — Central Science Laboratory (CSL), University of Tasmania, Hobart, Australia.

(5) Nathan Bindoff — Institute for Marine and Antarctic Studies (IMAS), Australian Research Council Centre of Excellence for Climate System Science, CSIRO Marine Atmospheric Research, ACE CRC, CAWCR, University of Tasmania, Hobart , Australia.
(6) Helen Bostock — NIWA, Wellington, New Zealand.
(7) Samuel L. Jaccard — Institute of Geological Sciences and Oeschger Centre for Climate Change Research, University of Bern, Switzerland.
(8) Helen Neil — NIWA, Wellington, New Zealand.
(9) Geraldine Jacobsend — Australian Nuclear Science and Technology Organisation (ANSTO), Lucas Heights, New South Wales, Australia.
(10) Priya Kitchener — Institute for Marine and Antarctic Studies (IMAS), University of Tasmania, Hobart (TAS), Australia.
(11) Emily Panietz — Institute for Marine and Antarctic Studies (IMAS), University of Tasmania, Hobart (TAS), Australia.
(12) Chelsea Long — Institute for Marine and Antarctic Studies (IMAS), University of Tasmania, Hobart (TAS), Australia.
(13) Nils Jansen — Institute for Marine and Antarctic Studies (IMAS), University of Tasmania, Hobart (TAS), Australia.
(14) Les Kinsley — Australian National University (ANU), Canberra, Australia.
(15) Karsten Goemann — Central Science Laboratory (CSL), University of Tasmania, Hobart, Australia.
(16) Sean Johnson — Centre of Excellence in Ore Deposits (CODES), University of Tasmania, Hobart, Australia.

Author's contributions

Chapters 2, 4 and 5 of this thesis have been prepared as manuscripts for submission to peer-reviewed journals. In all cases the design and implementation of the research, data analysis, interpretation of the results, and preparation of the manuscripts were the responsibility of the candidate but were carried out in consultation with supervisors and with the input of specialist contributors. These contributions are highlighted for each of these manuscripts below.

Chapter 2 (Paper 1): *Improved methodology for the microwave digestion of carbonate-rich environmental samples.*
A. Durand (first author): laboratory work, data processing, data analysis, manuscript writing.
Z. Chase (author 2): data analysis, manuscript writing.
A.T. Townsend (author 3): laboratory work, data processing, data analysis, manuscript writing.
T.L. Noble (author 4): data analysis, manuscript writing.
E. Panietz (author 5): laboratory work.
K. Goemann (author 6): laboratory work, data analysis, manuscript writing.

Chapter 4 (Paper 2): *Export production in the New-Zealand region since the last glacial maximum*
A. Durand (first author): laboratory work, data processing, data analysis, manuscript writing.
Z. Chase (author 2): laboratory work, data analysis, manuscript writing.

T.L. Noble (author 3): data analysis, manuscript writing.
H. Bostock (author 4): data analysis, manuscript writing.
S.L. Jaccard (author 5): data analysis, manuscript writing.
P. Kitchener (author 6): laboratory work, data analysis.
A.T. Townsend (author 7): laboratory work, data processing, data analysis, manuscript writing.
N. Jansen (author 8): laboratory work.
L. Kinsley (author 9): laboratory work.
G. Jacobsen (author 10): laboratory work, shared data.
S. Johnson (author 11): laboratory work
H. Neil (author 12): shared data.

Chapter 5 (Paper 3): *Sediment cores reveal a deoxygenated Southern Ocean surrounding New Zealand during the last glacial maximum*
A. Durand (first author): laboratory work, data processing, data analysis, manuscript writing.
Z. Chase (author 2): laboratory work, data analysis, manuscript writing.
T.L. Noble (author 3): data analysis, manuscript writing.
H. Bostock (author 4): data analysis, manuscript writing.
S.L. Jaccard (author 5): data analysis, manuscript writing.
A.T. Townsend (author 6): laboratory work, data analysis, manuscript writing.
N. Bindoff (author 7): data analysis.
H. Neil (author 8): laboratory work, shared data.
G. Jacobsen (author 9): laboratory work, shared data.
C. Long (author 10): laboratory work.

We the undersigned agree with the above stated 'proportion of work undertaken' for each of the above manuscripts contributing to this thesis:

Signed:

Dr. Zanna Chase
Supervisor
Institute for Marine and Antarctic Studies (IMAS)
University of Tasmania

Date: 22/04/2017

Signed:

Pr. Craig Johnson
Head of centre
Institute for Marine and Antarctic Studies (IMAS)
University of Tasmania

Date: 22/04/2017

Acknowledgements

First, I would like to thank Dr. Zanna Chase for giving me the opportunity to tackle this exciting project and guiding me all along. Thanks for your infinite patience, your help, your time, and for being such a great mentor. I have learned so much from you over these years. You have been an amazing supervisor and are a source of inspiration.

I would also really like to thank Dr. Ashley Townsend for your support all along this PhD journey. Particularly, thanks for the uncountable hours you spent sharing your passion and teaching me about Inductively Coupled Plasma-Mass Spectrometry. It has been a great privilege and an amazing experience to work together. Thanks for taking me under your wing.

Thanks to Dr. Taryn Noble for your involvement in this project. Thanks for the great ideas, the inspiring discussions about paleoceanography and the countless feedback that you gave on each of the chapters composing this thesis.

Thanks to Prof. Nathan Bindoff for taking the time to share your physical expertise and helping me understand what could have driven the oxygenation changes observed.

Thanks to those who have contributed to parts of this project. Many thanks to Samuel Jaccard and Helen Bostock for your interest and precious mentoring as developing chapter 4 and 5. Particular thanks to Samuel Jaccard for organising and funding a trip to Kiel to collect sediment samples. Thanks to Helen Neil and Priya Kitchener for sharing some data with me. Thanks to Emily Panietz and Chelsea Long for your help in the lab. Special thanks to Nils Jansen for setting up the opal measurement method in our facility and helping me with the samples. I am also very thankful to Les Kinsley who helped measuring samples on the Multi Collector-Inductively Coupled Plasma-Mass Spectrometer at the Australian National University. Thanks to Karsten Goemann for sharing your expertise in

scanning electron microscopy and for helping me characterise the insoluble precipitates in the digested samples. Thanks to Sean Johnson for the help you gave with the total carbon measurements. Thanks to Pearse for the amazing discussions about ocean deoxygenation and modelling. Thanks to Verena Lanny for making my trip to Switzerland easy and helping me analyse samples at the Institute of Geological Sciences and Oeschger Centre for Climate Change, Bern.

Thanks to the Tasmanian Graduate Research Scholarship that supported my four-year enrolment at the University of Tasmania. Many thanks to the Graduate Research Office as well as the Institute for Marine and Antarctic Studies and the Bottom of the Earth Society for co-funding my attendance to the 12th International Conference of Paleoceanography in Utrecht.

Thanks to my cheerful family for always supporting me in my choices. Thanks to all the friends who shared parts of this journey with me and always provided good distractions. Thanks to all my surf-mates: Malcolm, Guillaume, German, Martin, Marion, Jan, Pier and many more, for all the adventures and helping keeping me balanced and happy. Special thanks to Manu for being such a good friend. We have shared so many laughs together; I always had a big smile when returning to my desk after coffee breaks with you. Finally, thanks Delphi for sharing this adventure with me and making it such a happy and fun one. Thanks for the countless hours you spent reading and helping with my work and for always being so patient and interested. Thanks for cheering me up during the downs and having so much faith in me.

Thanks for the comments of Stephanie Kienast and Michael Ellwood, which greatly improved this thesis.

Contents

List of Figures

List of Tables

Chapter 1

Introduction

Observations have shown that oceans have lost 2% of their total oxygen content since 1960 (Schmidtko et al., 2017) and that this deoxygenation is increasing (Helm et al., 2011). Moreover, deoxygenation is widespread spatially and affects all oceans basins (Diaz and Rosenberg, 2008; Keeling et al., 2010; Matear et al., 2000; Stramma et al., 2008, 2010) (Figure 1.1). Regions accounting for the largest deoxygenation, up to 30 $mol.m^{-2}$ per decade since 1960, are located in the equatorial and north Pacific Ocean, the Southern Ocean and the south Atlantic Ocean (Schmidtko et al., 2017). In coastal areas deoxygenation has been mostly fuelled by riverine runoff of fertilizers, which boosted oxygen consumption by marine organisms (Diaz and Rosenberg, 2008). In the pelagic environment deoxygenation has been the result of higher temperatures which have decreased the oxygen solubility, and increased stratification which has reduced ventilation. The spreading of oxygen minimum zones (OMZ) as a result of this deoxygenation is of particular concern because of potentially large impacts on aerobic marine life (Diaz and Rosenberg, 2008; Karstensen et al., 2008; Stramma et al., 2008, 2010). The OMZ expansion could drive substantial changes in ecosystem dynamics, and could result in the collapse of some fisheries (Bograd et al., 2008; Chan et al., 2008; Chu and Tunnicliffe, 2015; DePasquale et al., 2015; Diaz and Rosenberg, 2008). Another consequence of deoxygenation is that it amplifies global warming by increasing denitrification which results in greater release of the greenhouse gas nitrous oxide (N_2O) (Babbin et al., 2015; Deutsch et al., 2007; Nevison et al., 1995). Moreover, because higher temperatures decrease oxygen solubility, deoxygenation is a self-reinforcing feedback to itself through enhancing global warming

(Keeling et al., 2010; Matear and Hirst, 2003). Unfortunately the future trends of ocean deoxygenation are still uncertain and a deeper understanding of key drivers will be essential to guide future decisions in order to mitigate deoxygenation consequences (Emerson and Bushinsky, 2014).

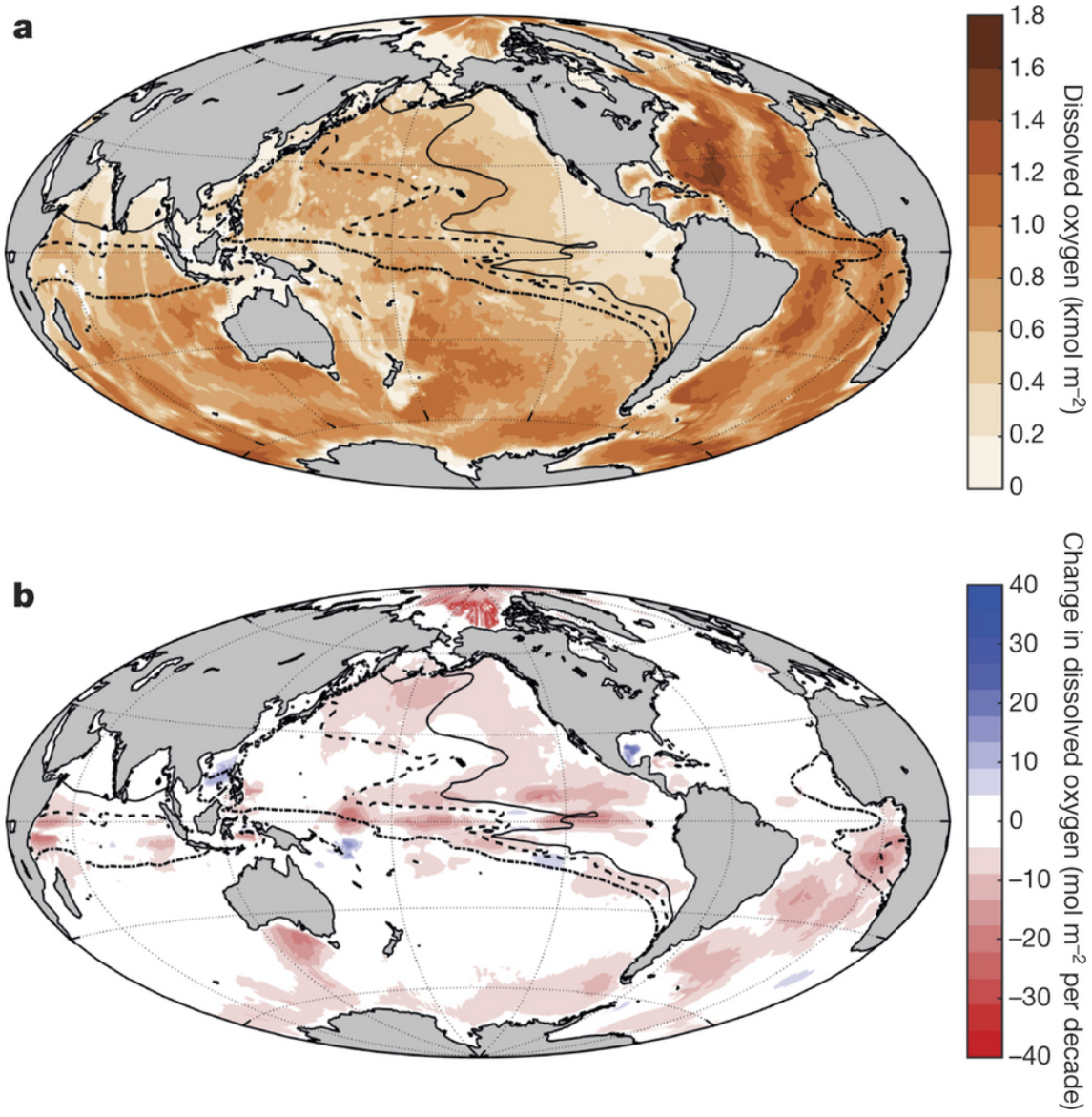

Figure 1.1: Amount of dissolved oxygen and changes per decade since 1960. (Figure from Schmidtko et al. (2017)). (a) Global dissolved oxygen inventory. Lines indicate boundaries of OMZs: dashed doted, region with less than 80 $\mu mol.kg^{-1}$ oxygen anywhere within the water column; dashed lines and solid lines similarly represent regions with less than 40 $\mu mol.kg^{-1}$ oxygen and 20 $\mu mol.kg^{-1}$ oxygen, respectively. (b) Changes in dissolved oxygen per decade. Lines show OMZs as in (a).

The oxygen content of the ocean interior is determined by the balance between the supply and the consumption of oxygen. Consumption of oxygen in the ocean is driven by

bacterial respiration of labile organic matter (remineralisation). Since labile organic matter is supplied by Export Production (EP), an increase in EP leads to oxygen depletion. On the other hand, the supply of oxygen to the ocean interior occurs through ventilation, the process whereby oxygen-rich surface waters are transported into the ocean interior through subduction (Helm et al., 2011). Therefore, the oxygen content of the subducted surface waters as well as their subduction rates and circulation influence the ocean interior oxygenation (Figure 1.2). The transfer of oxygen from the atmosphere to the surface ocean is driven by temperature and wind intensity, where strong winds and low temperature favour mixing and oxygen enrichment (Jaccard et al., 2014; Matear et al., 2000). Additionally, the production of dissolved oxygen by phytoplankton photosynthesis constitutes another process supplying dissolved oxygen to the mixed layer. The subduction of these surface waters, ventilating the ocean interior, occurs mostly through the formation of intermediate water masses, namely Subantarctic Mode Water (SAMW) and Antarctic Intermediate Water (AAIW) in subpolar regions of the Southern Ocean (Sloyan and Rintoul, 2001). Of the two water masses, AAIW is volumetrically the largest and dominates the oxygen supply to the ocean interior at low latitudes (Piola and Georgi, 1982).

As AAIW has a central role in ventilating the ocean interior, a large number of studies have tried to understand the drivers of its formation; however, large uncertainties remain. Antarctic intermediate water was first described in the 1930s as a fresh water mass of the ocean interior (Deacon, 1933; Wust, 1935). Over the years multiple possible mechanisms of AAIW formation have been identified (McCartney, 1979; Molinelli, 1981; Piola and Georgi, 1982; Rintoul and England, 2010; Sloyan et al., 2010); however they are still under debate today (Bostock et al., 2013). One theory is that AAIW is formed by convection during the Southern Hemisphere winter (McCartney, 1979; Sloyan and Rintoul, 2001; Sloyan et al., 2010). While travelling northward, Antarctic Surface Water (AASW) interacts with the atmosphere and as a result gets fresher and cooler. This increases the density of AASW and drives the convection process that leads to AAIW subduction. Prior to subduction, the northward advection at the surface is the result of Ekman transport driven by the westerly winds (Chiswell and Sutton, 1998; Hanawa and Talley, 2001;

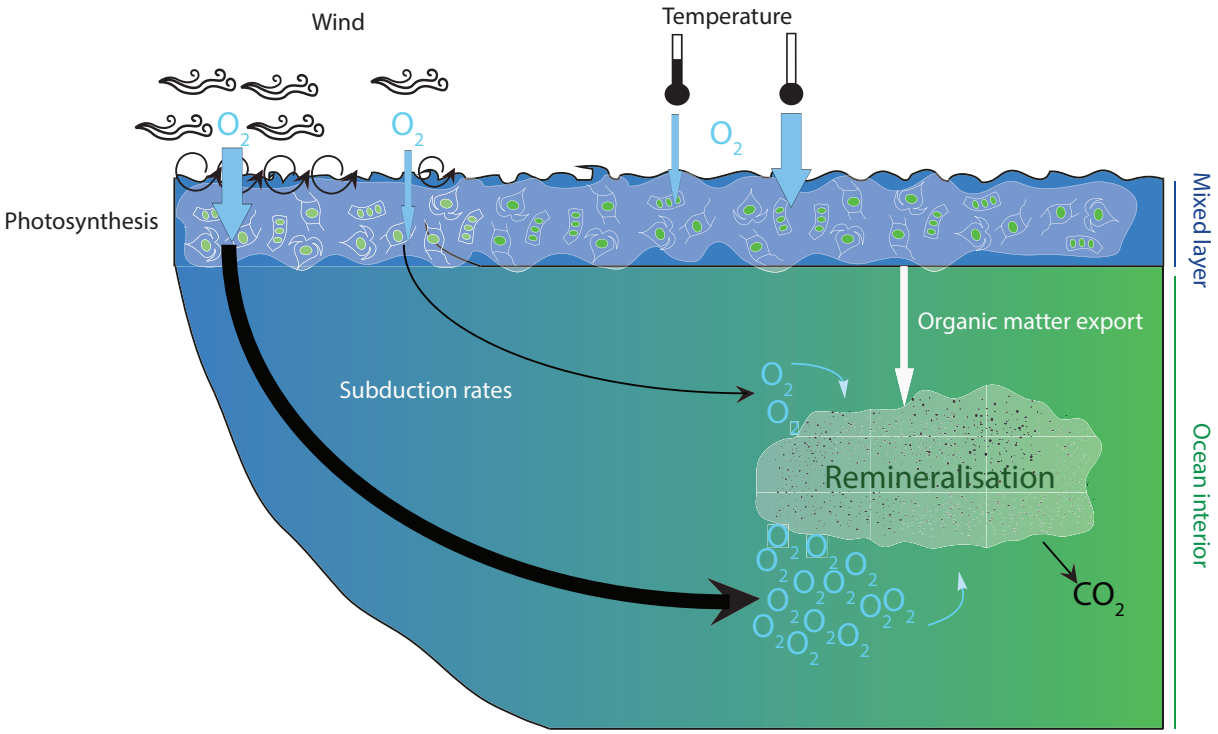

Figure 1.2: Summary of the processes driving variations in the oxygen content of the ocean interior.

Lachkar et al., 2007, 2009). Moreover, modelling studies have highlighted the essential role of shallow bathymetric features to explain why AAIW formation only occurs in a few hot spots in the Southern Ocean (Bostock et al., 2013; Reid, 1997; Sallee et al., 2010).

Changes in westerly wind stress have been reported as a major factor influencing AAIW ventilation (Downes et al., 2009, 2010, 2011). On one hand the intensity of the westerlies controls AAIW subduction: increased winds lead to increased subduction and enhanced ventilation (Downes et al., 2010). On the other hand, the position of the westerlies also influences AAIW subduction, where a southward shift in the mean position of the westerlies enhances AAIW ventilation (Downes et al., 2010). However, increased temperatures and rainfall have the opposite effect leading to an increase in buoyancy, which inhibits AAIW ventilation (Gille, 2002; Schmidtko and Johnson, 2012; Wong et al., 1999). Overall, a complex combination of drivers influence the AAIW formation and consequent oxygen delivery to the ocean interior, and the influence of climate change on these drivers and on the AAIW is yet to be fully understood.

By reconstructing past variations in oxygenation and their drivers, paleoceanographic

studies have a great potential to help better predict future oxygen changes. However, unlike past atmospheric gases, which can be preserved in bubbles trapped in icesheets, no seawater from the past remains trapped in an unaltered state. Rather, sediments form the best archive recording oceanic oxygenation changes. The variations of redox sensitive element concentrations in the sediments, such as Uranium (U) and Rhenium (Re), have been widely used as proxies to detect past oceanic oxygen changes (Colodner, 1991; Morford and Emerson, 1999; Tribovillard et al., 2006). Uranium and Re solubilities in seawater vary with the dissolved oxygen concentration of the seawater. When the oxygen concentration of seawater decreases, U and Re are reduced from their soluble forms ($UO_2(CO_3)_3)^{4-}$, $U(OH)_4$, and ReO_4^-) toward insoluble forms (UO_2 and $ReO_2.2H_2O$). This causes U and Re solid phases to accumulate in the sediments. In other words, when the concentration of dissolved oxygen in the water overlaying the sediment bed decreases, the concentrations of U and Re in sediments increase (Figure 1.3). This signal is then preserved and can be used as a proxy to reveal past oceanic oxygen changes (Figure 1.4). However, U and Re concentrations in sediments only reflect oxygenation changes of the water at the interface with the sediments and cannot be used to reveal oxygenation of surface waters. Another weakness is that the relationship between U and Re solubilities and dissolved oxygen is not linear and is close to a tipping point because the precipitation of U and Re solid phases occurs only when a redox threshold is reached (Crusius et al., 1996; Tribovillard et al., 2006). Therefore, U and Re can only be used as qualitative proxies for oxygenation change.

Other proxies, that directly relate to changes in the oxygen content of the water overlaying the sediment bed, include sediment lamination and foraminifera assemblages (Jaccard et al., 2014). Under very low oxygen concentrations (close to anoxia) the mixing of sediments by burrowing organisms stops. This allows the seasonal cyclicity in the sediment supply to be preserved as thin layers (lamination) (van Geen et al., 2003). Therefore, the presence of laminations reflects extremely low oxygen content of the water overlaying the sediment bed. Changes in foraminifera assemblages have also been used successfully to detect past oceanic oxygenation changes because they respond quickly

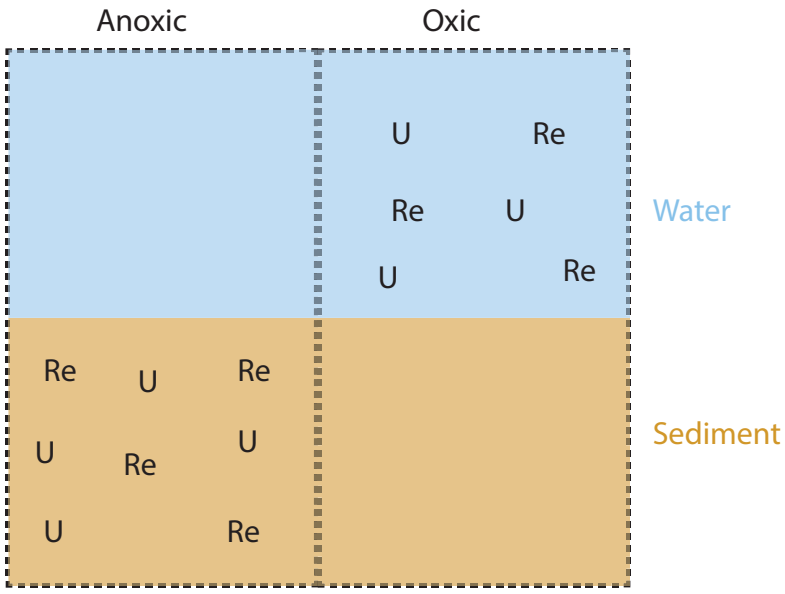

Figure 1.3: Summary of the conditions leading to U and Re enrichment in sediments.

to environmental changes. Thus, the absence of particular species can be used as a deoxygenation proxy (Corliss, 1985). However, there are considerable weaknesses to the use of lamination and foraminifera assemblages as oxygenation proxies (Jaccard et al., 2014). Lamination only occurs in nearly anoxic environments and therefore cannot detect subtle changes between two 'oxygenated' states. Moreover, laminations are only observed in areas of high sediment deposition, which limits its use. Finally, changes in foraminifera assemblages can be driven by changes independent of oxygenation such as temperature or organic matter availability. As a consequence, large uncertainties are often associated with their use as an oxygenation proxy.

In order to interpret changes in oxygenation inferred from redox sensitive metals it is helpful to also reconstruct water mass circulation and EP. It is beyond the scope of this chapter to detail every proxy used in paleoceanography that relates to circulation and EP; instead the ones that are used in this thesis are briefly described. Foraminifera $\delta^{13}C$ ($\delta^{13}C = (\frac{(\frac{^{13}C}{^{12}C})_{sample}}{(\frac{^{13}C}{^{12}C})_{standard}} - 1) * 1000$) is one of the most widely used proxies in paleoceanography because foraminifera preserve the past $\delta^{13}C$ signature of seawater in their shells. Spatial distribution of seawater $\delta^{13}C$ can be influenced by photosynthesis, remineralisation, air-sea gas exchange and circulation patterns; therefore, $\delta^{13}C$ is commonly used as

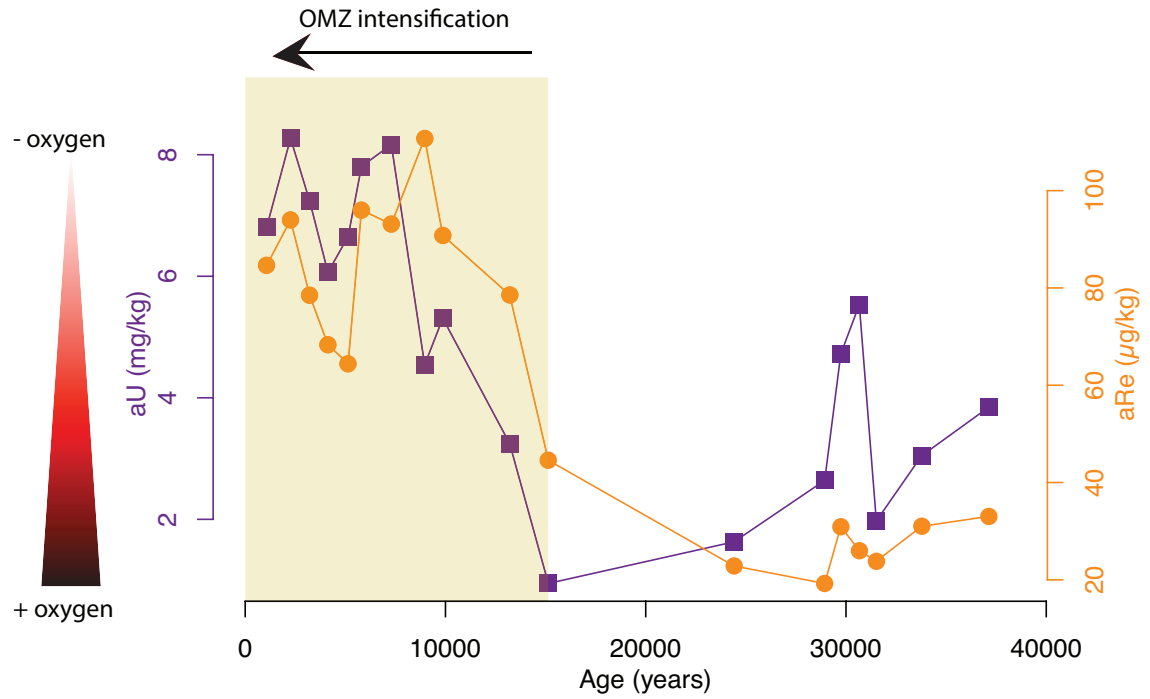

Figure 1.4: Authigenic Uranium (aU) and Rhenium (aRe) concentration variations with time in NH15P sediment core (Mexican continental margin). Enrichments of aU and aRe show the intensification of the Oxygen Minimum Zone (OMZ) above the core site. Data from Nameroff et al. (2004).

a proxy for both circulation and EP (Curry and Oppo, 2005; Kroopnick, 1985; Schmittner et al., 2013). Air-sea gas exchange buffers the surface $\delta^{13}C$ of the oceans allowing equilibration with the $\delta^{13}C$ of the atmospheric CO_2. Moreover, photosynthesis increases the $\delta^{13}C$ of surface waters by preferentially uptaking light ^{12}C. As a result, the organic matter produced from photosynthesis has low ^{13}C abundance and remineralisation of this organic matter decreases the $\delta^{13}C$ of deep waters. Finally, ocean circulation influences the spatial $\delta^{13}C$ distribution by mixing and transporting water masses of differing $\delta^{13}C$. Subsequently, because various factors influence $\delta^{13}C$, it can be difficult to separate their effects when they are subject to large variations. Although large uncertainties are associated with the use of $\delta^{13}C$, it is still widely used as a proxy to estimate changes in circulation and EP.

Alternatively, reconstruction of past EP changes can be accurately achieved by calculating fluxes of biogenic compounds preserved in sediments. Such compounds include

opal, barite, organic carbon and calcium carbonate (Chase et al., 2003; Paytan et al., 1996; Ragueneau et al., 1996). Increased flux of these compounds is linked to increased EP. However their accumulation in sediment is not only a function of the vertical supply, but also of the lateral redistribution (sediment winnowing and focussing), which can induce erroneous flux reconstructions (Francois et al., 2004). The sediment redistribution is particularly important in areas with strong bottom currents like the Southern Ocean (Dezileau et al., 2003; Frank et al., 1999). The traditional approach to calculate particulate flux to the seafloor uses sediment density and dated tie-points. However, this approach does not correct for sediment redistribution (Francois et al., 2004). Fortunately, the 230-Thorium (^{230}Th)-normalisation method has been widely used to solve this issue. This method is based on the fact that ^{230}Th is insoluble and consequently its removal from the water column by particle scavenging is equal to its known production rate by decay of 234-Uranium (^{234}U) (Francois et al., 2004). Because the dissolved U concentration in the ocean is essentially the same globally, the production of ^{230}Th occurs quasi-homogenously. As a consequence the expected flux of ^{230}Th reaching the seafloor is known and any deviations from it can be used to correct potential sediment redistribution. The development of this normalisation method only occurred recently so the results of a large number of studies prior to this advance have to be interpreted with care.

Using these and other proxies, paleo-studies have revealed that the Atlantic and Indian sectors of the Southern Ocean intermediate depths were better oxygenated during cold periods as a result of enhanced AAIW formation (Lynch-Stieglitz and Fairbanks, 1994; Rickaby and Elderfield, 2005). However, disagreement remains over the Pacific sector of the Southern Ocean. In the southeast Pacific, Muratli et al. (2009) showed that the intermediate depths were better oxygenated during Last Glacial Maximum (LGM) compared to the Holocene, using Re preserved in sediments. They attributed this increased ventilation to greater AAIW formation. Their results are in agreement with those from Jaccard and Galbraith (2012) and Jaccard et al. (2014), who showed that intermediate depths were generally better oxygenated during the LGM compared to the Holocene in the Pacific, based on a large scale data compilation. Conversely, several authors have

reported AAIW contraction during glacial periods in the southwest Pacific sector of the Southern Ocean, based on benthic foraminifera $\delta^{18}O$, $\delta^{30}Si$ and $\delta^{13}C$ (Elmore et al., 2015; Pahnke and Zahn, 2005; Ronge et al., 2015; Rousseau et al., 2016). They proposed that this AAIW contraction decreased the oxygen content at intermediate depths in this region. Unfortunately, the proxies used were not directly related to oxygen changes and as yet, no paleo-studies have directly investigated oxygenation changes in the southwest Pacific.

This thesis aims to reconstruct oxygenation changes at intermediate depths in the southwest Pacific sector of the Southern Ocean since the LGM, and thus fill key gaps in our understanding. To do so changes in oxygenation in parallel with their major drivers (circulation, EP) were directly investigated, using U, Re, $\delta^{13}C$ and Th-normalised biogenic fluxes from sediment cores of the New Zealand region (Figure 1.5). This approach has the potential to evaluate the likelihood of various scenarios and thus reveal the exact combination of factors driving the oxygenation changes.

The sediment cores used in this study were retrieved from the Campbell and Challenger Plateaux surrounding New Zealand. The sediment core depths span three out of the seven main water masses of this region, namely SAMW, AAIW and Upper Circumpolar Deep Water (UCDW) (Chiswell et al., 2015). Other water masses include Subantarctic Water (SAW), Subtropical Water (STW), Lower Circumpolar Deep Water (LCDW) and Antarctic Bottom Water (AABW). Subantarctic water and STW are the two shallowest water masses and are present at the interface with the atmosphere; therefore, their dissolved oxygen concentrations are at saturation. Subantarctic water is present south of the Subtropical Front (STF) in the Subantarctic Zone (SAZ, Figure 1.5), while STW is present north of the STF. Below these lie the oxygen rich SAMW (500-600 m) and AAIW (600-1200 m). Below the AAIW, a minimum in oxygen is observed between 1500 and 2500 m where the UCDW flows. Lower Circumpolar Deep Water flows between 2500 and 3000 m, and has intermediate oxygen content resulting from mixing of oxygen rich AABW and oxygen depleted UCDW. Even though it is the deepest water mass, the high dissolved oxygen content of AABW is due to the exchanges with the atmosphere that

occur at low temperature right before its subduction.

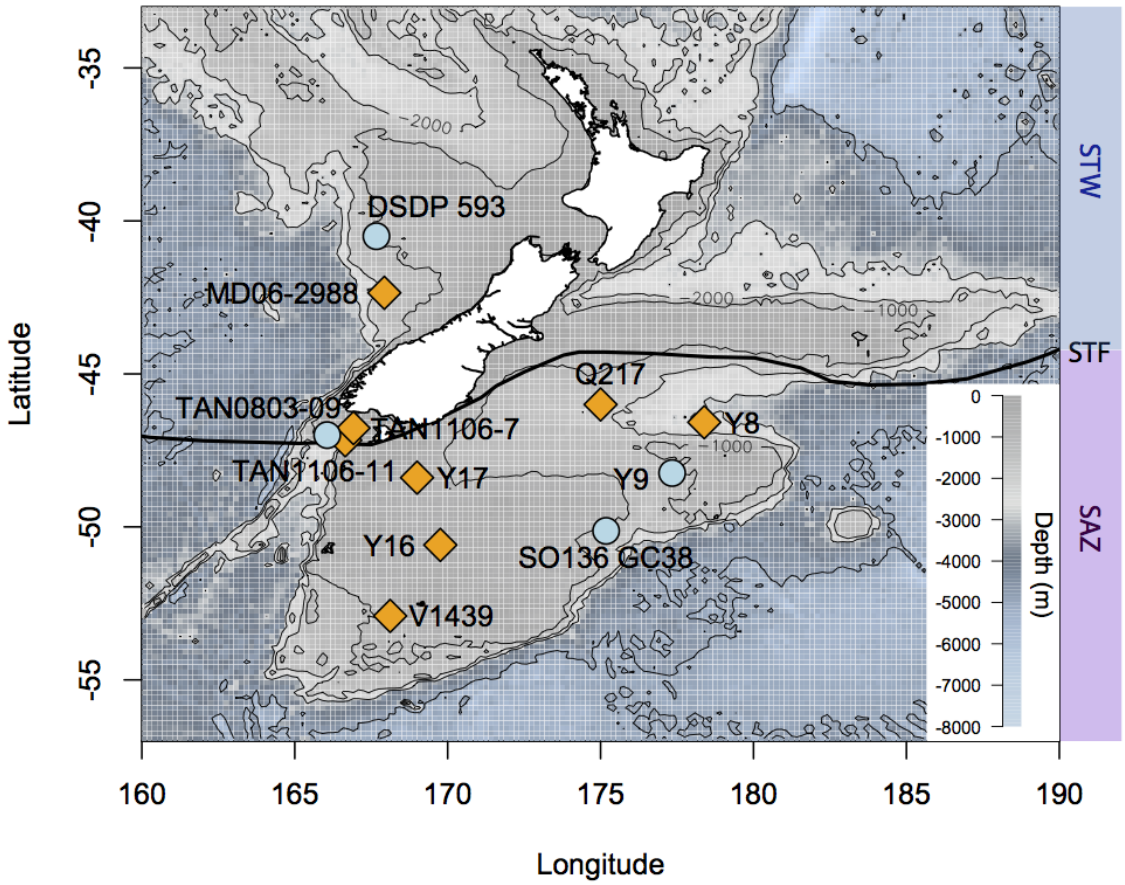

Figure 1.5: Map representing the bathymetry of the New Zealand region as well as sediment core locations. Orange diamonds show the cores where only oxygenation changes were investigated. Blue dots show the cores where both oxygenation and export production (EP) changes were reconstructed.

The precise quantification of U, Re and ^{230}Th, used in this thesis to identify oxygenation and EP changes, requires the complete dissolution (digestion) of the sediments. The complete digestion of solid material, such as sediments, occurs at high temperature and pressure in a cocktail of acids. In order to produce the high temperature and pressure, microwave assisted digestion is widely considered as the method of choice because of its efficiency, rapidity, increased safety, use of smaller acid volumes and the recovery of volatile samples (Flores, 2014; Kuss, 1992; Smith and Arsenault, 1996). Previous studies showed that microwave digestion in a mixture of Hydrochloric (HCl), Nitric (HNO_3)

and Hydrofluoric (HF) acids leads to the complete digestion of most marine sediments (Negre et al., 2009). However, all previously published methods failed to digest the sediments retrieved from New Zealand because their carbonate rich composition caused the formation of insoluble precipitates. **Chapter 2** addresses this problem and details the development of a new microwave assisted method for the complete digestion of carbonate rich environmental samples.

Once digested sediment composition needs to be assessed. However, even though the precise quantification of trace elements in sediments is an essential part of paleoceanography, it remains a challenge for many isotopes. **Chapter 3** details the isotopic dilution method used, as well as the analytical developments achieved, to measure precisely the low abundance isotopes ^{235}U, ^{234}U, ^{230}Th on a single collector Sector Field-ICP-MS.

As bacterial respiration associated with EP is the largest oxygen sink of the ocean interior, understanding EP changes is important for reconstructing past oxygenation changes. Several studies have already investigated past EP changes in this region, however, they presented contradicting results suggesting either no EP change (Ellwood et al., 2005), an increased EP during the LGM (Carter et al., 2000; Ikehara et al., 2000; Kowalski and A Meyers, 1997; Lean and McCave, 1998) or during the deglaciation (Carter and Manighetti, 2006). Moreover, these studies all used different EP proxies and therefore it is somewhat difficult to compare their results. Finally, these studies reconstructed the past fluxes of biological material without using the Th-normalisation method, which could result in erroneous interferences (Francois et al., 2004). To resolve these issues and reconstruct the overall EP trend in the southwest Pacific sector of the Southern Ocean, **chapter 4** presents for the first time Th-normalised fluxes of opal, $CaCO_3$, excess Barium ($_{xs}Ba$), and organic carbon (C_{org}) at four core sites in this region.

In **chapter 5** potential oxygenation changes are explored in the southwest Pacific sector of the Southern Ocean, by measuring U and Re contents of 12 sediment cores retrieved from the Campbell and Challenger Plateaux around New Zealand. These two plateaux have great potential to record ventilation changes to the Ocean interior because they are partly bathed by AAIW and therefore could record changes in the AAIW circu-

lation and/or oxygen content (Bostock et al., 2010; Chiswell et al., 2015; Forcén-Vàzquez, 2014). In order to understand whether circulation drove the changes observed, all benthic foraminiferal $\delta^{13}C$ data available in the New Zealand region were compiled.

As a conclusion, a general discussion of the main findings from this thesis as well as their importance for future research is detailed in **chapter 6**.

References

Babbin, A. R., Bianchi, D., Jayakumar, A., and Ward, B. B.: Rapid nitrous oxide cycling in the suboxic ocean, Science, 348, 1127–1129, 2015.

Bograd, S. J., Castro, C. G., Di Lorenzo, E., Palacios, D. M., Bailey, H., Gilly, W., and Chavez, F. P.: Oxygen declines and the shoaling of the hypoxic boundary in the California Current, Geophysical Research Letters, 35, 2008.

Bostock, H. C., Opdyke, B. N., and Williams, M. J.: Characterising the intermediate depth waters of the Pacific Ocean using δ 13 C and other geochemical tracers, Deep Sea Research Part I: Oceanographic Research Papers, 57, 847–859, 2010.

Bostock, H. C., Sutton, P. J., Williams, M. J., and Opdyke, B. N.: Reviewing the circulation and mixing of Antarctic Intermediate Water in the South Pacific using evidence from geochemical tracers and Argo float trajectories, Deep Sea Research Part I: Oceanographic Research Papers, 73, 84–98, 2013.

Carter, L. and Manighetti, B.: Glacial/interglacial control of terrigenous and biogenic fluxes in the deep ocean off a high input, collisional margin: A 139 kyr-record from New Zealand, Marine Geology, 226, 307–322, 2006.

Carter, L., Neil, H. L., and McCave, I. N.: Glacial to interglacial changes in non-carbonate and carbonate accumulation in the SW Pacific Ocean, New Zealand, Palaeogeography, Palaeoclimatology, Palaeoecology, 162, 333–356, 2000.

Chan, H. Y., Xu, W. Z., Shin, P. K. S., and Cheung, S. G.: Prolonged exposure to low dissolved oxygen affects early development and swimming behaviour in the gastropod Nassarius festivus (Nassariidae), Marine Biology, 153, 735–743, 2008.

Chase, Z., Anderson, R. F., Fleisher, M. Q., and Kubik, P. W.: Accumulation of biogenic and lithogenic material in the Pacific sector of the Southern Ocean during the past 40,000 years, Deep Sea Research Part II: Topical Studies in Oceanography, 50, 799–832, 2003.

Chiswell, S. M. and Sutton, P. J. H.: A Deep Eddy in the Antarctic Intermediate Water North of the Chatham Rise, Journal of Physical Oceanography, 28, 535–540, 1998.

Chiswell, S. M., Bostock, H. C., Sutton, P. J., and Williams, M. J.: Physical oceanography of the deep seas around New Zealand: a review, New Zealand Journal of Marine and Freshwater Research, 49, 1–32, 2015.

Chu, J. W. F. and Tunnicliffe, V.: Oxygen limitations on marine animal distributions and the collapse of epibenthic community structure during shoaling hypoxia, Global Change Biology, 21, 2989–3004, 2015.

Colodner, D.: PhD thesis: The marine geochemistry of rhenium, iridium and platinum, Massachusetts Institute of Technology, 1991.

Corliss, B. H.: Microhabitats of benthic foraminifera within deep-sea sediments, Nature, 314, 435–438, 1985.

Crusius, J., Calvert, S., Pedersen, T., and Sage, D.: Rhenium and molybdenum enrichments in sediments as indicators of oxic, suboxic and sulfidic conditions of deposition, Earth and Planetary Science Letters, 145, 65–78, 1996.

Curry, W. B. and Oppo, D. W.: Glacial water mass geometry and the distribution of δ13C of ΣCO2 in the western Atlantic Ocean, Paleoceanography, 20, 2005.

Deacon, M.: A general account of the hydrology of the South Atlantic Ocean, 1933.

DePasquale, E., Baumann, H., and Gobler, C. J.: Vulnerability of early life stage Northwest Atlantic forage fish to ocean acidification and low oxygen, Marine Ecology Progress Series, 523, 145–156, 2015.

Deutsch, C., Sarmiento, J. L., Sigman, D. M., Gruber, N., and Dunne, J. P.: Spatial coupling of nitrogen inputs and losses in the ocean, Nature, 445, 163–167, 2007.

Dezileau, L., Bareille, G., and Reyss, J. L.: The 231Pa/230Th ratio as a proxy for past changes in opal fluxes in the Indian sector of the Southern Ocean, Marine Chemistry, 81, 105–117, 2003.

Diaz, R. J. and Rosenberg, R.: Spreading dead zones and consequences for marine ecosystems, Science, 321, 926–929, 2008.

Downes, S. M., Bindoff, N. L., and Rintoul, S. R.: Impacts of climate change on the subduction of mode and intermediate water masses in the Southern Ocean, Journal of Climate, 22, 3289–3302, 2009.

Downes, S. M., Bindoff, N. L., and Rintoul, S. R.: Changes in the subduction of Southern Ocean water masses at the end of the twenty-first century in eight IPCC models, Journal of Climate, 23, 6526–6541, 2010.

Downes, S. M., Budnick, A. S., Sarmiento, J. L., and Farneti, R.: Impacts of wind stress on the Antarctic Circumpolar Current fronts and associated subduction, Geophysical Research Letters, 38, 2011.

Ellwood, M. J., Kelly, M., Neil, H., and Nodder, S. D.: Reconstruction of paleo–particulate organic carbon fluxes for the Campbell Plateau region of southern New Zealand using the zinc content of sponge spicules, Paleoceanography, 20, 2005.

Elmore, A. C., McClymont, E. L., Elderfield, H., Kender, S., Cook, M. R., Leng, M. J., Greaves, M., and Misra, S.: Antarctic Intermediate Water properties since 400 ka recorded in infaunal (Uvigerina peregrina) and epifaunal (Planulina wuellerstorfi) benthic foraminifera, Earth and Planetary Science Letters, 428, 193–203, 2015.

Emerson, S. R. and Bushinsky, S.: Oxygen Concentrations and Biological Fluxes in the Open Ocean, Oceanography, 27, 168–171, 2014.

Flores, E. M. M.: Microwave-assisted sample preparation for trace element determination, Elsevier, Amsterdam, 2014.

Forcén-Vàzquez, A.: PhD thesis: Oceanography of the New Zealand subantarctic region, University of Wellington, 2014.

Francois, R., Frank, M., Rutgers van der Loeff, M. M., and Bacon, M. P.: 230Th normalization: An essential tool for interpreting sedimentary fluxes during the late Quaternary, Paleoceanography, 19, 2004.

Frank, M., Gersonde, R., and Mangini, A.: Sediment Redistribution, 230Thex- Normalization and Implications for the Reconstruction of Particle Flux and Export Paleoproductivity, in: Use of Proxies in Paleoceanography, pp. 409–426, Springer Berlin Heidelberg, Berlin, Heidelberg, 1999.

Gille, S. T.: Warming of the Southern Ocean since the 1950s, Science, 295, 1275–1277, 2002.

Hanawa, K. and Talley, L. D.: Mode waters, International Geophysics Series, 77, 373–386, 2001.

Helm, K. P., Bindoff, N. L., and Church, J. A.: Observed decreases in oxygen content of the global ocean, Geophysical Research Letters, 38, 2011.

Ikehara, M., Kawamura, K., Ohkouchi, N., Murayama, M., Nakamura, T., and Taira, A.: Variations of terrestrial input and marine productivity in the Southern Ocean (48°S) during the last two deglaciations, Paleoceanography, 15, 170–180, 2000.

Jaccard, S. L. and Galbraith, E. D.: Large climate-driven changes of oceanic oxygen concentrations during the last deglaciation, Nature Geoscience, 5, 151–156, 2012.

Jaccard, S. L., Galbraith, E. D., Froelicher, T. L., and Gruber, N.: Ocean (De)Oxygenation across the last deglaciation, insights for the future, Oceanography, 27, 26–35, 2014.

Karstensen, J., Stramma, L., and Visbeck, M.: Oxygen minimum zones in the eastern tropical Atlantic and Pacific oceans, Progress in Oceanography, 77, 331–350, 2008.

Keeling, R. F., Körtzinger, A., and Gruber, N.: Ocean deoxygenation in a warming world, Annual Review of Marine Science, 2, 199–229, 2010.

Kowalski, E. A. and A Meyers, P.: Glacial–interglacial variations in Quaternary production of marine organic matter at DSDP Site 594, Chatham Rise, southeastern New Zealand margin, Marine Geology, 140, 249–263, 1997.

Kroopnick, P. M.: The distribution of 13C of ΣCO2 in the world oceans, Deep Sea Research Part A. Oceanographic Research Papers, 32, 57–84, 1985.

Kuss, H.-M.: Applications of microwave digestion technique for elemental analyses, Fresenius' Journal of Analytical Chemistry, 343, 788–793, 1992.

Lachkar, Z., Orr, J. C., Dutay, J. C., and Delecluse, P.: Effects of mesoscale eddies on global ocean distributions of CFC-11, CO2, and Delta C-14, Ocean Science, 3, 461–482, 2007.

Lachkar, Z., Orr, J. C., Dutay, J.-C., and Delecluse, P.: On the role of mesoscale eddies in the ventilation of Antarctic intermediate water, Deep Sea Research Part I: Oceanographic Research Papers, 56, 909–925, 2009.

Lean, C. M. B. and McCave, I. N.: Glacial to interglacial mineral magnetic and palaeoceanographic changes at Chatham Rise, SW Pacific Ocean, Earth and Planetary Science Letters, 163, 247–260, 1998.

Lynch-Stieglitz, J. and Fairbanks, R. G.: Glacial-interglacial history of Antarctic Intermediate Water: relative strengths of Antarctic versus Indian Ocean sources, Paleoceanography, 9, 7–29, 1994.

Matear, R. and Hirst, A.: Long-term changes in dissolved oxygen concentrations in the ocean caused by protracted global warming, Global Biogeochemical Cycles, 17, 2003.

Matear, R., Hirst, A., and McNeil, B.: Changes in dissolved oxygen in the Southern Ocean with climate change, Geochemistry, Geophysics, Geosystems, 1, 1050, 2000.

McCartney, M. S.: Subantarctic Mode Water, Woods Hole Oceanographic Institution, Woods Hole, 1979.

Molinelli, E. J.: The Antarctic influence on Antarctic intermediate water, Journal of Marine Research, 39, 267–293, 1981.

Morford, J. L. and Emerson, S.: The geochemistry of redox sensitive trace metals in sediments, Geochimica et Cosmochimica Acta, 63, 1735–1750, 1999.

Muratli, J., Chase, Z., Mix, A., and McManus, J.: Increased glacial-age ventilation of the Chilean margin by Antarctic Intermediate Water, Nature Geoscience, 3, 23–26, 2009.

Nameroff, T. J., Calvert, S. E., and Murray, J. W.: Glacial-interglacial variability in the eastern tropical North Pacific oxygen minimum zone recorded by redox-sensitive trace metals, Paleoceanography, 19, n/a–n/a, doi:10.1029/2003PA000912, URL `http://dx.doi.org/10.1029/2003PA000912`, pA1010, 2004.

Negre, C., Thomas, A. L., Mas, J. L., Garcia-Orellana, J., Henderson, G. M., Masqué, P., and Zahn, R.: Separation and measurement of Pa, Th, and U isotopes in marine sediments by microwave-assisted digestion and multiple collector inductively coupled plasma mass spectrometry, Analytical Chemistry, 81, 1914–1919, 2009.

Nevison, C. D., Weiss, R. F., and Erickson, D. J.: Global oceanic emissions of nitrous oxide, Journal of Geophysical Research, 100, 15 809–15 820, 1995.

Pahnke, K. and Zahn, R.: Southern Hemisphere water mass conversion linked with North Atlantic climate variability, Science, 307, 1741–1746, 2005.

Paytan, A., Kastner, M., and Chavez, F. P.: Glacial to interglacial fluctuations in productivity in the equatorial Pacific as indicated by marine barite, Science, 274, 1355–1357, 1996.

Piola, A. R. and Georgi, D. T.: Circumpolar properties of Antarctic intermediate water and Subantarctic Mode Water, Deep Sea Research Part A. Oceanographic Research Papers, 29, 687–711, 1982.

Ragueneau, O., Leynaert, A., Tréguer, P., Demaster, D. J., and Anderson, R. F.: Opal studied as a marker of paleoproductivity, Eos, Transactions American Geophysical Union, 77, 491–491, 1996.

Reid, J. L.: On the total geostrophic circulation of the Pacific Ocean: flow patterns, tracers, and transports, Progress in Oceanography, 39, 263–352, 1997.

Rickaby, R. and Elderfield, H.: Evidence from the high-latitude North Atlantic for variations in Antarctic Intermediate water flow during the last deglaciation, Geochemistry, Geophysics, Geosystems, 6, 2005.

Rintoul, S. R. and England, M. H.: Ekman Transport Dominates Local Air–Sea Fluxes in Driving Variability of Subantarctic Mode Water, Journal of Physical Oceanography, 32, 1308–1321, 2010.

Ronge, T. A., Steph, S., Tiedemann, R., Prange, M., Merkel, U., Nürnberg, D., and Kuhn, G.: Pushing the boundaries: Glacial/Interglacial variability of intermediate- and deep-waters in the southwest Pacific over the last 350,000 years, Paleoceanography, 30, 23–38, 2015.

Rousseau, J., Ellwood, M. J., Bostock, H. C., and Neil, H.: Estimates of late Quaternary mode and intermediate water silicic acid concentration in the Pacific Southern Ocean, Earth and Planetary Science Letters, 439, 101–108, 2016.

Sallee, J.-B., Speer, K., Rintoul, S., and Wijffels, S.: Southern Ocean Thermocline Ventilation, Journal of Physical Oceanography, 40, 509–529, 2010.

Schmidtko, S. and Johnson, G. C.: Multidecadal Warming and Shoaling of Antarctic Intermediate Water, Journal of Climate, 25, 207–221, 2012.

Schmidtko, S., Stramma, L., and Visbeck, M.: Decline in global oceanic oxygen content during the past five decades, Nature, 542, 335–339, 2017.

Schmittner, A., Gruber, N., Mix, A. C., Key, R. M., Tagliabue, A., and Westberry, T. K.: Biology and air-sea gas exchange controls on the distribution of carbon isotope ratios ($\delta^{13}C$) in the ocean, Biogeosciences, 10, 5793–5816, 2013.

Sloyan, B. M. and Rintoul, S. R.: Circulation, Renewal, and Modification of Antarctic Mode and Intermediate Water, Journal of Physical Oceanography, 31, 1005–1030, 2001.

Sloyan, B. M., Talley, L. D., Chereskin, T. K., Fine, R., and Holte, J.: Antarctic Intermediate Water and Subantarctic Mode Water Formation in the Southeast Pacific: The Role of Turbulent Mixing, Journal of Physical Oceanography, 40, 1558–1574, 2010.

Smith, F. E. and Arsenault, E. A.: Microwave-assisted sample preparation in analytical chemistry, Talanta, 43, 1207–1268, 1996.

Stramma, L., Johnson, G. C., Sprintall, J., and Mohrholz, V.: Expanding oxygen-minimum zones in the tropical oceans., Science, 320, 655–658, 2008.

Stramma, L., Schmidtko, S., Levin, L. A., and Johnson, G. C.: Ocean oxygen minima expansions and their biological impacts, Deep Sea Research Part I: Oceanographic Research Papers, 57, 587–595, 2010.

Tribovillard, N., Algeo, T. J., Lyons, T., and Riboulleau, A.: Trace metals as paleoredox and paleoproductivity proxies: An update, Chemical Geology, 232, 12–32, 2006.

van Geen, A., Zheng, Y., Bernhard, J. M., Cannariato, K. G., Carriquiry, J., Dean, W. E., Eakins, B. W., Ortiz, J. D., and Pike, J.: On the preservation of laminated sediments along the western margin of North America, Paleoceanography, 18, 2003.

Wong, A. P. S., Bindoff, N. L., and Church, J. A.: Large-scale freshening of intermediate waters in the Pacific and Indian Oceans, Nature, 400, 440–443, 1999.

Wust, G.: The stratosphere of the Atlantic Ocean, The German Meteor expedition 1925-1927, 1935.

Chapter 2

Improved methodology for the microwave digestion of carbonate-rich environmental samples

This chapter was published as an article under the same title in International Journal of Environmental and Analytical Chemistry, 2016, by Taylor & Francis, doi: 10.1080/03067319.2015.1137904.

Axel Durand[1], Zanna Chase[1], Ashley T. Townsend[2], Taryn L. Noble[1], Emily Panietz[1], Karsten Goemann[2]

[1]Institute for Marine and Antarctic Studies, University of Tasmania, Hobart, Australia
[2]Central Science Laboratory, University of Tasmania, Hobart, Australia

Abstract

Microwave assisted digestion permits a rapid and total dissolution of sediments and various other sample types, allowing easier and more accurate multi-element determinations. In this study, we present an optimised microwave digestion method for the complete digestion of 200 mg of carbonate-rich sediments. The optimised method prevents the formation of precipitates and assures a complete dissolution of the material. The optimised method involves treatment with concentrated hydrochloric acid (HCl) prior to microwave digestion, which prevents the formation of an insoluble calcium fluoride precipitate associated with the use of hydrofluoric acid (HF). Three different certified reference samples along with a pure calcium carbonate standard and a carbonate-rich in-house marine sediment sample were considered. Sediments were found to only be partially digested if insufficient HF was present, while a noticeable fluoride based precipitate was found if excess HF was present. Twenty elements were analysed using sector field ICP-MS (Al, Ag, Ba, Ca, Cd, Co, Cr, Cu, Fe, Mg, Mn, Mo, Na, Ni, Sr, Th, Ti, U, V and Zn). A total sample digestion with average elemental recoveries above 90% was obtained by reacting carbonate-rich samples with HCl on a hotplate at 150 °C for 2 h (time for the total release of generated CO_2), prior to any microwave digestion step. This extra step prevented the accumulation of gas in the sealed vessels during digestion, which would otherwise influence the carbonate chemical equilibria and make insoluble calcium available for precipitation. After this initial treatment, the improved digestion method consisted of microwave attack employing a mix of concentrated HCl, nitric acid (HNO_3) and HF (4 mL / 10 mL / 2 mL), followed by evaporation on a hotplate. The limits of detection (LOD) obtained using the optimised microwave protocol and ICP-MS measurements were below 0.1 µg/kg for the trace elements and below 0.2 mg/kg for major elements.

2.1 Introduction

Scientists quickly saw the advantages of using microwave energy in their laboratories after household microwave ovens were introduced into kitchens in the 1950s. One of the first studies to use a microwave as a digestion instrument was published in 1975 and was used on various biological samples (Abu-Samra et al., 1975), marking the start of a microwave revolution in the earth and environmental science fields. Since the 1970s the technique has been continuously improved, and

made safer with the introduction of sealed vessels and pressure and temperature control (Agazzi and Pirola, 2000). Microwave digestion procedures have been developed in parallel with the acceptance and widespread use of inductively coupled plasma mass spectrometry (ICP-MS) as a multi trace element technique (Linge and Jarvis, 2009). Many sample digestion methods have now been developed and have been shown to be suitable for multi trace element work for a variety of sample matrices including sediment, soil and biological materials (Bettinelli et al., 2000; Flores, 2014; Mann et al., 1992; Mester and Sturgeon, 2003). The success of microwave digestion comes from its rapidity, efficiency, increased safety, use of smaller acid volumes, increased recovery of volatile elements, reduced contamination and the applicability of the microwave approach across a range of sample types (Kuss, 1992). Furthermore, the fact that only the liquid phase is heated by the microwave energy provides a unique advantage in that very high temperatures (200 to 300 °C) can be reached in the reaction vessel at relatively low pressures which increases both the safety and the speed of the digestion (Abu-Samra et al., 1975; Bettinelli et al., 2000). Several studies have compared the technique for the digestion of different sample types (e.g., biological, sediments) to either conventional hotplate or ultrasound assisted extractions, with microwave techniques providing faster digestions with similar or improved results and increased recoveries (Kuss, 1992; Lima et al., 2000; Mann et al., 1992).

Marine sediments with high carbonate contents remain a challenge to digest and analyse when the use of perchloric acid ($HClO_4$) and boric acid (H_3BO_3) is avoided (Kemp and Brown, 1990; Muratli et al., 2012). Perchloric acid works efficiently at decomposing many samples but is extremely dangerous (highly flammable at room temperature). Boric acid is used to neutralise residual HF following sample digestion but often increases blank levels (Wu et al., 1996).

Several investigators have reported precipitate formation when digesting carbonate-rich sediments and assessed the precipitate to likely be calcium fluoride (CaF_2), resulting from reaction between the carbonate and HF (Colodner et al., 1993; Kemp and Brown, 1990) (Equation 2.1).

$$2HF + CaCO_3 \rightarrow CaF_2 + CO_2 \tag{2.1}$$

Likewise, in preliminary work in our laboratory, when conventional acid based (HF, HCl, HNO_3) digestion methods were applied to carbonate-rich ($\geq$70% $CaCO_3$) sediments from the

Campbell Plateau (south of New Zealand) (Negre et al., 2009), we observed the presence of a grey/white solid residue. This solid matter is a potential adsorption site and presents a risk in the recovery of highly particle reactive elements such as Th (Geibert and Usbeck, 2004; Roberts et al., 2009).

It has been suggested that the use of microwave technology may increase the precipitation reaction between $CaCO_3$ and HF (Kemp and Brown, 1990). Sealed microwave vessels prevent any CO_2 formed during the reaction from escaping. The accumulation of gas in the vessel affects the carbonate dissolution equilibria by decreasing the speed of the reactions and leaving carbonate partially undigested (Kemp and Brown, 1990) (Equation 2.2, 2.3, 2.4). A precipitation reaction can then occur between undigested carbonate and HF (Kemp and Brown, 1990) (Equation 2.1).

$$CO_{2(g)} \rightleftharpoons CO_{2(dissolved)} \tag{2.2}$$

$$CO_{2(dissolved)} + H_2O \rightleftharpoons H_2CO_3 \rightleftharpoons HCO_3^- + H^+ \rightleftharpoons CO_3^{2-} + 2H^+ \tag{2.3}$$

$$CaCO_3 \rightleftharpoons Ca^{2+} + CO_3^{2-} \tag{2.4}$$

Colodner et al. (1993) addressed this problem, and proposed a multi-step method involving a first microwave step to pre-digest the carbonate fraction. The liquid fraction was then separated from the solid residue. The isolated solid residue remaining was then digested using a second microwave step using HF. Finally the two digested fractions were re-united. This method effectively digests carbonate rich sediment by suppressing any direct contact between the carbonate and HF thereby preventing CaF_2 formation. However the method developed by Colodner et al. (1993) involves multiple and complex digestion and separation steps increasing the time, the cost, the volume of acids used and the risk of contamination. Latimer and Filippelli (2003) were able to limit the precipitate reaction by reducing the volume of HF used. Muratli et al. (2012), working with lithogenic-dominated sediment ($CaCO_3 \leq 20\%$), re-dissolved the fluoride complexes by heating prior to analysis. In our preliminary work with carbonate-rich sediment, precipitate remained even after reducing HF volume and using a post-digestion heating step. Finally Kemp and Brown (1990) used a pre-digestion step with acetic acid followed by a microwave digestion step to successfully digest carbonate rich material. Unfortunately this method

combines the use of large volumes of acids ($\geq$ 30 mL) with the use of boric acid which increases the contamination (Wu et al., 1996), the sample time preparation (drying the acids) and the cost.

In this study, we present the development of an efficient digestion method for carbonate-rich sediment that minimises the formation of precipitates through the addition of a simple step to existing microwave protocols (Muratli et al., 2012; Negre et al., 2009). The recovery of a range of elements was assessed using SF-ICP-MS analysis, with quantitation using external calibration standards providing a practical balance between sample throughput and fit-for-purpose analytical data.

2.2 Experimental section

2.2.1 Reagents and material

High purity acids, namely HCl 32% Ultrex II (J. T. Baker), HF 40% Ultrex II (J. T. Baker) and HNO_3 65% Ultrex II (J. T. Baker), were used to minimise contamination.

All bottles used were Teflon© (polytetrafluoroethylene), low density polyethylene (LDPE) or polypropylene.

New and used sample bottles and microwave vessels were rinsed five times with Milli-Q water and then soaked in a 10% Decon 90 (Aldrich) solution for at least 48 h. They were then rinsed five times with Milli-Q water and soaked in a 6 N HCl solution (Aldrich ACS reagent) for at least 48 h. Sample bottles were rinsed 10 times with Milli-Q water, dried in a laminar flow hood, and stored capped. Pipette tips were cleaned immediately prior to use with two rinses of 6 N Ultrex II HCl (J. T. Baker) followed by one rinse of Milli-Q water following an adaptation of the GEOTRACES recommendations (Cutter et al., 2010).

2.2.2 Samples and certified materials

A range of samples and certified materials were considered in order to test the method across a wide range of matrices (Table 2.1). HISS-1 (NRCC, Canada) is a marine sediment reference material for trace metals and other constituents and was collected from Hibernia Shelf, off the coast of Newfoundland. The sediment is primarily lithogenic, with low carbonate content ($\leq$

3%). HISS-1 was freeze dried, screened (125 µm) and blended by the manufacturer. This standard was used to confirm that any changes made to the digestion process would not affect the quality of the digestion on sediments with a low carbonate composition. GSD-11 is a river sediment from the Shizhuyan ore field in Binzhou, Hunan province, China. The rocks of the drainage basin include biotite granite, carbonates, granite and granodiorite (Xie et al., 1989). GSD-11 was dried, milled in an alumina ceramic vessel with alumina ceramic balls and screened by the manufacturer. GSR-6 is a limestone rock sample from Tongling, Anhui, China. The major component of this standard is calcite (Xie et al., 1989). GSR-6 rock was broken into pieces ($\leq$ 10 cm), washed with water, dried, crushed into 3 to 5 mm pieces prior to milling and screening by the manufacturer. A sample of pure calcium carbonate (ELTRA, Germany) was also used as a standard, providing a suite of reference materials covering a broad range of carbonate compositions. D-178 is a marine sediment from the Campbell plateau of New Zealand and has a matrix rich in carbonate. It was analysed after freeze drying and crushing.

Table 2.1: Description of samples considered.

	Sample type	***Origin***	***Carbonate content (g/100g)***
HISS-1	marine	Canada, Hibernia Shelf	3
GSR-6	rock	China, Tongling	64
GSD-11	stream	China, Shizhuyan	1
D-178	marine	New Zealand, Tasman Plateau	76
$CaCO_3$	pure carbonate	Synthesised	100

The mineralogical composition of the certified reference materials used in this study has not been reported. The carbonate content of all the reference materials was therefore estimated based on the assumption that all the Ca is present as $CaCO_3$ (Table 2.1). This assumption was made because the carbonate content of the samples considered in this study is either extremely high ($\geq$ 63%) or extremely low ($\leq$ 3%). When carbonate is the major fraction of the sediment, the impact of any Ca not present as $CaCO_3$ on the estimated carbonate content is minimal because most of the Ca is present as $CaCO_3$. Similarly when the carbonate fraction is extremely small ($\leq$ 3%) low carbonate concentrations will be slightly overestimated (by 1-2%) using this approach.

2.2.3 Microwave instrument and sequence

A Milestone Ethos EZ laboratory microwave oven with SK-12 (medium pressure) rotor was used for digestions with a maximum power, temperature and pressure of 1500 W, 300 °C and 35 bar, respectively. The unit has a maximum capacity of 12 x 100 mL vessels made from PTFE-TFM (Polytetrafluoroethylene with additional modifier Perfluorpropylvinylether). The sequence for acid digestion was as follows: temperature ramping over 10 min to 180 °C, stabilisation at this temperature for 40 min, before final increase to 200 °C over 4 min. The reaction vessel was held at this temperature for 20 min. Applied microwave power was adjusted automatically by the unit to perform the sequence described above. This microwave sequence was adapted from US EPA 3051 and 3052 processes for the digestion of marine sediments (Agazzi and Pirola, 2000). The maximum temperature was higher in our protocol, 200 °C, compared with the maximum temperatures suggested for US EPA methods, 180 °C and 185 °C, respectively. Furthermore, heating was applied for a longer period (74 min) compared with US EPA 3051 and 3052 methods (15 min and 20 min, respectively). This protocol with increased temperature and digestion time compared to the US EPA 3051 and 3051 methods was chosen in agreement with the manufacturer recommendations (Milestone) to limit the risk of overpressure and to maximise the sample digestion.

2.2.4 Digestion procedures

Two different approaches to eliminate precipitate formation and completely digest carbonate samples were considered in this study. The first attempted to minimise the volume of HF used during the microwave digestion process. The second approach considered the addition of a hotplate digestion step using HCl prior to microwave attack. Every digestion treatment was applied 4 times (n = 4) to each reference material. At least one digestion blank was included in each digestion batch run on the microwave. The blanks considered were process blanks taken through the entire sample handling procedure. The method limits of detection (LOD) of the 20 elements analysed were calculated as three standard deviations of 17 digestion blank replicates added to the mean value of the 17 replicates (Table 2.2). The overall reproducibility of the optimised protocol was tested by digesting D-178 19 times over a three months period.

Table 2.2: Determined elemental concentrations with relative errors following ICP-MS analysis, for different volumes of HF used during the digestion (n=4).

I.D	Vol of HF Added	[Al]	[Ca]	[Fe]	[Mg]	[Na]	[Ag]	[Ba]	[Cd]	[Co]	[Cr]
HISS-1	0mL	2330 ± 662	9670 ± 850	2070 ± 143	622 ± 81.5	2180 ± 380	-	-	0.03 ± 0.01	0.49 ± 0.04	9.05 ± 2.26
HISS-1	1mL	6490 ± 444	9870 ± 811	2160 ± 117	683 ± 73.5	3130 ± 609	-	-	0.03 ± 0.01	0.6 ± 0.07	17.37 ± 5.4
HISS-1	1mL P.D.	6040 ± 612	9050 ± 247	2140 ± 63.8	628 ± 33.1	2940 ± 186	-	-	0.03 ± 0.02	0.55 ± 0.01	16.43 ± 2.93
HISS-1	2mL P.D.	6420 ± 537	9840 ± 1010	2130 ± 140	666 ± 106	3820 ± 112	-	-	0.03 ± 0.01	0.55 ± 0.03	23.35 ± 3.35
HISS-1	3mL P.D.	6780 ± 784	9750 ± 1300	2240 ± 325	676 ± 92.2	3270 ± 458	-	-	0.03 ± 0.01	0.59 ± 0.1	23.21 ± 4.35
HISS-1	3mL	6420 ± 419	9660 ± 1150	2150 ± 126	700 ± 80.2	3270 ± 565	-	-	0.03 ± 0.01	0.56 ± 0.05	19.38 ± 3.91
HISS-1	6mL	6650 ± 614	9650 ± 293	2160 ± 170	701 ± 35.9	3360 ± 184	-	-	0.03 ± 0.01	0.55 ± 0.08	19.06 ± 0.96
HISS-1	*certified*	*7300 ± 599*	*11400 ± 1000*	*2460 ± 100*	*750 ± 200*	*3730 ± 300*	-	-	*0.02 ± 0.01*	*0.65* ± -	*30 ± 6.8*
D-178	0mL	3650 ± 739	302000 ± 44200	5480 ± 351	2690 ± 274	7230 ± 510	0.04 ± 0.03	133 ± 14	0.57 ± 0.03	1.67 ± 0.17	9.47 ± 0.96
D-178	1mL	5280 ± 1100	308000 ± 23600	5840 ± 407	2850 ± 138	7360 ± 740	0.06 ± 0.03	154 ± 10	0.64 ± 0.09	1.84 ± 0.06	10.71 ± 1.13
D-178	1mL P.D.	5880 ± 123	294000 ± 6970	5910 ± 65.7	3110 ± 507	7160 ± 643	0.11 ± 0.01	151 ± 6	0.58 ± 0.09	1.77 ± 0.1	10.88 ± 0.44
D-178	2mL P.D.	5710 ± 207	306000 ± 22500	5740 ± 253	2840 ± 247	7640 ± 840	0.09 ± 0.02	145 ± 3	0.54 ± 0.06	1.72 ± 0.05	10.93 ± 0.67
D-178	3mL P.D.	5730 ± 78.3	285000 ± 2800	5910 ± 53.7	2730 ± 55.2	7170 ± 691	0.09 ± 0.01	146 ± 2	0.57 ± 0.05	1.67 ± 0.05	10.8 ± 0.16
D-178	3mL	5520 ± 527	300000 ± 48300	5740 ± 370	2760 ± 350	8100 ± 2190	0.08 ± 0.02	144 ± 11	0.54 ± 0.03	1.6 ± 0.13	10.59 ± 1.09
D-178	6mL	5490 ± 418	292000 ± 45800	5500 ± 424	2690 ± 269	8760 ± 836	0.07 ± 0.03	145 ± 13	0.54 ± 0.03	1.68 ± 0.13	10.54 ± 0.82
D-178	19 replicates 2mL	5512 ± 334	305858 ± 23849	5702 ± 307	2763 ± 181	7201 ± 1233	0.15 ± 0.02	147 ± 11	0.52 ± 0.03	1.68 ± 0.1	10.47 ± 0.68
GSR-6	0mL	22300 ± 677	232000 ± 26500	15000 ± 33.4	26100 ± 356	153 ± 54.5	-	122 ± 7	0.06 ± 0	9.06 ± 1.33	26.85 ± 0.96
GSR-6	1mL	22900 ± 1240	220000 ± 23400	14800 ± 625	26100 ± 1190	273 ± 5.99	-	123 ± 4	0.1 ± 0.01	8.08 ± 0.6	27.78 ± 1.23
GSR-6	2mL P.D.	23900 ± 1200	237000 ± 17400	15100 ± 347	26300 ± 1760	415 ± 72.9	-	123 ± 1	0.08 ± 0	8.27 ± 0.51	27.91 ± 1.84
GSR-6	3mL	22900 ± 1190	219000 ± 18900	14700 ± 450	25600 ± 1070	270 ± 23.3	-	124 ± 2	0.09 ± 0.02	8.14 ± 0.2	27.45 ± 0.97
GSR-6	6mL	21900 ± 819	232000 ± 3540	14800 ± 269	25100 ± 620	269 ± 44.5	-	126 ± 3	0.06 ± 0.02	8.16 ± 0.38	27.77 ± 0.5
GSR-6	*certified*	*26500* ± -	*255000* ± -	*17400* ± -	*31100* ± -	*460* ± -	-	*120 ± 4*	*0.07 ± 0*	*9 ± 0.75*	*35 ± 0.9*
GSD-11	0mL	33900 ± 577	2880 ± 187	25700 ± 689	2920 ± 116	558 ± 163	2.39 ± 0.26	181 ± 5	1.98 ± 0.09	7.02 ± 0.11	33.34 ± 0.91
GSD-11	1mL	17200 ± 1900	2610 ± 162	26100 ± 441	642 ± 71.8	2640 ± 509	2.94 ± 0.25	207 ± 11	1.94 ± 0.08	7.3 ± 0.34	35.16 ± 1.55
GSD-11	2mL P.D.	23400 ± 2570	2460 ± 94.3	25700 ± 299	1110 ± 70.2	2760 ± 16.7	2.89 ± 0.05	185 ± 1	2.09 ± 0.37	7.25 ± 0.07	34.41 ± 0.36
GSD-11	3mL	27900 ± 3090	2630 ± 52.2	26200 ± 498	1180 ± 342	2580 ± 445	3.1 ± 0.29	193 ± 9	1.99 ± 0.2	7.35 ± 0.19	36.21 ± 1.57
GSD-11	6mL	38100 ± 4450	2670 ± 46.1	25700 ± 338	1810 ± 424	2900 ± 380	2.89 ± 0.16	189 ± 7	2.02 ± 0.11	7.24 ± 0.19	35.25 ± 0.74
GSD-11	*certified*	*55000 ± 423*	*3430 ± 37.4*	*30700 ± 240*	*3660* ± -	*3410* ± -	*3.2 ± 0.46*	*258 ± 10*	*2.3* ± -	*8.5 ± 0.42*	*39.6 ± 1.84*
Limit of detection		*7.58E-003*	*6.83E-002*	*1.41E-003*	*2.81E-003*	*2.02E-001*	*1.06E-003*	*2.81E-004*	2.17E-005	*1.79E-005*	*3.84E-005*

I.D	Vol of HF Added	[Cu]	[Mn]	[Mo]	[Ni]	[Sr]	[Th]	[Ti]	[U]	[V]	[Zn]
HISS-1	0mL	1.73 ± 0.09	60.9 ± 5.29	-	-	83.4 ± 5.49	-	503 ± 23.6	0.22 ± 0.009	6.05 ± 0.242	-
HISS-1	1mL	2.11 ± 0.22	65.1 ± 2.92	-	-	104 ± 4.02	-	721 ± 43.4	0.255 ± 0.022	6.57 ± 0.201	-
HISS-1	1mL P.D.	2.14 ± 0.175	61.8 ± 3.09	-	-	95 ± 2.34	-	695 ± 38.5	0.267 ± 0.029	6.25 ± 0.149	-
HISS-1	2mL P.D.	1.88 ± 0.05	63.7 ± 4.22	-	-	100 ± 4.24	-	719 ± 57.4	0.246 ± 0.008	6.7 ± 0.496	-
HISS-1	3mL P.D.	2.11 ± 0.08	63.4 ± 7.33	-	-	107 ± 15.2	-	767 ± 117	0.276 ± 0.048	7.02 ± 1.07	-
HISS-1	3mL	2.04 ± 0.09	65.3 ± 6.79	-	-	102 ± 5.68	-	739 ± 55.5	0.286 ± 0.035	6.44 ± 0.279	-
HISS-1	6mL	2.09 ± 0.28	64.2 ± 0.899	-	-	104 ± 5.02	-	735 ± 40.1	0.278 ± 0.012	6.63 ± 0.658	-
HISS-1	*certified*	*2.29 ± 0.37*	*66.1 ± 4.2*	-	-	*96.9 ± 11.2*	-	*760 ± 0*	*0.26*	*6.8 ± 0.78*	-
D-178	0mL	5.02 ± 0.368	40.7 ± 3.87	-	0.543 ± 0.931	1250 ± 77.3	0.657 ± 0.13	712 ± 52.6	0.594 ± 0.025	11.2 ± 0.738	17.75 ± 1.30
D-178	1mL	5.84 ± 0.735	48.3 ± 3.35	-	1.36 ± 0.592	1370 ± 90.6	0.786 ± 0.186	799 ± 104	0.656 ± 0.036	11.1 ± 2.53	18.53 ± 1.60
D-178	1mL P.D.	5.41 ± 0.276	49.6 ± 6.18	-	0.876 ± 0.076	1370 ± 18	0.85 ± 0.0217	824 ± 22.3	0.576 ± 0.025	12.4 ± 0.224	20.49 ± 1.11
D-178	2mL P.D.	4.84 ± 0.269	46.6 ± 1.82	-	1.48 ± 0.195	1320 ± 53.5	0.99 ± 0.0918	803 ± 20.3	0.62 ± 0.019	12.2 ± 0.251	17.98 ± 0.59
D-178	3mL P.D.	5.18 ± 0.122	45.3 ± 0.56	-	1.28 ± 0.463	1330 ± 12.9	0.959 ± 0.118	818 ± 8.29	0.593 ± 0.014	12.3 ± 0.112	19.62 ± 0.85
D-178	3mL	5.22 ± 0.487	46.3 ± 5.14	-	1.23 ± 1.43	1270 ± 107	0.867 ± 0.0543	792 ± 58.6	0.609 ± 0.062	12 ± 1.16	18.505 ± 0.25
D-178	6mL	5 ± 0.233	44.3 ± 4.53	-	0.613 ± 0.841	1250 ± 83.9	0.843 ± 0.0606	767 ± 51	0.615 ± 0.064	11.7 ± 0.839	16.90 ± 1.52
D-178	19 replicates 2mL	4.42 ± 0.290	43.3 ± 1.79	-	1.3 ± 0.478	1301 ± 103.5	0.732 ± 0.1346	807 ± 42	0.619 ± 0.057	12.1 ± 0.80	16.59 ± 2.16
GSR-6	0mL	20.2 ± 0.679	414 ± 20.4	0.258 ± 0.005	13.4 ± 0.943	942 ± 42.6	2.85 ± 0.416	965 ± 33.7	-	35.6 ± 1.79	38.37 ± 5.36
GSR-6	1mL	20.3 ± 0.642	409 ± 23.2	0.309 ± 0.08	15.7 ± 0.959	922 ± 46.6	3.9 ± 0.499	1770 ± 66.2	-	36.6 ± 2.23	39.62 ± 4.98
GSR-6	2mL P.D.	20.1 ± 0.628	402 ± 12.1	0.397 ± 0.072	15 ± 1.45	937 ± 47.6	3.99 ± 0.0563	1780 ± 60.1	-	38.1 ± 1.6	42.64 ± 4.41
GSR-6	3mL	20.3 ± 1.35	410 ± 16.7	0.339 ± 0.145	15.9 ± 0.267	928 ± 16	4.15 ± 0.218	1800 ± 75.2	-	37 ± 1.67	41.04 ± 5.63
GSR-6	6mL	20 ± 1.51	406 ± 14	0.414 ± 0.058	15.1 ± 0.271	941 ± 23.6	4.21 ± 0.161	1790 ± 30.7	-	36.7 ± 0.544	39.17 ± 5.44
GSR-6	*certified*	*23.4 ± 0.8*	*440 ± -*	*0.38 ± 0.09*	*17.6 ± 0.6*	*900 ± 22*	*4.4 ± 0.01*	*1950 ± -*	-	*34 ± 2.2*	*52 ± 2.4*
GSD-11	0mL	73.3 ± 2.48	2250 ± 19.8	6.5 ± 0.203	10.8 ± 1.59	14.4 ± 0.658	21.6 ± 0.924	617 ± 44	8.78 ± 0.173	38.1 ± 1.36	317.10 ± 49.83
GSD-11	1mL	74.4 ± 2.85	2240 ± 67	6.71 ± 0.497	12.2 ± 0.597	23.7 ± 1.82	5.21 ± 2.82	1830 ± 81.6	8.72 ± 0.695	39.8 ± 1.37	316.30 ± 39.94
GSD-11	2mL P.D.	71.4 ± 7.97	2130 ± 54.7	6.94 ± 0.803	12.8 ± 0.0852	18.7 ± 0.0578	11.1 ± 0.763	1840 ± 2.38	8.93 ± 0.163	39.8 ± 0.572	316.65 ± 65.07
GSD-11	3mL	72 ± 4.36	2250 ± 36.2	6.7 ± 0.399	13.3 ± 0.427	21.6 ± 0.896	12.4 ± 3.29	1880 ± 51.7	9.49 ± 0.862	40.1 ± 0.467	319.57 ± 44.52
GSD-11	6mL	72.6 ± 4.22	2240 ± 38	6.83 ± 0.168	13.7 ± 1.9	21.1 ± 1.07	13.5 ± 4.1	1880 ± 48.9	9.49 ± 0.72	40 ± 0.779	325.47 ± 56.29
GSD-11	*certified*	*79 ± 1.72*	*2500 ± 11.7*	*6.2 ± 1.49*	*14.4 ± 1.68*	*29 ± 0.325*	*23 ± 2*	*2110 ± 37.4*	*9 ± 1.4*	*46 ± 1.9*	*375 ± 5.95*
Limit of detection		8.20E-005	1.00E-004	7.77E-005	2.60E-003	2.06E-004	3.23E-006	1.87E-004	2.45E-006	2.17E-005	1.03E-003

Note : certified concentrations and associated standard errors are also provided. P.D. stands for Pre-Digestion step when the optimised protocol was used. The limits of detection calculated on 17 digestion blank replicates are included. The standard deviations of the 19 replicates (digestion of D-178 using the optimised protocol) are also included. The concentrations are given in mg/kg.

HF gradient digestion

The basic digestion procedure applied was an adaptation of two methods already published (Muratli et al., 2012; Negre et al., 2009). Four different volumes of HF were considered: 6 mL (Kemp and Brown, 1990), 3 mL, 1 mL and a digestion without HF, reflecting the diversity of methods found in the literature (Pena-Icart et al., 2011).

Two hundred milligrams of freeze-dried and crushed sediment were weighed into 100 mL microwave vessels. The large sample size (200 mg) was necessary because we are ultimately interested in extracting and analysing 230-Thorium (^{230}Th) (Negre et al., 2009). 230-Thorium has a really small isotopic abundance compared to ^{232}Th, therefore large sediment weights need to be digested for a precise measurement of ^{230}Th, however ^{230}Th results are beyond the scope of this manuscript. The sides of the vessels were rinsed two times with 1 mL of Milli-Q water to remove any attached sediment. In a fume hood 4 mL of concentrated HCl, 10 mL of concentrated HNO_3 and either 0, 1, 3 or 6 mL of concentrated HF were added. The vessels were immediately transferred to the microwave oven and exposed to the sequence described previously. The vessels were allowed to cool for up to 1 h with the fan of the microwave turned on to accelerate cooling. Each solution was carefully transferred into a clean 50 mL Teflon© (polytetrafluoroethylene) beaker. The microwave vessels and their lids were rinsed two times with 1 mL of concentrated HNO_3 to collect as much of the digested sediments as possible. Observations to assess the quality of the digestions were recorded (Table 2.3). The solutions were then heated on a hotplate at 105 °C and taken to incipient dryness. Six milliliters of concentrated HNO_3 were then added and taken to dryness at 110 °C. This last step was repeated once. When nearly desiccated, the samples were taken up in 4 mL of 7.5 N HNO_3 and their weights recorded. A four hundred microliter aliquot of this solution was diluted in 15 mL of 12.5% HNO_3 (weights recorded) in 30 mL acid-cleaned LDPE Nalgene bottles. This aliquot was used to quantify the 20 elements presented in this study. The reminder of the 4 mL solution was used to analyse the ^{230}Th fraction of the sediment (not presented in this study). Just prior to ICP-MS analysis the bottles were heated on a hotplate at 60 °C for 24 h and then further diluted by a factor five. At this stage Indium (^{115}In) was added as the internal standard.

Table 2.3: Visual observations and solid matter compositions following digestion with different volumes of HF. The solid compositions were determined using SEM analysis. N.E. corresponds to 'Not Enough' sample for the x-ray characterisation. '$\leq$' and '$\ll$' indicate the dominant elemental component(s) when multiple elements were characterised.

References	0 mL of HF added	1 mL of HF added	2mL of HF added Pre-digestion step	3mL of HF added	6mL of HF added
HISS-1	Grey residue SiO_2	Grey residue N.E	Clear	Clear	Clear
GSR-6	Grey residue SiO_2	Clear	Clear	Clear	White residue Ca Mg $\ll$ Ca F
GSD-11	Grey residue SiO_2	Grey residue Ca $\leq$ Mg $\ll$ Al F	White suspension N.E.	White 'sandy' residue Ca $\leq$ Mg $\ll$ Al F	White 'sandy' residue Ca $\leq$ Mg $\ll$ Al F
$CaCO_3$	Clear	White 'sandy' residue	White suspension N.E.	White 'sandy' residue N.E.	White 'sandy' residue
D-178 (core sample)	Grey residue SiO_2	Clear	Clear	White 'sandy' residue N.E.	White 'sandy' residue CaF_2

Optimised procedure with pre-digestion in HCl

Two hundred milligrams of crushed and dried sediment were placed in the microwave vessels. In a fume hood 4 mL of concentrated HCl was added and the beakers were placed on a hotplate at 150 °C for 2 h to allow CO_2 to be released. The vessels were left to cool for 1 h with lids on, in the fume hood. Ten milliliters of concentrated HNO_3 and 2 mL of concentrated HF were added. For HISS-1 and D-178 reference materials the method was also tested using 1 mL and 3 mL of HF. The procedures for microwave digestion and the sample preparation prior to ICP-MS analysis were then followed as described above.

2.2.5 Detection instrumentation and techniques

ICP-MS instrumentation and analysis

An ELEMENT 2 sector field ICP-MS from Thermo Fisher Scientific was used to perform all analyses. Both low (m/Δm $\approx$ 400) and medium (m/Δm $\approx$ 4500) spectral resolution modes were used. Low resolution was selected for those higher mass isotopes known to have minimal overlap from polyatomic interferences (^{88}Sr, ^{95}Mo, ^{107}Ag, ^{109}Ag, ^{111}Cd, ^{137}Ba, ^{185}Re, ^{232}Th and ^{238}U). The instrument operated in this mode offers maximum sensitivity and measurement precision. Medium resolution was utilised for those low mass isotopes well known to suffer from polyatomic interferences (^{47}Ti, ^{51}V, ^{52}Cr, ^{55}Mn, ^{56}Fe, ^{59}Co, ^{60}Ni, ^{63}Cu and ^{66}Zn). Major species (e.g. ^{23}Na, ^{24}Mg and ^{42}Ca) were also analysed in this manner to prolong detector life. A range of

polyatomic species associated with the presence of argon and acid digestion reagents could form in the ICP and interfere with some targeted elements. For example $^{35}Cl^{16}O^{+}$, $^{36}Ar^{16}O^{+}$ and $^{38}Ar^{14}N^{+}$ $^{40}Ar^{16}O^{+}$, $^{43}Ca^{16}O^{+}$, $^{40}Ar^{23}Na^{+}$ interfere with ^{51}V, ^{52}Cr, ^{56}Fe, ^{59}Co, and ^{63}Cu, respectively. Access to increased spectral resolution through the use of sector field ICP-MS allows interference free measurement of many low mass isotopes (Townsend, 2000). Details can be found elsewhere (Giessman and Greb, 1994). The instrument was tuned daily to optimise signal sensitivity and stability. The method of external calibration was used for elemental quantification. Multi-element calibration solutions were prepared by serial dilution from 100 $\mu g.mL^{-1}$ standard solutions (QCD Analysts, Spring Lake, USA). Although potentially offering increased analytical accuracy through closer matrix matching between standards and unknown samples, quantitation using a standard additions approach was not employed in this work given the varied range of samples with unique compositions considered and to provide maximum sample throughput. Indium was used as an internal standard following addition to all samples, standards and blanks. A typical analysis sequence consisted of a four point calibration followed by in-house drift correction, instrument blanks and external reference materials. Samples then followed, grouped according to matrix and expected elemental concentrations. Sample groups never exceeded four or five samples and were bracketed by in-house quality control standards. Further sample handling protocols and typical instrument operating conditions can be found elsewhere (Mann et al., 1992). Table 2.4 summarises the instrument conditions and measurement parameters.

The 20 elements selected for analysis were chosen to provide the best understanding around the performance of acid digestion procedures across a range of sample matrices. The ultimate application of the developed method is to better understand the past redox conditions of marine sediments. Elements including U or Mo are used to reconstruct past redox conditions (Morford and Emerson, 1999; Tribovillard et al., 2006). However understanding their deposition processes is essential and can only be made by looking at a wider range of elements.

Precipitate characterisation - Scanning Electron Microscopy

The composition of various solid residues resulting from possible incomplete digestion or precipitation were assessed using a Scanning Electron Microscope (SEM, Hitachi SU-70 field emission SEM) and energy dispersive x-ray microanalysis (EDS, Oxford AZtec 2.2 XMax80 system). Op-

Table 2.4: Typical instrument conditions and measurement parameters.

Instrument	ELEMENT 2 sector field ICP-MS (Thermo Fisher, Bremen, Germany)
Torch	Fassel type (Thermo Fisher, Germany)
Spray chamber	20 mL Cyclonic (Glass Expansion, Australia)
Nebuliser	0.2 mL/min Micromist (Glass Expansion, Australia)
RF power	1350 W
Cool gas flow	$\approx$ 15 L/min
Auxiliary gas flow	$\approx$ 0.7 L/min
Sample gas flow	$\approx$ 0.95 L/min
Sample uptake	100 s with pumping
Sample rinse	150 s, 5% nitric acid solution
Scan type	E-scan
Isotopes monitored in low resolution (m/Δm $\approx$ 400)	^{88}Sr,^{95}Mo,^{107}Ag,^{109}Ag,^{111}Cd,^{137}Ba,^{232}Th and ^{238}U
Isotopes monitored in medium resolution (m/Δm $\approx$ 4500)	^{23}Na,^{24}Mg,^{27}Al,^{42}Ca,^{47}Ti,^{51}V,^{52}Cr,^{55}Mn,^{56}Fe,^{59}Co, ^{60}Ni,^{63}Cu and ^{66}Zn
Internal standard	^{115}In, both resolution modes

erating conditions employed were 15 kV accelerating voltage and around 2 nA probe current. Prior to analysis residues were extracted from HNO_3 solution by centrifugation (5 min at 1000 rpm). The liquid fraction was removed and the solid phase was washed out of the tubes with 3 x 1 mL of Milli-Q water. The solutions containing the residues were transferred into Teflon© (polytetrafluoroethylene) beakers and dried on a hotplate at 100 °C. Once totally dried the residues were crushed in a ziplock bag. Small amounts of powder were attached to SEM pin holders using double-sided carbon sticky tape, and coated with around 20 nm of carbon using a Ladd 40000 carbon evaporator. For each residue, three sites were considered and 10 x-ray analysis measurements were performed on each site. Areas on the holders with low powder coverage where individual particles are well separated were chosen for analysis to minimise charging effects and contribution of multiple particles to individual analyses. The global composition of the residue was calculated by averaging the 30 spectra recorded. Due to the irregular surface topography and small size of the analysed particles, the compositional information obtained was normalised to 100% total and can only be considered semi-quantitative.

2.3 Results

Digestion recoveries across all 20 elements (Figure 2.1) and deviations from certified values for representative elements (Figure 2.2) were calculated for all sediments from concentration data (Table 2.2). D-178 recoveries and deviations are relative to the maximum concentrations measured for this sample, since it is not a certified reference material.

A one way anova (analysis of variance) was used to test for differences between treatments.

When one treatment was compared to more than one other treatment, the respective highest or lowest p value was reported.

2.3.1 HISS-1

HISS-1 element recoveries were all close to the certified values ($\geq$ 92% for 1 to 6 mL of HF added) (Figures 2.1, 2.2; Table 2.2). Clear solutions with no apparent residue were observed when between 2 and 6 mL of HF was used (Table 3). Elemental recoveries when not using HF were comparatively low (75%), with a residue identified as SiO_2 being present. Higher recoveries were observed when a volume larger than 1 mL of HF was used ($p \leq 0.05$). A maximal recovery of 95% was observed when 6 mL of HF were used, although the use of 1 and 3 mL of HF gave statistically similar results with 92% and 94% of recovery, respectively. An average recovery of 94% was achieved using the optimised protocol, but this was not statistically different from recoveries using no pre-digestion and at least 1 mL of HF. The use of 1 and 3 mL of HF with the pre-digestion step was also tested for HISS-1. Smaller but statistically similar recoveries were observed compared to the use of 2 mL HF with the pre-digestion step (Table 2.2).

Of the major elements, Al was not recovered when no HF was used ($p \leq 0.05$ between the Al recovery with no HF used and all the other recoveries for each other volume of HF used). Considering Na, the optimised protocol gave the highest recovery and was also the only recovery in agreement with the certified concentration of HISS-1 (Figure 2.2, $p \leq 0.001$). A similar variation pattern was observed for Cr, with high recovery when the optimised protocol was applied (Table 2.2). Minimal differences were noted for U for the different volumes of HF applied (Figure 2.2). The absence of HF during the digestion strongly decreased the recoveries of Th and Ti (Figure 2.2).

Trace elements had a higher recovery compared to the major elements (Figure 2.1, p=0.007). All element concentrations using the optimised procedure agreed within error with the certified concentrations (Figure 2.2), with the exception of Fe, which was slightly lower than the certified value.

2.3.2 GSR-6

Average elemental recoveries of 83%, 94%, 91% and 88% were noted for GSR-6 when 0, 1, 3 and 6 mL of HF were used without the pre-digestion step (Figure 2.1). An average recovery of 94%

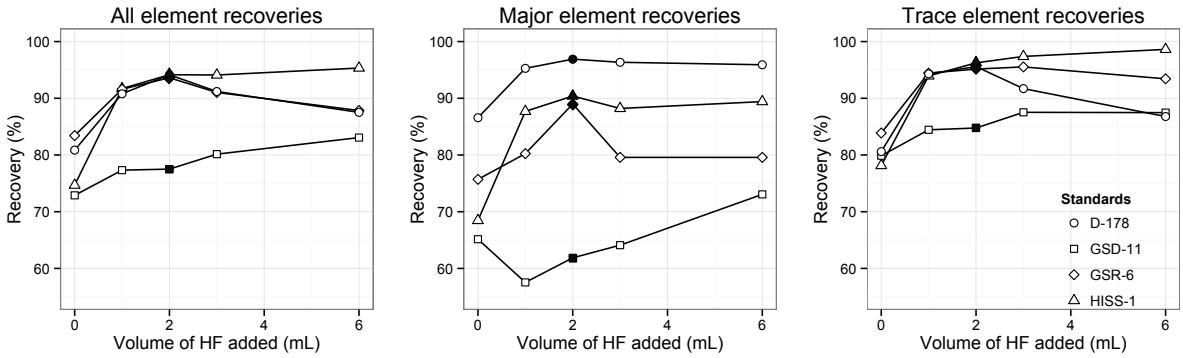

Figure 2.1: From left to right : Average overall element recoveries against volume HF added during digestion; Average overall major element recoveries (Ca, Mg, Al, Fe and Na) against the volume HF added during digestion; average overall trace element recoveries (Cd, Co, Cr, Cu, Mn, Sr, Ti, U and V) against the volume HF added during digestion. Black symbols highlight the proposed optimised procedure (pre-treatment with HCl (32%) on hotplate followed by microwave digestion with 2 mL of HF). The averaged recoveries for the different groups (all elements, major elements, trace elements) presented were calculated by averaging the recovery of each individual element for each group.

was observed when the optimised protocol was used (Figure 2.1). The three highest recoveries (1, 2 and 3 mL of HF) corresponded to visibly clear digestion solutions with no residue observed (Table 2.3) and were statistically similar. The residues observed when no HF and 6 mL of HF were used were identified as SiO_2 and CaF_2 respectively (Table 2.3).

For GSR-6 the major elements displayed lower recoveries compared to the trace elements (p=0.01). The use of the optimised protocol increased the major element recoveries compared to the trace element recoveries (Figure 2.1), mainly driven by increased recovery of Na. No statistically supported variations for the trace element recoveries were observed when different volumes of HF were used (Figure 2.2).

2.3.3 GSD-11

GSD-11 displayed low and statistically similar recoveries for all volumes of HF used, both with and without the pre-digestion step (Figure 2.1, 2.2; Table 2.2, 2.3). The best recovery of 83% corresponded to the use of 6 mL of HF. GSD-11 digestions were all unsuccessful, with a SiO_2 residue when small volumes of HF were added and an aluminum fluoride precipitate when larger volumes of HF were added (Table 2.3).

Trace elements displayed better recoveries compared to major elements (Figure 1 and 2, p=0.0002). Some trace elements (Cr, Cu, Mo, U, Ti) were well recovered independently of the

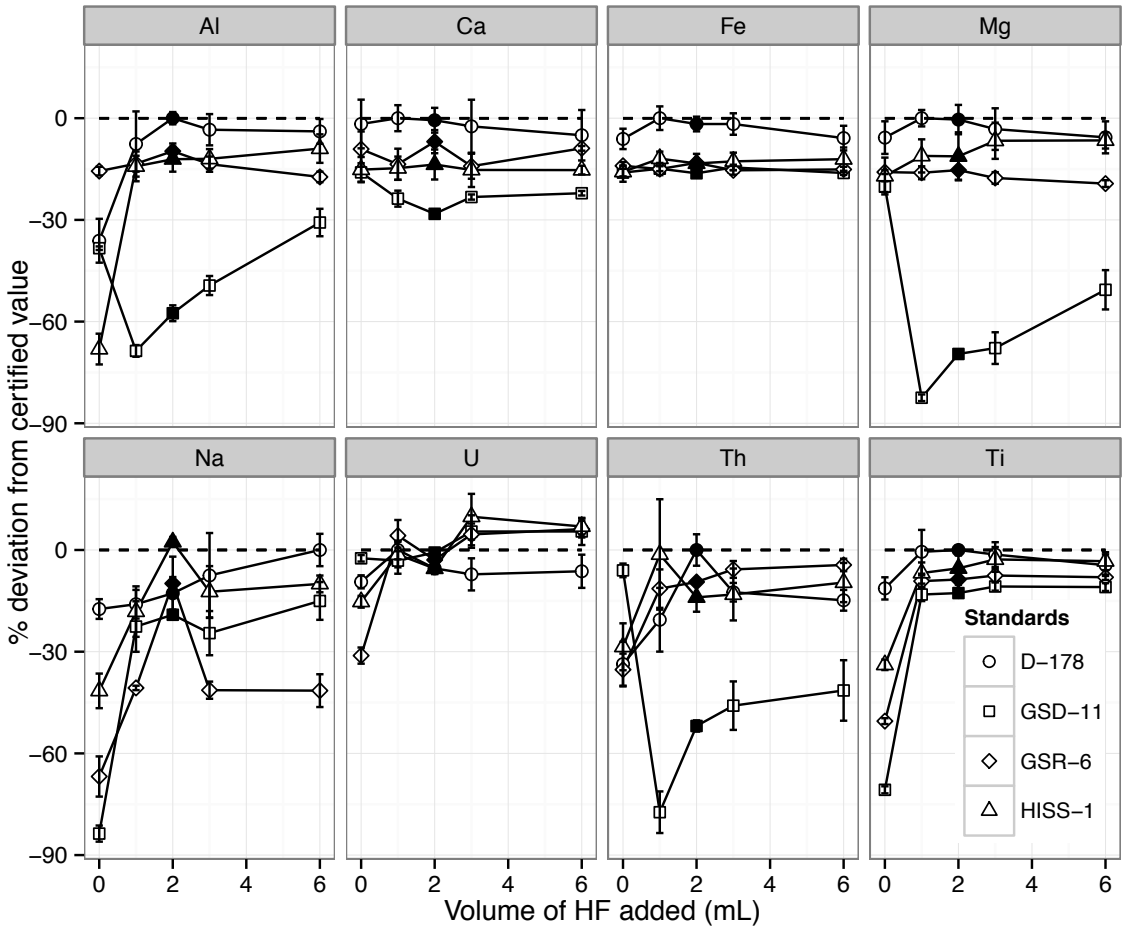

Figure 2.2: Deviation from certified concentrations for representative elements in HISS-1, GSR-6 and GSD-11 after ICP-MS analysis. The deviation represented for D-178 is from the maximal concentration observed. The data for 2 mL of HF added correspond to the proposed optimised procedure, black symbols highlight the proposed optimised procedure (pre-treatment with HCl (32%)) on hotplate followed by microwave digestion); the error bars shown for n=4 represent the standard error.

volume of HF used (Figure 2.2, Table 2.2).

The recovery of Al, Mg and Th showed a distinct trend with respect to the volume of HF added (Figure 2.2): maximum elemental recovery was observed without any HF addition and a minimum when 1 mL was used, followed by increasing elemental recoveries with volumes of 2, 3 or 6 mL HF. This trend can also be observed in the average major element recoveries (Figure 2.1) and is statistically supported; most recoveries were statistically different ($p \leq 0.05$) except the two recoveries between 2 mL and 3 mL of HF used and 1 mL and 2 mL of HF used.

2.3.4 D-178

Elemental recoveries in D-178 varied with the volume of HF added in a similar fashion as GSR-6: high and statistically similar recoveries were observed when intermediate volumes of HF were added (Figure 2.1). An average recovery of 91% was observed when both 1 and 3 mL of HF was added and a recovery of 94% was observed when 2 mL of HF with the pre-digestion step was used (all statistically similar). As with HISS-1, D-178 recoveries tended to be lower when 1 or 3 mL of HF were used with the pre-digestion step instead of 2 mL of HF (Table 2.2). The use of 1 mL of HF and 2 mL of HF with the pre-digestion step produced the only clear solutions for this sediment. For all other volumes of HF considered a noticeable residue was observed. The residues were found to be SiO_2 when no HF was added and CaF_2 when more HF was added (3 mL and 6 mL) (Table 2.3).

For the major elements, only small variations in Ca, Fe and Mg recoveries were observed across the volumes of HF added, with average recoveries observed between 86 and 96% (Figure 2.1). The recovery of Na and Al were more strongly affected by HF volume, with Na showing the highest recovery using 6 mL of HF and Al showing the highest recovery using the optimised protocol (Figure 2.2).

High trace element recoveries were observed when either 1 mL of HF was added or when the optimised protocol was used (Figure 2.1). Nickel, Ag and Th showed clearer variations with the volume of HF added compared to the other elements (Table 2.2, Figure 2.1). High recoveries for all trace elements and smaller errors were observed when the optimised protocol was used (Figure 2.2, Table 2.2).

The long term reproducibility of the optimised protocol was tested on D-178 and displayed in Table 2.2. For most elements the respective standard error over the 19 replicates was less than 10%. For the most abundant elements (Ca, Mg, Na, Fe, Al) the standard error of the 19 replicates was around 5%. Higher errors were observed for low-abundance trace elements like Ag and Mo (Table 2.2).

2.3.5 Calcium carbonate reference

Calcium carbonate digestion replicates were only clear when no HF was used in the digestion process (Table 2.3).

2.3.6 Summary of the results

Distinct residues were identified using SEM for each sample considered (Table 2.3). One was identified as SiO_2 (grey residue), which was present in three of the four certified reference materials post acid attack, when low volumes of HF were added, corresponding to incomplete digestions. Fluoride precipitates (white solid) were observed when higher volumes of HF were employed. Calcium carbonate digestion replicates were only clear when no HF was used in the digestion process.

Overall the optimised protocol gave the best results in terms of elemental recovery and digest clarity, for HISS-1, GSR-6 and D-178. Exceptions were noted for the pure $CaCO_3$ reference and for GSD-11 that produced a slight white suspension after the use of the optimised protocol. The amount of solid matter present in GSD-11 solutions after digestion was approximately 10 times smaller in weight using the optimised protocol compared to the standard methods without the pre-digestion step. The LOD were consistently at three to four orders of magnitude smaller (at minimum) than the analyte concentrations (Table 2.2). While the precision of the analyses did not vary consistently with the digestion method, the overall reproducibility using the optimised pre-digestion method was good, with relative standard errors generally of less than 10% (Table 2.2). The poorest precision, considering all the elements, was observed for HISS-1 when 1 mL of HF was used (Table 2.2).

2.4 Discussion

Two potential solutions were investigated to eliminate the fluoride precipitate found after digestion. The first was to reduce the volume of HF added to limit its availability for parallel reactions. The second was the addition of a simple hotplate pre-digestion step in concentrated HCl.

The volume of HF needed to produce a complete digestion was different for each of the four certified materials considered, due to their varied compositions. Adapting the volume of HF to every sample composition and matrix is not satisfactory as it requires extra work and potential unsuccessful digestions to determine the optimal volume of HF to use. The use of the pre-digestion step allowed a single digestion protocol to be applied across a wide range of carbonate rich materials.

2.4.1 Low carbonate marine sediment: HISS-1

HISS-1 with a low carbonate and high silicate content needed more HF to attack and solubilise its matrix. At low HF volumes (0 and 1 mL) sediments remained undigested (SiO_2 present), whereas the use of 3 and 6 mL of HF resulted in complete digestions (Figures 2.1, 2.2, Table 2.2, 2.3). The use of 2 mL (with pre-digestion), 3 mL and 6 mL of HF gave recoveries around 95% corresponding to total digestions. The effect of the optimised protocol was not the same across all the elements analysed. Particular elemental recoveries (Na, Cr) were only in agreement with the certified concentrations when the optimised protocol was used (Figure 2.2, Table 2.2). For the other elements (Ca, Mg, Cu, Mn, U) the recoveries observed were all close to the certified concentrations with no variations associated with the different volumes of HF used. We propose that these elements (Ca, Mg, Cu, Mn, U) were easily dissolved without a complete dissolution of the samples (Table 2.3) while Na or Cr needed a more aggressive treatment to be completely dissolved.

2.4.2 High carbonate materials: D-178, GSR-6 and calcium carbonate

The volumes of HF needed to provide complete digestion for GSR-6, D-178 and pure $CaCO_3$ (with their higher concentrations of carbonate) were lower than for HISS-1 (Figures 2.1, 2.2). Sediments with more carbonate required less HF because this mineral type can be digested relatively easily with HCl (Tiessen et al., 1983). Calcium carbonate digestions were only clear when no HF was used in the digestion process. In this extreme case the use of HF and HNO_3 was unnecessary as carbonate was adequately dissolved by HCl alone (Table 2.3).

Initially in this study, microwave vessels were allowed to sit overnight to outgas any CO_2 liberated (after the addition of HNO_3 and HCl, with lids loosely capped and without heating). Although CO_2 effervescence had ceased, solid matter was still observed in carbonate-rich samples post microwave digestion. This indicates that dissolving $CaCO_3$ in open vessels on a hotplate before any microwave treatment limits the accumulation of gas in the closed environment and prevents the formation of a precipitate.

The use of the optimised protocol resulted in a 10% increase in GSR-6 major element recoveries in comparison with the use of 1 and 3 mL of HF without the pre-digestions step (Figure

2.1, 2.2). This increase was predominantly associated with a better Na recovery (Figure 2.2). It is proposed that the optimised protocol not only reduces the formation of CaF_2. A Na complex, present in GSR-6, might also be better dissolved using the combination of the pre-digestion step and microwave digestion compared with using microwave digestion in isolation. A similar trend was observed for Ni in D-178 with highest recovery following the use of the optimised protocol (Figure 2.2). Again the pre-digestion could facilitate the dissolution of a Ni complex by increasing the time of contact between the solid and HCl.

The optimised protocol gave the smallest deviations from certified or consensus values with clear solutions for D-178 and GSR-6, allowing a single protocol to be applied to digest sediments with different matrices (Table 2.2). The reproducibility of the method when tested on D-178 gave good results for all elements except really low abundance ones like Ag and Mo. The concentrations of these elements in D-178 were so low that their direct analysis on the ICP-MS was challenging. For a precise determination of elements like Ag and Mo in D-178 an Isotopic Dilution technique (ID-ICP-MS) could be considered (Heumann, 1992).

2.4.3 Low carbonate, high Al sediment: GSD-11

GSD-11 displayed the lowest average elemental recoveries (around 80%) of the standards considered. This can be linked to incomplete digestion (0 and 1 mL of HF added) and fluoride based precipitate formation (3 and 6 mL of HF added) (Figures 2.1 and Table 2.3). Trace elements were better recovered than the major elements as the precipitate formed was composed of Al and Mg (two highly abundant elements) (Figure 2.1, 2.2). It is possible that the trace elements were in easily dissolvable phases, or easily leached out of residual phases, or both.

The inefficiency of the optimised protocol developed when applied to GSD-11 arises due to the different composition of the precipitate formed. When using larger volumes of HF for dissolution, an aluminum fluoride precipitate formed, also containing Mg (less than 10%) and Ca (less than 5%) (Table 2.2). For Mg, Th and Al the relationship between recovery and volume of HF added was quite different from the pattern observed for the other elements (Figure 2.2). This unique pattern suggests that the recovery variations displayed by Mg, Th and Al are affected by the presence of any fluoride-based precipitate. Indeed, excess HF has the capacity to cause precipitation with Mg and Al in solution to produce complexes such as $CaMgAlF_{12}$, $CaAlF_5$, and $Na_{0.88}Mg_{0.88}Al_{1.12}(F,OH)_6.H_2O$ (Kitano and Okumura, 1973; Yokoyama et al., 1999). The

reduced recoveries of Mg, Al and Th when 1 mL of HF was added to the digestion mixture can be explained as follows: the relative proportion of the complexes formed may be related to the amount of HF available, and the original compositional matrix of the sample (Yokoyama et al., 1999). It is possible that increasing the amount of HF available in the solution impacts the thermodynamics of the different precipitation reactions to predominantly produce a precipitate containing less Al and Mg and containing more Ca or Na (Kitano and Okumura, 1973; Yokoyama et al., 1999). Of all reference samples considered in this study aluminum fluoride precipitation was unique to GSD-11 (Figure 2.2). GSD-11 has much more Al than the other standards, with Ca:Al of 0.1, compared to 1.6 and 9.6 for HISS-1 and GSR-6, respectively. During digestion Ca and Al compete to react with HF. Hence an increased abundance of Al in this standard increases the chance of a reaction between Al and HF in comparison to others.

Thorium is a known particle reactive element (Kretschmer et al., 2011) and may adsorb to any precipitate formed following sample digestion. As such Th can be used as a tool to understand and quantify interferences from any solid residue formed. In digests of GSD-11, Th only co-varied with Al and Mg (Figure 2.3). Therefore the possibility that any solid matter other than the fluoride precipitate composed of Mg and Al was present after the digestion can be excluded. If another residue was present a co-variation between Th and the elements composing this solid residue may have been observed. The fluoride precipitate containing more Ca and Na, as described in the above paragraph, could have been dissolved during earlier hotplate stages (Muratli et al., 2012), while obviously aluminum fluoride was not. Additionally, variations noted for a less particle reactive element, like Ba, were not correlated with Al ($r^2 = 35\%$), eliminating other sources of analytical error such as sample loss or weighing error, or incomplete digestion, which would reduce the recovery of all elements (Figure 2.3).

To facilitate a total digestion of GSD-11 without using $HClO_4$ or $HBrO_3$, a digestion in two steps should be considered: A first microwave step using HCl and HNO_3 to digest the carbonate fraction and the Mg and Al oxides followed by the extraction of the liquid phase containing the Al and Mg (Fraction 1). Then the leftover solid could be digested by a second microwave step in HNO_3 and HF to solubilise the silicate fraction (Fraction 2). The resultant Fraction 2 taken up in HNO_3 could then be combined with Fraction 1. This approach would minimise interaction between Ca, Mg, Al and HF.

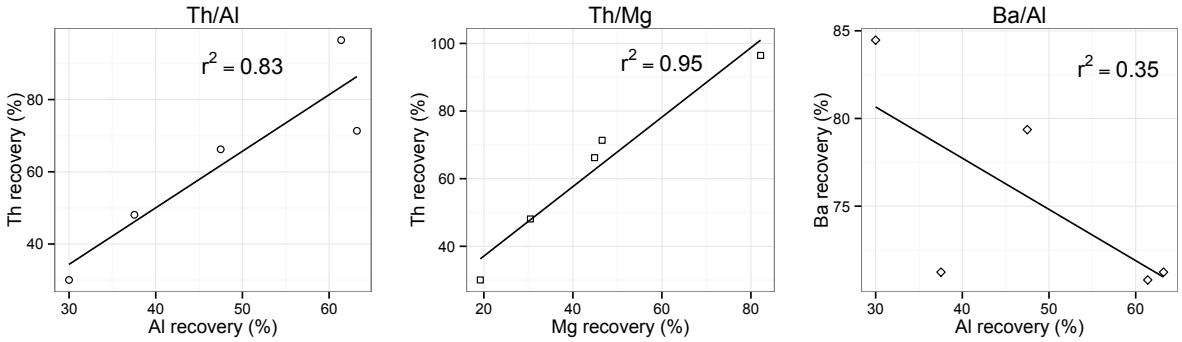

Figure 2.3: Trends between Al and Th, Mg and Th, and Al and Ba for different volumes of HF used during digestion considering sample GSD-11, including the suggested improved protocol.

2.5 Conclusion

The mechanisms and causes of carbonate precipitation following microwave digestion for a range of certified materials and carbonate-rich samples were considered in this study. A simple and general solution to avoid incomplete digestion and digestion precipitation was proposed, namely the use of a hotplate digestion step with HCl prior to microwave digestion with a reduced volume of HF (2 mL) for 200 mg of sediments.

A wide range of carbonate-rich materials can be successfully digested using the method developed in this study. Sediment (marine and riverine) and carbonate rock sample digestions were successfully completed using the combination of a simple pre-digestion step with a standard microwave protocol. Materials containing as much as 76% carbonate (D-178) and as low as 3% carbonate (HISS-1) were completely digested using the same method. The acid volumes used were dramatically reduced in comparison to other digestion methods. However, as the objective of this method was to investigate a new and straightforward digestion method for carbonate-rich materials, it should be noted that samples containing a small carbonate fraction (e.g. GSD-11) can still be easily digested using other techniques (previously published). We recommend its use with carbonate-rich samples that remain a challenge to digest with conventional methods.

2.6 Acknowledgements

This work was supported by the Australia-New Zealand IODP Consortium (ANZIC) and by an ARC Future Fellowship awarded to ZC (FT120100759). Access to ICP-MS instrumentation was

supported through ARC LIEF funds (LE0989539).

References

Abu-Samra, A., Morris, J. S., and Koirtyohann, S.: Wet ashing of some biological samples in a microwave oven, Analytical Chemistry, 47, 1475–1477, 1975.

Agazzi, A. and Pirola, C.: Fundamentals, methods and future trends of environmental microwave sample preparation, Microchemical Journal, 67, 337–341, 2000.

Bettinelli, M., Beone, G., Spezia, S., and Baffi, C.: Determination of heavy metals in soils and sediments by microwave-assisted digestion and inductively coupled plasma optical emission spectrometry analysis, Analytica Chimica Acta, 424, 289–296, 2000.

Colodner, D. C., Boyle, E. A., and Edmond, J. M.: Determination of rhenium and platinum in natural waters and sediments, and iridium in sediments by flow injection isotope dilution inductively coupled plasma mass spectrometry, Analytical Chemistry, 65, 1419–1425, 1993.

Cutter, G., Andersson, P., Codispoti, L., Croot, P., Francois, R., Lohan, M. C., Obata, H., and Rutgers v d Loeff, M.: Sampling and Sample-handling Protocols for GEOTRACES Cruises, 2010.

Flores, E. M. M.: Microwave-assisted sample preparation for trace element determination, Elsevier, Amsterdam, 2014.

Geibert, W. and Usbeck, R.: Adsorption of thorium and protactinium onto different particle types: experimental findings, Geochimica et Cosmochimica Acta, 68, 1489–1501, 2004.

Giessman, U. and Greb, U.: High-Resolution Icp-Ms - a New Concept for Elemental Mass-Spectrometry, Fresenius' Journal of Analytical Chemistry, 350, 186–193, 1994.

Heumann, K. G.: Isotope dilution mass spectrometry, International Journal of Mass Spectrometry and Ion Processes, 118-119, 575–592, 1992.

Kemp, A. J. and Brown, C. J.: Microwave digestion of carbonate rock samples for chemical analysis, Analyst, 115, 1197–1199, 1990.

Kitano, Y. and Okumura, M.: Coprecipitation of fluoride with calcium carbonate, Geochemical Journal, 7, 37–49, 1973.

Kretschmer, S., Geibert, W., van der Loeff, M. M. R., Schnabel, C., Xu, S., and Mollenhauer, G.: Fractionation of 230Th, 231Pa, and 10Be induced by particle size and composition within an opal-rich sediment of the Atlantic Southern Ocean, Geochimica et Cosmochimica Acta, 75, 6971–6987, 2011.

Kuss, H.-M.: Applications of microwave digestion technique for elemental analyses, Fresenius' Journal of Analytical Chemistry, 343, 788–793, 1992.

Latimer, J. C. and Filippelli, G. M.: Data report: sediment geochemical results from ODP Leg 189, Site 1171 – eocene to present, Proceedings of the Ocean Drilling Program, Scientific Results, 189, 1–16, 2003.

Lima, É. C., Barbosa Jr, F., Krug, F. J., Silva, M. M., and Vale, M. G.: Comparison of ultrasound-assisted extraction, slurry sampling and microwave-assisted digestion for cadmium, copper and lead determination in biological and sediment samples by electrothermal atomic absorption spectrometry, Journal of Analytical Atomic Spectrometry, 15, 995–1000, 2000.

Linge, K. L. and Jarvis, K. E.: Quadrupole ICP-MS: Introduction to Instrumentation, Measurement Techniques and Analytical Capabilities, Geostandards and Geoanalytical Research, 33, 445–467, 2009.

Mann, D. K., Oatts, T. J., and Wong, G. T.: The determination of leachable uranium in marine and lacustrine sediments by steam digestion., Talanta, 39, 1199–1203, 1992.

Mester, Z. and Sturgeon, R. E.: Sample preparation for trace element analysis, vol. 41, Elsevier, Amsterdam, 2003.

Morford, J. L. and Emerson, S.: The geochemistry of redox sensitive trace metals in sediments, Geochimica et Cosmochimica Acta, 63, 1735–1750, 1999.

Muratli, J. M., McManus, J., Mix, A., and Chase, Z.: Dissolution of fluoride complexes following microwave-assisted hydrofluoric acid digestion of marine sediments, Talanta, 89, 195–200, 2012.

Negre, C., Thomas, A. L., Mas, J. L., Garcia-Orellana, J., Henderson, G. M., Masqué, P., and Zahn, R.: Separation and measurement of Pa, Th, and U isotopes in marine sediments by microwave-assisted digestion and multiple collector inductively coupled plasma mass spectrometry, Analytical Chemistry, 81, 1914–1919, 2009.

Pena-Icart, M., Villanueva Tagle, M. E., Alonso-Hernandez, C., Rodriguez Hernandez, J., Behar, M., and Pomares Alfonso, M. S.: Comparative study of digestion methods EPA 3050B (HNO(3)–H(2)O(2)–HCl) and ISO 11466.3 (aqua regia) for Cu, Ni and Pb contamination assessment in marine sediments., Marine Environmental Research, 72, 60–66, 2011.

Roberts, K. A., Xu, C., Hung, C.-C., Conte, M. H., and Santschi, P. H.: Scavenging and fractionation of thorium vs. protactinium in the ocean, as determined from particle–water partitioning experiments with sediment trap material from the Gulf of Mexico and Sargasso Sea, Earth and Planetary Science Letters, 286, 131–138, 2009.

Tiessen, H., Roberts, T. L., and Stewart, J.: Carbonate analysis in soils and minerals by acid digestion and two-endpoint titration, Communications in Soil Science and Plant Analysis, 14, 161–166, 1983.

Townsend, A. T.: Enhanced sensitivity for Os isotope ratios by magnetic sector ICP-MS with a capacitive decoupling Pt guard electrode, Fresenius' Journal of Analytical Chemistry, 367, 614–620, 2000.

Tribovillard, N., Algeo, T. J., Lyons, T., and Riboulleau, A.: Trace metals as paleoredox and paleoproductivity proxies: An update, Chemical Geology, 232, 12–32, 2006.

Wu, S., Zhao, Y.-h., Feng, X., and Wittmeier, A.: Application of inductively coupled plasma mass spectrometry for total metal determination in silicon-containing solid samples using the microwave-assisted nitric acid–hydrofluoric acid–hydrogen peroxide–boric acid digestion system, Journal of Analytical Atomic Spectrometry, 11, 287–296, 1996.

Xie, X., Yan, M., Wang, C., Li, L., and Shen, H.: Geochemical standard reference samples GSD 9–12, GSS 1–8 and GSR 1–6, Geostandards Newsletter, 13, 83–179, 1989.

Yokoyama, T., Makishima, A., and Nakamura, E.: Evaluation of the coprecipitation of incompatible trace elements with fluoride during silicate rock dissolution by acid digestion, Chemical geology, 157, 175–187, 1999.

Chapter 3

Determination of trace isotope concentrations in sediment digests by isotopic dilution using a single collector sector field inductively coupled plasma mass spectrometer

Abstract

This chapter reports the development of capability for measuring concentrations of trace isotopes 238-Uranium (^{238}U), 232-Thorium (^{232}Th) and 230-Thorium (^{230}Th) in sediment digests by single collector inductively coupled plasma-mass spectrometer (ICP-MS; Element 2) isotopic dilution (ID) at the University of Tasmania. Application of the instrument in standard configuration mode does not allow practical measurement of these isotopes due to low sensitivity. To address this issue, the configured ICP-MS guard electrode (GE) was activated, enhancing sensitivity 10x. Sensitivity was further enhanced another 10x by replacing the standard wet aerosol introduction system with a micro-concentric desolvating nebuliser. The micro-concentric desolvating nebuliser also minimised known overlapping water based polyatomic interferences (hydrides, oxides). Agreement between values determined using the developed method with those found using external ID-Multi Collector-ICP-MS, as well as those found using traditional external calibration, demonstrates that in its optimised configuration (ID + GE on + micro-concentric nebuliser) concentrations of ^{238}U, ^{232}Th and ^{230}Th can be measured successfully. Applying this approach to sediment digests (n=4), ^{238}U, ^{232}Th and ^{230}Th concentrations within these replicates agreed to within 5%.

3.1 Introduction

Investigating past changes in export production in the New Zealand region is a critical part of this thesis. Using material preserved in sediments, accurate reconstruction of past export production can be achieved by calculating the fluxes of biogenic compounds reaching the seafloor (Chase et al., 2003; Paytan and Kastner, 1996; Ragueneau et al., 1996). However, the lateral redistribution of sediments on the seafloor can induce erroneous flux reconstructions in areas of strong bottom currents, like the Southern Ocean (Dezileau et al., 2003; Frank et al., 1999). To resolve this problem the 230-Thorium (^{230}Th)-normalisation method has been widely used (Francois et al., 2004). 230-Thorium is produced quasi-homogenously in the water column by the decay of 234-Uranium. Moreover, because ^{230}Th is very insoluble, its removal from the water column by particle advection and scavenging is almost equal to its production rate. Therefore, the expected flux of ^{230}Th reaching the seafloor can be calculated at any given location and any deviation from it can be used to correct for sediment redistribution on the seafloor (Francois et al., 2004).

230-Thorium only represents a few parts per billion of the sediment material and therefore its precise quantification remains a challenge. Instruments employed for analysis of trace isotopes such as ^{230}Th include Thermal Ionisation Mass Spectrometers (TIMS) or more recently Inductively Coupled Plasma-Mass Spectrometers (ICP-MS). Today, ICP-MS have become more prevalent than TIMS because they require much less sample preparation, have superior sensitivity, shorter measurement times, and allow analysis of smaller samples (Shen et al., 2002).

Together with ICP-MS, the use of Isotopic Dilution (ID) as a quantification method allows extremely precise quantification of low abundance isotopes (Sargent et al., 2002). Isotopic dilution is based on the external addition of an isotope-enriched spike (Ia) of the targeted isotope (It) to the sample, before any physical or chemical alteration of the original sample (Figure 3.1). The ratio between Ia and It is then measured and used to calculate the concentration of It. Because isotopes have the same chemical properties and reaction behaviour, any loss of It will consequently affect Ia in the same way. Therefore, the ratio between Ia and It is independent of any chemical reaction that would induce a loss in the recovery of It. By measuring Ia/It instead of It concentration directly, it enables incomplete recovery at any stage of the sample preparation and analysis to be corrected.

Since the signals of at least two isotopes need to be acquired in order to use ID, Multi Collec-

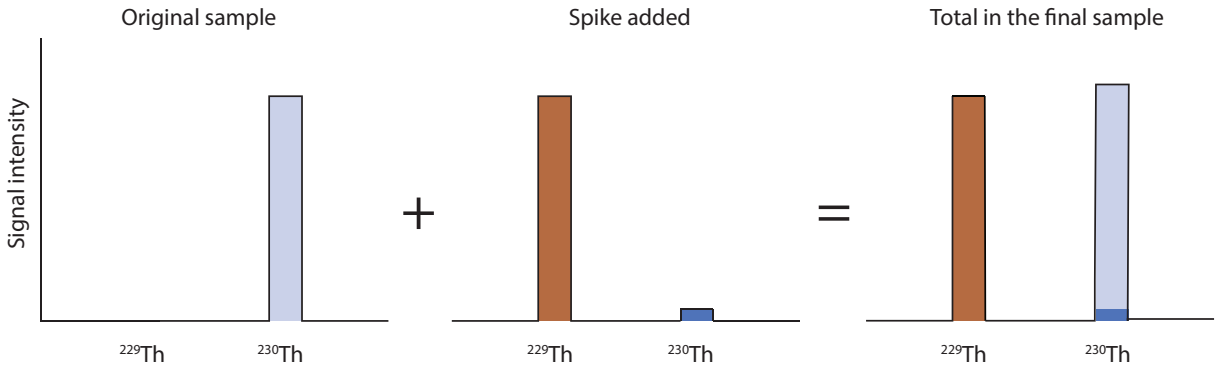

Figure 3.1: Example of the ID technique used for the measurement of ^{230}Th when ^{229}Th is added as a spike.

tor (MC) ICP-MS are particularly adapted to isotopic measurements. Multi Collector ICP-MS allow simultaneous detection of several different ions on different detectors. This increases both the precision and accuracy of the measurements compared to single collector ICP-MS, which can only monitor one ion mass at a time (Wieser et al., 2012). Nevertheless single collector ICP-MS in a fast scanning regime can approach quasi-simultaneous measurements, and accordingly can produce consistent isotopic measurements. On occasion these can be considered as an alternative to MC-ICP-MS for trace isotope concentration measurements (Hinrichs and Schnetger, 1999).

This chapter describes the application of previously published methods (Cheng et al., 2000; Choi et al., 2001; Hinrichs and Schnetger, 1999; Shen et al., 2002) to the single collector ICP-MS instrument in our facility (Element 2, Central Science Laboratory-CSL, University of Tasmania-UTAS) to achieve measurements of 238-Uranium (^{238}U), ^{232}Th and ^{230}Th concentrations in sediment digests by ID. Additionally, the accuracy of the measurements presented is assessed through intercomparisons with two other approaches. Firstly, $^{229}Th/^{230}Th$ ratios measured using the method detailed in this work, are compared to MC-ICP-MS values measured at an external laboratory (School of Earth Sciences, Australian National University-ANU). Secondly, ^{232}Th and ^{238}U concentrations measured in sediments using the ID-ICP-MS method detailed here are compared to values determined via the method of external calibration using the same single collector ICP-MS. The precision of the developed method is also assessed by analysis of multiple digest replicates.

3.2 Material and methods

3.2.1 Sediment material, spikes and standards

229-Thorium (SRM-4328C) and ^{236}U (IRMM-3660a) spikes were used for the quantification of U and Th isotopes in this study. Both spikes were calibrated by reverse ID on a MC-ICP-MS (Neptune) using CRM 145B for ^{236}U and a Th standard (10 59-1, high purity standards) for ^{229}Th. Solutions made by dilution of an uranyl acetate salt were used as in-house references. Sediment samples from sediment cores 1171B (-48.5°, 149.11°; Tasman Sea), TAN0803-09 (-47°, 166.06°; Solander Trough), as well as surface sediment D-178 (Campbell Plateau, New Zealand) were digested and analysed.

3.2.2 Sediment digestion

Two hundred mg of freeze-dried and crushed sediments were spiked with ^{229}Th (0.32 Bq) and ^{236}U (36 mBq). The mixture was digested in a mix of hydrochloric (HCl), nitric (HNO_3) and hydrofluoric (HF) acids using the same method as described in detail in **chapter 2**. The digested solution was separated into two aliquots as detailed in **chapter 5**. The first aliquot was used for external calibration measurements and the second aliquot was used for measurements by ID. Thorium and U were separated from the second aliquot using Dowex AG1-X8 anion exchange resin following the method of Negre et al. (2009). This separation step is also detailed in **chapter 5**. Before analysis, the Th and U fractions were dried on a hotplate at 150 °C and taken into 1 mL of a 2% HNO_3, 0.1% HF solution. Uranium and Th fractions (in 1 mL of a 2% HNO_3, 0.1% HF solution) were combined before analysis for a final sample volume of 2 mL. Samples were prepared in batches of 12. Each batch included 10 sediment samples, one in-house reference (D-178), and one procedural blank.

3.2.3 Analysis

The measurements of ^{229}Th, ^{230}Th, ^{232}Th, ^{234}U, ^{235}U, ^{236}U and ^{238}U were carried out using an Element 2 sector field ICP-MS from Thermo Fischer Scientific (Bremen, Germany) in low resolution mode ($m/\Delta m \approx 400$). The instrument was tuned daily for a compromise between sensitivity and signal stability with minimal polyatomic (hydride/oxide) formation. A

tuning solution containing only Indium and U was used. Due to its extremely low solubility and inherent 'stickiness', Th was excluded from the tuning solution to prevent instrumental contamination. Measurements were made across a range of masses, namely: 238, 236, 235 amu for U; and 232, 230.5, 230, 229.5, and 229 amu for Th. Thorium and U measurements were undertaken alternatively using two different instrumental methods (one for Th, one for U) on a single sample solution. Two hundred scans of a 5% window for each peak (100 lines elected), allowed measurement times to be less than 2 minutes for each of the Th and U methods. To maximise signal sensitivity the instrument capacitive guard electrode (GE) was activated (offering intensity enhancement of the order of 10x), while an Aridus II micro-concentric desolvating nebuliser (DSN) sample introduction system (CETAC) was employed to minimise unresolvable interferences related to hydride, oxide and hydroxide formation. Typical DSN gas flows were approximately 5 L/min for argon sweep gas (across membrane) and 10 mL/min for nitrogen (added to dry sample stream to enhance sensitivity). Using these gas flows, oxide and hydroxide formation rates of U and Th were consistently less than 0.05%. To improve instrumental signal stability and to keep background levels low during day-to-day operation, the micro-concentric DSN spray chamber was removed at the end of each day and soaked overnight in 50% HNO_3. It was rinsed with Milli-Q water and dried before being re-installed.

The isotopes of Th and U vary significantly in abundance leading to large signal intensity differences to be measured by the ICP-MS instrument. This issue was addressed by measuring different isotopes in different detection modes. With the Element 2 sector field ICP-MS instrument, two detection modes are available, namely: counting (amplified signal) and analog (non amplified signal). 232, 236 and 238 amu were typically measured in analog mode because of their high intensities. Low signals at 235, 234, 230.5, 230, 229.5, and 229 amu were measured in counting mode. This difference in the detection mode results in a bias, the gain bias (Cheng et al., 2000; Choi et al., 2001; Shen et al., 2002). The gain bias was corrected by successively measuring the $^{238}U/^{235}U$ ratio in CRM-145 with ^{238}U and ^{235}U both in counting mode ($^{238}U_{counting}/^{235}U_{counting}$) and then ^{238}U in analog mode, with ^{235}U remaining in counting mode ($^{238}U_{analog}/^{235}U_{counting}$). The gain bias was obtained by correcting the measured $^{238}U_{counting}/^{235}U_{counting}$ to the value of the $^{238}U_{analog}/^{235}U_{counting}$ as described by others (Choi et al., 2001; Hinrichs and Schnetger, 1999; Shen et al., 2002). This gain bias was used to correct the $^{232}Th/^{230}Th$ and $^{238}U/^{235}U$ ratios. In order to keep the gain bias as small as possible the

instrumental analog to counting correction factor was checked and updated every six samples.

Different instrumental responses for ions of different masses produce a mass bias. Instrument mass bias was estimated by regularly monitoring the $^{238}U_{counting}/^{235}U_{counting}$ ratio of the U standard CRM-145 and comparing the measured value to the certified ratio. The mass bias was corrected using a log-law as detailed in Shen et al. (2002). Mass and gain biases were generally less than 5%. To correct for any instrumental drift, groups of 6 samples were bracketed by the measurement of the CRM-145 in duplicate. Drift for the mass bias was less than 1% across 6 samples; gain bias drift was up to 10% across six samples.

The tailing effect from the ^{232}Th peak to the baseline of the ^{230}Th peak was corrected by subtracting the logmeans of the half masses at 229.5 and 230.5 amu from ^{230}Th counts (Shen et al., 2002). To minimise the carry over between samples the sample introduction system was rinsed for 10 minutes between each sample with a solution of 2% HNO_3 (Ultrex II, J.T. Baker) and 0.1% HF (Ultrex II, J.T. Baker) in Milli-Q water. The same rinse solution was also used to rinse the instrument for one hour between each group of six samples. Prior to the analysis of each group of six samples, acid blanks made of the rinse solution were measured in duplicate to monitor contamination and carry over. Procedural blanks, which went through the entire sample-handling procedure (digestion + separation) were also measured prior to sediment samples. The ^{238}U, ^{232}Th, and ^{230}Th concentrations in the procedural blanks were calculated using ID calculations against ^{236}U and ^{229}Th. These concentrations as well as the counts of each amu from the acid blanks were used to correct the samples concentrations. Over the course of one day (≈8 h), 12 samples were measured.

As a means of validating the ID method, concentrations of ^{232}Th and ^{238}U in sediment samples TAN0803-09 and D-178 were measured using an external calibration method on the same single collector ICP-MS instrument. Details of the external calibration and associated sample handling procedure and instrumental conditions can be found in **chapter 2**.

As another intercomparison, $^{229}Th/^{230}Th$ ratios from 1171B and D-178 digests were also measured on a Thermo Fisher Neptune Plus MC-ICP-MS at the Research School of Earth Sciences, Australian National University (ANU). Measurements from this MC-ICP-MS and the UTAS instrument were carried out using the same solutions to avoid unwanted sample preparation bias. For MC analysis, an Apex HF sample introduction system was used. Thorium fractions were analysed in peak jumping mode using a retarding potential quadrupole (RPQ)

to minimise the tail of ^{232}Th. As detailed earlier, tailing effects were corrected by measuring the half masses around ^{230}Th peak. Mass bias and SEM/Faraday cup yield were corrected by standard bracketing using the uranium standard CRM-145.

3.2.4 Instrument detector dead-time determination

Instrument detector (single collector, CSL) dead-time was determined by measuring $^{238}U/^{235}U$ ratios of five solutions of different concentrations across different pre-selected dead-times values (Figure 3.2) (Nelms et al., 2001; Russ, 1989). The solutions were made by gravimetrical dilution from a mother solution made by dissolution of the uranyl acetate salt (of non-natural isotopic abundance). Concentrations considered were 2, 5, 7.5, 10 and 12.5 µg/kg. The range of concentrations selected was chosen to keep the detection of both isotopes (^{235}U and ^{238}U) in the same detection mode (counting) to avoid inducing any bias from detector mode of operation. Five different dead-times between zero and 30 ns were chosen at which ratios were measured. For each solution the $^{238}U/^{235}U$ ratios vs dead-time values are plotted as a line (Figure 3.2).

3.2.5 Isotopic dilution calculations

The concentrations of ^{238}U and ^{230}Th ($[^{238}U]$ and $[^{230}Th]$) in the sediment digests were calculated as follows from the $^{229}Th/^{230}Th$ and $^{238}U/^{236}U$ ratios measured (Vanhaecke and Moens, 2004):

$$[^{230}Th] = \frac{230}{229}.[^{229}Th]_{spike}.\frac{W_{spike}}{W_s}.\frac{R_{sp} - R_s}{R_s(R_{sp} + 1)} \tag{3.1}$$

$$[^{238}U] = \frac{238}{236}.[^{236}U]_{spike}.\frac{W_{spike}}{W_s}.\frac{R_{sp} - R_s}{R_s(R_{sp} + 1)} \tag{3.2}$$

Where $[^{229}Th]_{spike}$ and $[^{236}U]_{spike}$ are the concentrations (mg/kg) of ^{229}Th and ^{236}U in the spike solutions; W_{spike} and W_s are the weights of the spike added and the total weight of the dry sediments; R_{sp} are the $^{229}Th/^{230}Th$ ratios measured in the spike for equation 3.1, and $^{238}U/^{236}U$ ratios for equation 3.2. Finally, R_s are the $^{229}Th/^{230}Th$ ratios (mass bias and blank corrected) measured in the samples for equation 3.1 and the $^{238}U/^{236}U$ ratios (mass bias and blank corrected) for equation 3.2.

The concentrations of ^{232}Th were calculated as follows from the $^{232}Th/^{230}Th$ ratios measured:

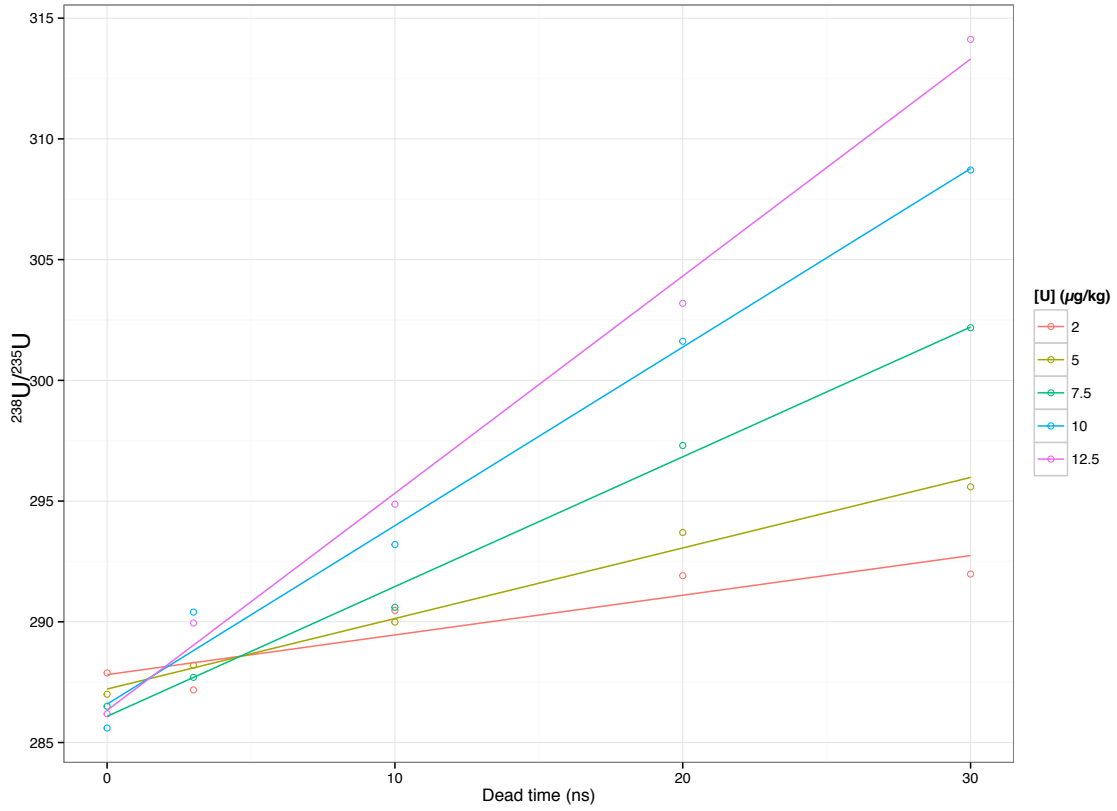

Figure 3.2: Variation of measured $^{238}U/^{235}U$ ratio with preselected instrument dead-time for different dilutions of the same 'mother' solution. Intersecting ratio responses correspond to optimal dead-time value.

$$[^{232}Th] = R_s[^{230}Th] \tag{3.3}$$

Where R_s are the mass/gain biases and blank corrected $^{232}Th/^{230}Th$ sample ratios measured.

3.3 Results and discussion

The Element 2 sector field ICP-MS in standard configuration and operation cannot quantify low abundance Th and U isotopes by ID due to a lack of instrument sensitivity and precision. In the following sections, the analytical developments implemented in order to resolve these issues are outlined. Firstly, the importance of a correct dead-time adjustment to perform accurate isotopic ratio measurements is discussed. Secondly, sensitivity enhancement and improved ratio precision associated with the use of the GE and micro-concentric DSN are outlined. Finally, the accuracy

and precision of the measurement approach using the optimised method is assessed through comparison with results from ID-MC-ICP-MS (Neptune), external calibration measurements (Element 2) and repeated analysis of an in-house standard.

3.3.1 Importance of instrumental dead-time determination

Instrument dead-time correction is a key parameter of the ICP-MS detection system that needs to be determined and set for accurate isotopic measurements. Detector dead-time refers to the small period of time (in ns) required by instrument/detector electronics for sequential ion impacts to be successfully measured. During this dead-time, the detector is blind and if another ion hits the detector it may not be accurately recorded. Therefore, a predetermined and accurate dead-time value is critical for challenging isotopic ratio measurements. As an example, consider several solutions that have different U concentrations but the same $^{238}U/^{235}U$ ratio. If the dead-time of the detector is set appropriately, then the same $^{238}U/^{235}U$ ratio will be measured in the different solutions, irrespective of analyte concentration. However, if the dead-time is not set appropriately the concentration differences will induce a bias, resulting in different $^{238}U/^{235}U$ ratios determined for the different solutions. Detector dead-time varies with instrument type, detector type and detector age.

The dead-time determination method used in this study closely followed the work of Nelms et al. (2001) and Russ (1989), with the optimum dead-time corresponding to the point at which the signal response lines best intercept (Figure 3.2). From the results presented in Figure 3.2, a detector dead-time of 2 ns was selected for isotopic measurements during the period of analysis.

During the period of analysis the detector of the instrument was replaced. As a consequence, the instrumental dead-time was measured a second time following the same method described previously (results not shown). The dead-time was found to be 2 ns again.

3.3.2 Method enhancements associated with use of guard electrode and micro-concentric desolvating nebuliser

Two options were employed to increase the sensitivity of the Element 2 instrument from our facility, namely the use of the instrumental GE and the use of a micro-concentric DSN.

A capacitive decoupling platinum GE consists of a quartz cylinder coated with platinum

surrounding the torch of the ICP-MS. The platinum part can be either connected to the electrical system (floating GE, on) or isolated (grounded GE, off) (Appelblad et al., 2000). The GE decreases the energy loss of the ions in the plasma by focussing them into a more coherent distribution, thus increasing the ion transmission and the sensitivity (Appelblad et al., 2000; Townsend, 2000). Use of the GE increased the signal intensity by a factor 10 compared to a standard configuration (Figure 3.3). This result is consistent with previous work that reported an increased sensitivity by a factor five to ten associated with the use of the GE (Townsend, 2000). Unfortunately, as a consequence of GE use, increased formation of oxide/hydroxide/hydride and doubly charged ion results (such as UO^+ or ThH^+), which can interfere and obstruct the accurate determination of targeted isotopes (Appelblad et al., 2000; Townsend, 2000). However, in this work the sensitivity enhancement provided by the GE is advantageous and required to precisely and accurately quantify low abundance isotope concentrations.

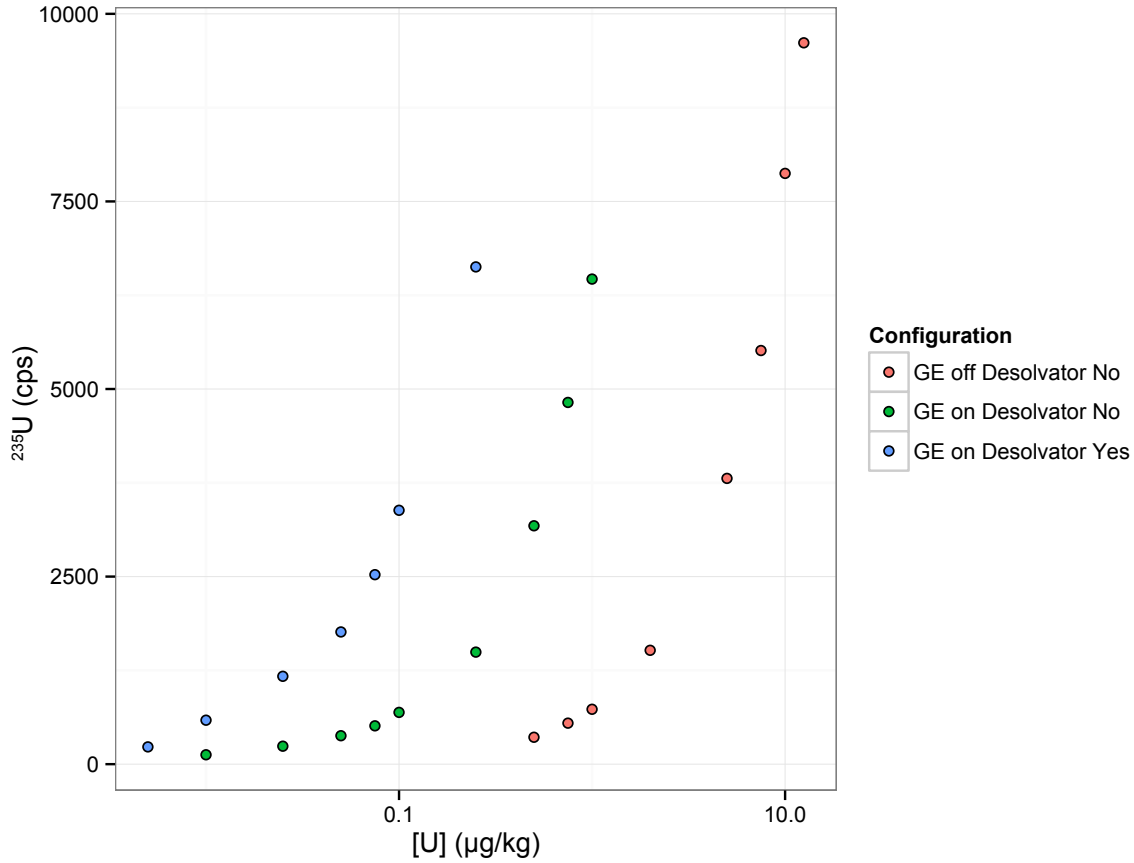

Figure 3.3: Influence of GE and micro-concentric DSN on instrument sensitivity (^{235}U shown as an example). Solutions of different U concentrations were made by dissolution of an in-house uranyl acetate salt, with resultant counts shown for different instrumental configurations.

One method to enhance sensitivity as well as minimise hydride, oxide and hydroxide polyatomics forming in the plasma (from atomic combinations aided by the aqueous sample media acting as a source of H and O) is to use a micro-concentric DSN. Whereas a classic nebuliser introduces a wet spray into the plasma, a DSN introduces a dry aerosol after separation of the dominant solvent from the sample analytes (Coedo et al., 1999; D'Ilio et al., 2006; Jensen et al., 2003; Martin and Volmer, 1999). With optimisation of the argon and nitrogen gas flows of the DSN, oxide/hydroxide formation rates of U and Th were less than 0.05%, even with GE activated. In standard configuration mode, the typical UO formation level is around 1-2%, and rises to values of the order of 10-20% with GE activated. The use of the DSN together with the GE also increased the signal sensitivity by a factor 10 compared to the standard wet aerosol introduction with GE on (Figure 3.3).

The use of a low sample flow DSN (200 µL/min) also allowed a reduction in the sample volume presented to the instrument $\leq$ 2 mL, providing opportunity to pre-concentrate samples to greater levels before ICP-MS analysis.

In summary, use of a DSN in combination with ICP-MS GE increased the signal sensitivity by a factor 100 compared to standard wet aerosol introduction without GE active. This allowed the use of smaller more concentrated sample volumes, while decreasing oxide/hydroxide/hydride formation rates for U and Th to negligible levels of less than 0.05%. In this optimised mode, standard deviations across ten $^{235}U/^{238}U$ ratio measurements on CRM-145 ([U] $\approx$ 100 µg.kg) were less than 5%. Moreover, in this configuration, reproducibility was tested on four D-178 procedural replicates for elemental concentrations, carried out over a three month period. For $[^{238}U]$, $[^{232}Th]$ and $[^{230}Th]$ standard deviations between replicates were less than 5%.

3.3.3 Intercalibrations

To assess the quality of the measurements, $^{229}Th/^{230}Th$ ratios of 12 sediment sample digests from 1171B and D-178 were measured using the method detailed here as well as by MC-ICP-MS on a Neptune instrument. The same solutions were measured on both the single and multi-collector instruments to avoid inducing any bias due to sample preparation differences. An impressive agreement was found between the CSL single collector ICP-MS measurements and those measured using MC-ICP-MS at ANU (Figure 3.4). Deviations between the two sets of measurements were less than 1%. The state-of-the-art in terms of isotopic measurements

typically involves MC-ICP-MS, such as shown here using the ANU Neptune (Frank Vanhaecke, 2012). Therefore, the agreement between the Element 2 measurements and those from the Neptune shows that the analytical developments achieved allow the single collector ICP-MS from our facility to perform fit-for-purpose isotopic ratio measurements.

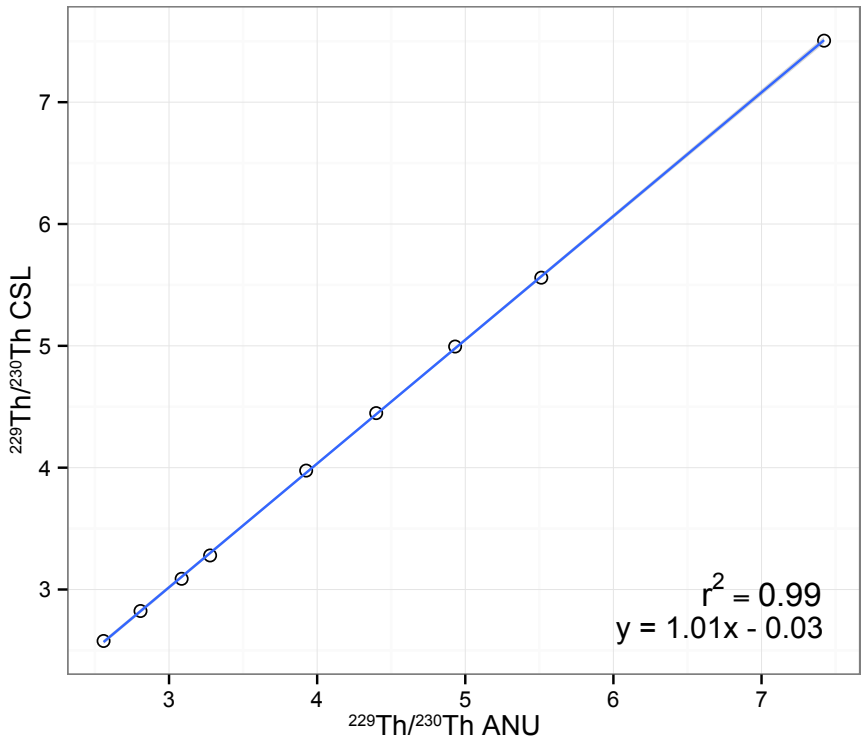

Figure 3.4: Comparison between $^{229}Th/^{230}Th$ ratios measured by MC-ICP-MS (ANU) and ICP-MS (UTAS, method applied) from 1171B and D-178 sediment digests. The 95% probability is represented as shaded area (largely indistinguishable from the line).

Elemental concentrations measured using the ID-ICPMS method developed here were also compared to those found using the traditional external calibration ICP-MS approach. To do so ^{232}Th and ^{238}U concentrations in TAN0803-09 and D-178 digests were measured using both methods (Figure 3.5). As ^{232}Th and ^{238}U concentrations in sediments are relatively high (mg/kg), their measurement by external calibration ICP-MS has been proved to be accurate (Durand et al., 2016; Mann et al., 1992). Overall, good agreement was observed for ^{232}Th and ^{238}U concentrations between the two ICP-MS methods, with differences generally less than 5% for ^{232}Th measurements and less than 10% for ^{238}U, respectively. These deviations are within the errors reported for external calibration measurements of these two isotopes (Durand et al., 2016).

The success of the intercomparison studies demonstrates the accuracy of the method devel-

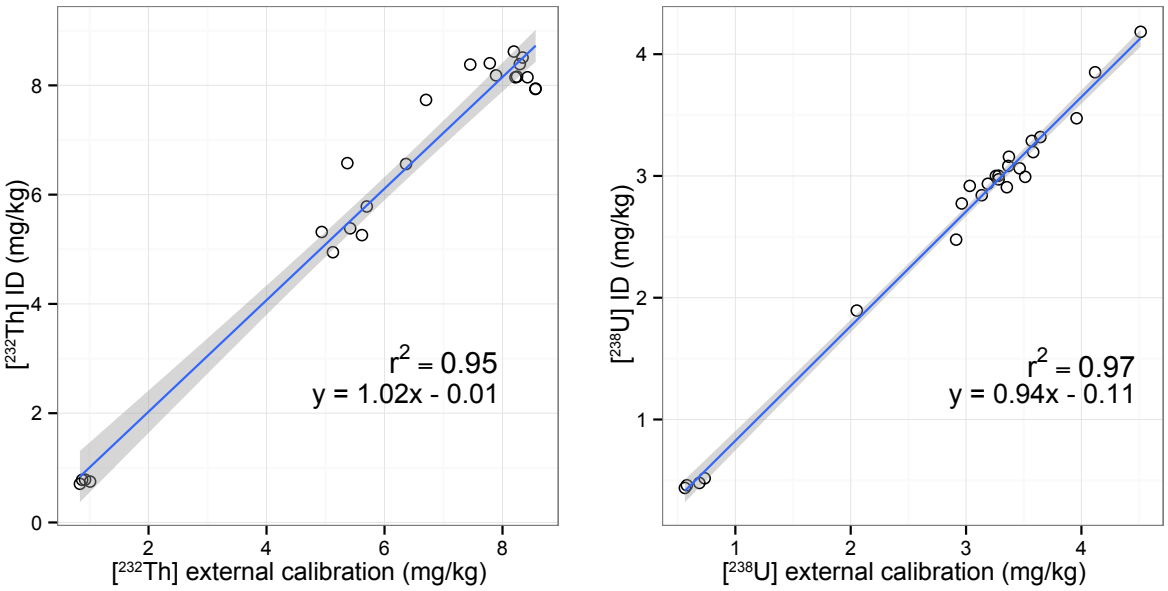

Figure 3.5: Comparison between ^{238}U and ^{232}Th concentrations measured by ID-ICP-MS and external calibration ICP-MS, both using the UTAS instrument (Element 2), from TAN0803-09 and D-178 sediment digests. The 95% confidence interval is represented as shaded area.

oped here to measure trace concentrations of ^{238}U, ^{232}Th and ^{230}Th, in sediment digests. It is recommended that future work, to further investigate the accuracy of the method developed, consists of measuring ^{238}U and ^{230}Th concentrations in some certified reference materials such as Table Mountain Latite (Cheng et al., 2000). Moreover, repeated runs of procedural blanks would also allow the procedural limit of detections to be calculated. Only three procedural blanks were measured in the work outlined here, with ^{238}U, ^{232}Th concentrations in the blanks at least three orders or magnitude lower compared to the sample concentrations. 230-Thorium concentrations in the three procedural blanks were at least four orders of magnitude smaller compared to sample concentrations.

3.3.4 Technical issues and recommendations

While developing the method detailed here a signal stability issue was faced. Signal intensity losses, up to 90% of the total signal, for less than a second, recurring randomly resulted in poor signal stability, jeopardising measurement quality. This signal instability was only observed with the ICP-MS in most sensitive 'counting' detection mode. Trial and error experience suggested that some elements, in high concentrations in the samples, deposited inside the DSN spray

chamber. During analysis this deposit was occasionally removed by the gas flow and ionised, leading to intense ion impacts on the detector. This sudden increase in the number of ion impacts was enough to overload the detector in counting mode, leading to a loss of signal (detector saturation). Removing the DSN spray chamber at the end of each analysis day and soaking in concentrated acid (as described in the method section) minimised the accumulation of such deposit and generally resolved the signal sensitivity issue.

Large gain bias drift, up to 10% across six samples, was observed. Changing the detector of the instrument resolved this issue and limited drift across six samples to less than 5%.

Here, ^{232}Th and ^{230}Th concentrations in sediment digests were measured by ID over ^{229}Th. Since ^{229}Th was added to match the concentration of ^{230}Th in the samples, large differences between ^{232}Th and ^{229}Th concentrations existed. These large differences were not ideal when using ID. Therefore, other techniques may be more appropriate to determine ^{232}Th concentrations in sediment digests. Digesting each sample twice, spiking one with ^{229}Th matched to ^{230}Th concentration, and the other to ^{232}Th, would be a option. Alternatively, external calibration measurement is a suitable method (Durand et al., 2016; Mann et al., 1992).

3.4 Conclusion

In this work analytical methodology required to perform reliable and fit-for-purpose measurements of low abundance isotope concentrations in sediment digests on a single-collector ICP-MS by ID was developed at UTAS. Use of a micro-concentric DSN with the ICP-MS GE activated increased the sensitivity of the single-collector ICP-MS by a factor 100 compared to standard wet aerosol introduction (no GE). This increased sensitivity was necessary to measure low abundance concentrations of isotopes such as ^{230}Th. Data integrity was also confirmed through intercomparison studies with other established methods. Strong agreement between the method developed here compared to ID-MC-ICP-MS and external calibration ICP-MS demonstrates that trace isotope concentrations can be measured accurately by ID using a single-collector ICP-MS (Element 2).

References

Appelblad, P. K., Rodushkin, I., and Baxter, D. C.: The use of Pt guard electrode in inductively coupled plasma sector field mass spectrometry: advantages and limitations, Journal of Analytical Atomic Spectrometry, 15, 359–364, 2000.

Chase, Z., Anderson, R. F., Fleisher, M. Q., and Kubik, P. W.: Accumulation of biogenic and lithogenic material in the Pacific sector of the Southern Ocean during the past 40,000 years, Deep Sea Research Part II: Topical Studies in Oceanography, 50, 799–832, 2003.

Cheng, H., Edwards, R. L., Hoff, J., Gallup, C. D., Richards, D. A., and Asmerom, Y.: The half-lives of uranium-234 and thorium-230, Chemical Geology, 169, 17–33, 2000.

Choi, M. S., Francois, R., Sims, K., Bacon, M. P., Brown-Leger, S., Fleer, A. P., Ball, L., Schneider, D., and Pichat, S.: Rapid determination of 230Th and 231Pa in seawater by desolvated micro-nebulization Inductively Coupled Plasma Magnetic Sector Mass Spectrometry, Marine Chemistry, 76, 99–112, 2001.

Coedo, A. G., Dorado, T., and Padilla, I.: Evaluation of a desolvating microconcentric nebulizer in inductively coupled plasma mass spectrometry to improve the determination of arsenic in steels, Applied Spectroscopy, 53, 974–978, 1999.

Dezileau, L., Bareille, G., and Reyss, J. L.: The 231Pa/230Th ratio as a proxy for past changes in opal fluxes in the Indian sector of the Southern Ocean, Marine Chemistry, 81, 105–117, 2003.

D'Ilio, S., Violante, N., Caimi, S., Di Gregorio, M., Petrucci, F., and Senofonte, O.: Determination of trace elements in serum by dynamic reaction cell inductively coupled plasma mass spectrometry - Developing of a method with a desolvating system nebulizer, Analytica Chimica Acta, 573, 432–438, 2006.

Durand, A., Chase, Z., Townsend, A. T., Noble, T., Panietz, E., and Goemann, K.: Improved methodology for the microwave digestion of carbonate-rich environmental samples, International Journal of Environmental Analytical Chemistry, 96, 119–136, 2016.

Francois, R., Frank, M., Rutgers van der Loeff, M. M., and Bacon, M. P.: 230Th normalization: An essential tool for interpreting sedimentary fluxes during the late Quaternary, Paleoceanography, 19, 2004.

Frank, M., Gersonde, R., and Mangini, A.: Sediment Redistribution, 230Thex- Normalization and Implications for the Reconstruction of Particle Flux and Export Paleoproductivity, in: Use of Proxies in Paleoceanography, pp. 409–426, Springer Berlin Heidelberg, Berlin, Heidelberg, 1999.

Frank Vanhaecke, P. D.: Isotopic analysis: fundamentals and applications using ICP-MS, John Wiley & Sons, 2012.

Hinrichs, J. and Schnetger, B.: A fast method for the simultaneous determination of Th-230, U-234 and U-235 with isotope dilution sector field ICP-MS, Analyst, 124, 927–932, 1999.

Jensen, B. P., Gammelgaard, B., Hansen, S. H., and Andersen, J. V.: Comparison of direct injection nebulizer and desolvating microconcentric nebulizer for analysis of chlorine-, bromine- and iodine-containing compounds by reversed phase HPLC with ICP-MS detection, Journal of Analytical Atomic Spectrometry, 18, 891–896, 2003.

Mann, D. K., Oatts, T. J., and Wong, G. T.: The determination of leachable uranium in marine and lacustrine sediments by steam digestion., Talanta, 39, 1199–1203, 1992.

Martin, M. and Volmer, D. A.: Examining the analytical capabilities of a desolvating microconcent nebulizer for inductively coupled plasma-mass spectrometry, Rapid Communications in Mass Spectrometry, 13, 84–86, 1999.

Negre, C., Thomas, A. L., Mas, J. L., Garcia-Orellana, J., Henderson, G. M., Masqué, P., and Zahn, R.: Separation and measurement of Pa, Th, and U isotopes in marine sediments by microwave-assisted digestion and multiple collector inductively coupled plasma mass spectrometry, Analytical Chemistry, 81, 1914–1919, 2009.

Nelms, S. M., Quetel, C. R., Prohaska, T., Vogl, J., and Taylor, P.: Evaluation of detector dead time calculation models for ICP-MS, Journal of Analytical Atomic Spectrometry, 16, 333–338, 2001.

Paytan, A. and Kastner, M.: Benthic Ba fluxes in the central Equatorial Pacific, implications for the oceanic Ba cycle, Earth and Planetary Science Letters, 142, 439–450, 1996.

Ragueneau, O., Leynaert, A., Tréguer, P., Demaster, D. J., and Anderson, R. F.: Opal studied as a marker of paleoproductivity, Eos, Transactions American Geophysical Union, 77, 491–491, 1996.

Russ, G. P. I.: Isotope ratio measurements using ICP-MS, in: Applications of inductively coupled plasma mass spectrometry, pp. 90–114, Glasgow, 1989.

Sargent, M., Harrington, C., and Harte, R.: Guidelines for Achieving High Accuracy in Isotope Dilution Mass Spectrometry (IDMS), Royal Society of Chemistry, 2002.

Shen, C.-C., Lawrence Edwards, R., Cheng, H., Dorale, J. A., Thomas, R. B., Bradley Moran, S., Weinstein, S. E., and Edmonds, H. N.: Uranium and thorium isotopic and concentration measurements by magnetic sector inductively coupled plasma mass spectrometry, Chemical Geology, 185, 165–178, 2002.

Townsend, A. T.: Enhanced sensitivity for Os isotope ratios by magnetic sector ICP-MS with a capacitive decoupling Pt guard electrode, Fresenius' Journal of Analytical Chemistry, 367, 614–620, 2000.

Vanhaecke, F. and Moens, L.: Overcoming spectral overlap in isotopic analysis via single- and multi-collector ICP–mass spectrometry, Analytical and Bioanalytical Chemistry, 378, 232–240, 2004.

Wieser, M., Schwieters, J., and Douthitt, C.: Multi-Collector Inductively Coupled Plasma Mass Spectrometry, Multi-Collector Inductively Coupled Plasma Mass Spectrometry, fundamentals and applications using ICP-MS, Wiley & Sons, Weinheim, Germany, 2012.

Chapter 4

Export production in the New-Zealand region since the last glacial maximum

This chapter has been accepted for publication as an article in Earth and Planetary Science Letters.

Axel Durand[1], Zanna Chase[1], Taryn L. Noble[1], Helen Bostock[2], Samuel Jaccard[3], Priya Kitchener[1], Ashley T. Townsend[4], Nils Jansen[1], Les Kinsley[5], Geraldine Jacobsen[6], Sean Johnson[7], Helen Neil[2]

[1]Institute for Marine and Antarctic Studies, University of Tasmania, Hobart, Australia
[2]NIWA, Wellington, New Zealand
[3]Institute of Geological Sciences and Oeschger Centre for Climate Change Research, University of Bern, Switzerland
[4]Central Science Laboratory, University of Tasmania, Hobart, Australia
[5]Australian National University, Canberra, Australia
[6]Australian Nuclear Science and Technology Organisation (ANSTO), Lucas Heights, New South Wales, Australia
[7]Centre of Excellence in Ore Deposits (CODES), University of Tasmania, Hobart, Australia

Abstract

Increased export production (EP) in the Subantarctic Zone (SAZ) of the Southern Ocean due to iron fertilisation has been proposed as a key mechanism for explaining carbon drawdown during the last glacial maximum (LGM). This work reconstructs marine EP since the LGM at four sites around New Zealand. For the first time in this region, 230-Thorium-normalised fluxes of biogenic opal, carbonate, excess barium, and organic carbon are presented. In Subtropical Waters and the SAZ, these flux variations show that EP has not changed markedly since the LGM. The only exception is a site currently north of the subtropical front. At this site it is suggested the subtropical front shifted over the core site between 18 and 12 ka, driving increased EP. To understand why EP remained mostly low and constant, lithogenic fluxes at the four sites were measured to investigate changes in dust deposition. At all sites, lithogenic fluxes were greater during the LGM compared to the Holocene. The positive temporal correlation between the Antarctic dust record and lithogenic flux at a site in the Tasman Sea shows that regionally, increased dust deposition contributed to the high glacial lithogenic fluxes. Additionally, it is inferred that lithogenic material from erosion and glacier melting deposited on the Campbell Plateau during the deglaciation (18-12 ka). From these observations, it is proposed that even though increased glacial dust deposition may have relieved iron limitation within the SAZ around New Zealand, the availability of silicic acid limited diatom growth and thus any resultant increase in carbon export during the LGM. Therefore, silicic acid concentrations have remained low since the LGM. This result suggests that both silicic acid and iron co-limit EP in the SAZ around New Zealand, consistent with modern process studies.

4.1 Introduction

Air bubbles trapped in Antarctic ice revealed that atmospheric CO_2 concentrations were 80 ppm lower during the last glacial maximum (LGM, 18-21 ka) compared to pre-industrial levels (Genthon et al., 1987; Neftel et al., 1988). Previous studies highlighted an essential role of the Southern Ocean in regulating atmospheric CO_2 concentrations on glacial-interglacial timescales (Sigman and Boyle, 2000; Sigman et al., 2010). Specifically, increased biological activity, from enhanced iron (Fe)-bearing dust deposition, in a stratified Southern Ocean, is thought to have been one of the drivers of the glacial carbon storage (Hain et al., 2010; Jaccard et al., 2013;

Kohfeld et al., 2005; Kumar et al., 1995; Martínez-Garcia et al., 2014). However, there remains uncertainty as to whether export production (EP) increased across the Southern Ocean as a whole during past ice ages. Paleoceanographic records revealed a northward displacement of the maximum EP zone from the Antarctic Zone (AZ) toward the Subantarctic Zone (SAZ) of the Southern Ocean during the LGM (Anderson et al., 2002; Chase et al., 2003). Furthermore, disparities have been observed between the different sectors of the Southern Ocean. In the Atlantic sector, several studies reported increased EP in the SAZ during the LGM compared to present (Anderson et al., 2002; Chase et al., 2001; Martínez-Garcia et al., 2014), while in the Pacific sector, Chase et al. (2003) inferred that EP in the SAZ has remained rather invariant since the LGM. Several authors suggested that the remoteness of the Pacific sector of the Southern Ocean from terrestrial Fe sources could explain why EP was not significantly higher during the LGM compared to the Holocene (5-12 ka) (Bostock et al., 2013; Chase et al., 2003). Recently, Lamy et al. (2014) showed that glacial dust deposition in the SAZ was 50% lower in the Pacific sector compared to the Atlantic sector of the Southern Ocean.

Despite being an extremely large area of the Southern Ocean, there is little past EP data in the South Pacific, particularly in the New Zealand region, compared to the South Atlantic. Up to this date little is known about how EP in the New Zealand region might have changed with time. So far previous studies disagree about EP changes since the LGM (Figure 4.1 and supplementary material see section 4.7). Increased organic carbon (C_{org}) mass accumulation rate (MAR) at sites DSDP 594 and CHAT-1K during the LGM was used to infer increased glacial EP in the Chatham Rise area (Kowalski and A Meyers, 1997; Lean and McCave, 1998). Similarly, $CaCO_3$ MARs increased during the LGM over the Chatham Rise (Carter et al., 2000). However, a later study presented conflicting results: using opal and $CaCO_3$ MARs, Carter and Manighetti (2006) suggested that EP in the Chatham Rise area increased during the deglaciation (18-12 ka) instead of the LGM. Furthermore, on the Campbell Plateau, Ellwood et al. (2005) found no EP change since the LGM based on zinc/silicon (Zn/Si) ratios of sponge spicules. These studies used different EP proxies and therefore it is somewhat difficult to extract a consistent EP trend in the New Zealand region (Figure 4.1). Moreover, the absence of 230-Thorium (^{230}Th) normalised accumulation rates in a region characterised by strong bottom currents, which can re-suspend and redistribute sediment material on the seafloor, potentially results in erroneous inferences about vertical rain rates (Francois et al., 2004).

The lack of accurate EP reconstructions within New Zealand region makes it hard to compare the importance of New Zealand region EP relatively to other areas of the Southern Ocean. Therefore, new accurate reconstructions of EP changes and their drivers are essential to fill these key gaps in our understanding. In addition, a large part of the New Zealand region's waters are located within the SAZ and the SAZ EP is known to have played a major role in driving glacial CO_2 sequestration. Consequently, it is critical to understand how and why EP might have changed in this region across glacial-interglacial transitions.

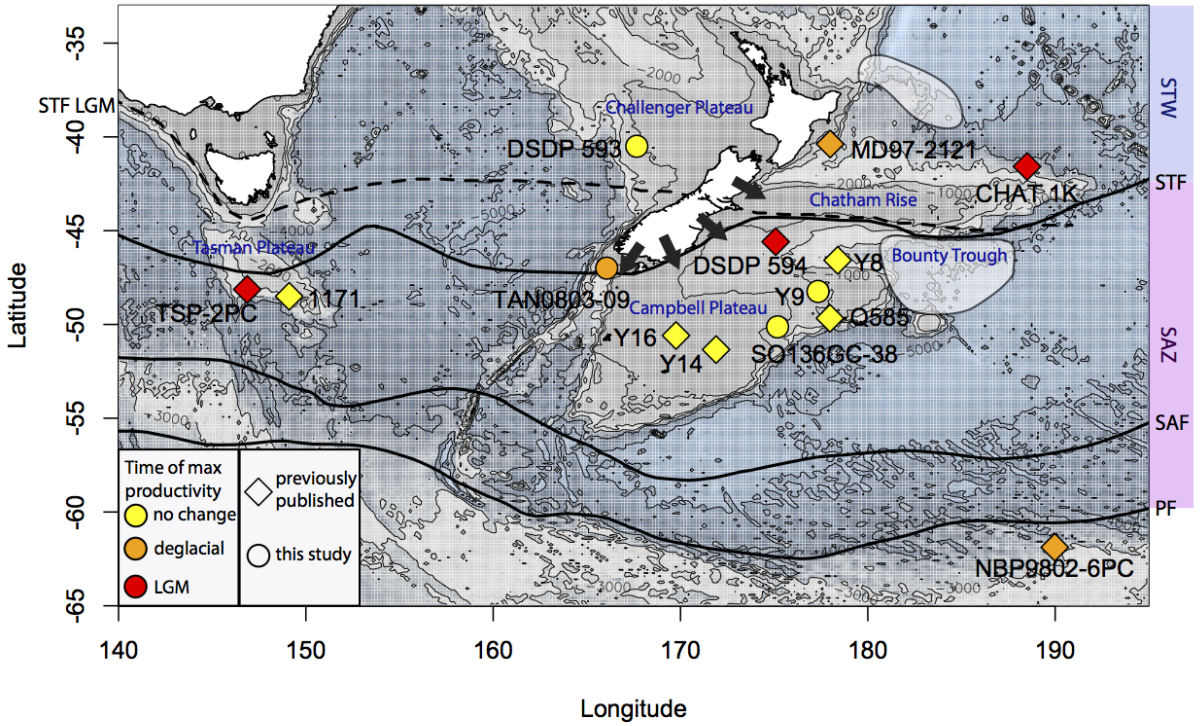

Figure 4.1: Productivity changes at different core sites since the LGM. Yellow colour indicates similar productivity across the LGM-Holocene transition, while orange and red means higher productivity during the deglacial (18-12 ka) and LGM (18-21 ka), respectively. Dots represent new data from this study, diamonds represent previously published data. All the data available for this region were included. A list of the different proxies used for each core is available in the supplementary material section. The background represents bathymetry. The mean present (Orsi et al., 1995) and LGM (Bostock et al., 2015) positions of the STF are represented as plain and dashed lines, respectively. Major glaciogenic sediment deposition zones during the LGM are represented as white polygons (Carter et al., 2000). Arrows show major lithogenic river discharges during the LGM.

Today, the New Zealand region is characterised by highly variable temporal and spatial patterns of biological activity (Chiswell et al., 2013; Murphy et al., 2001). Areas of high biological

Table 4.1: Summary of the sediment core locations, depths, and age models.

Core	Latitude	Longitude	Depth (m)	Location	Age model
DSDP 593	-40.5	167.67	1068	Challenger Plateau	Radiocarbon (this study) + $\delta^{18}O$ alignment with LR04 stack (Martinez et al. 1994)
TAN0803-09	-47	166.06	1648	Solander Trough	Radiocarbon (Bostock et al. 2015) + $\delta^{18}O$ alignment with LR04 stack (Neil, Bostock, NIWA; unpublished)
Y9	-48.24	177.34	1267	Campbell Plateau	Radiocarbon (Neil et al. 2004) + $\delta^{18}O$ alignment with LR04 stack (Neil et al. 2004)
SO136GC-38	-50.13	175.18	1359	Campbell Plateau	Age model from Neil et al. (2004)

activity are generally observed along the coast as well as in the Bounty Trough region, in austral spring and summer. Averaged over the year the chlorophyll-a concentrations of the SAZ and Subtropical Waters (STW) are low ($\leq 0.5\ mg.m^{-3}$) (Figure 4.2). Iron and nitrogen limit biological activity of the SAZ and STW, respectively (Boyd et al., 1999). Elevated biological activity is observed along the Chatham Rise and between the Solander Trough and Campbell Plateau associated with the Sub-Tropical Front (STF), where warm, Fe-rich STW mixes with cold, nutrient-rich Subantarctic Waters (SAW) (Boyd et al., 1999) (Figure 4.2). A sediment trap study shows that C_{org} export is similar in New Zealand STW compared to the global average (6-7 $mg.m^{-2}.d^{-1}$) while C_{org} export is lower in New Zealand SAZ compared to the global average (3 $mg.m^{-2}.d^{-1}$) (Nodder et al., 2016).

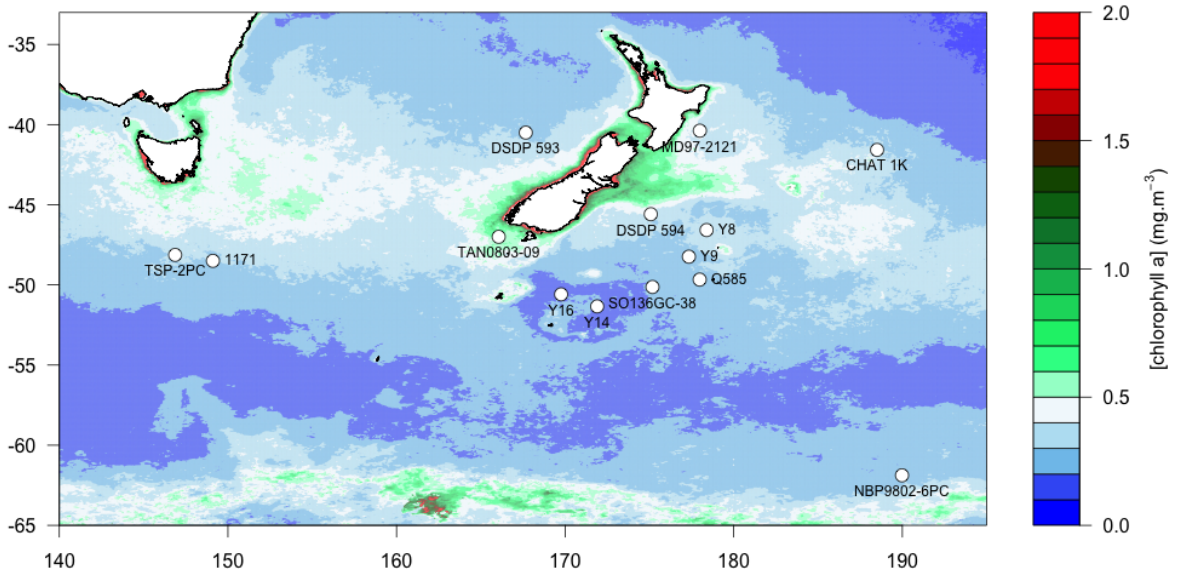

Figure 4.2: Mean chlorophyll-a concentration (2014-2016) from SeaWIFS data. The positions of sediment cores discussed in this paper are indicated.

In this study Th-normalised accumulation of biogenic opal, $CaCO_3$, $_{xs}Ba$ and C_{org} were used to reconstruct EP in the New Zealand region between the LGM and present. Increased sedimentary accumulation of these biogenic constituents has been related to increased EP; however, the accumulation of each of these components in sediments is controlled by specific factors. Opal and $CaCO_3$ are produced in surface waters by siliceous and calcareous plankton species, respectively. Therefore, their rain rates inform about the abundance of these organisms and the preservation of their skeletal remains in the sedimentary record (Ragueneau et al., 1996). On the other hand, C_{org} and $_{xs}Ba$ rain rates are not specific to any plankton group and relate to total carbon export. Excess Ba accumulation is driven by barite precipitation that occurs in certain micro-environments, which are rich in decaying organic matter (Paytan et al., 1996). To resolve spatial changes in EP, our data were compared with all New Zealand/Tasman Sea paleo-EP data available from the literature and a selection of other sites in the Southern Ocean (Figure 4.1 and supplementary material see section 4.7).

4.2 Methods

4.2.1 Age models

A previously published age model was used without modification for SO136GC-38 (Neil et al., 2004). Age models for cores DSDP 593, Y9 and TAN0803-09, were updated by combining radiocarbon ages and pre-existing down core foraminiferal $\delta^{18}O$ data. Radiocarbon dates were used as absolute time markers, and the $\delta^{18}O$ records were correlated to the LR04 stack (Lisiecki and Raymo, 2005) using Analyseries (Paillard et al., 1996). Radiocarbon ages from Neil et al. (2004) were used for Y9, while new radiocarbon dates were determined for DSDP 593 and TAN0803-09. The new radiocarbon measurements were conducted at the ANSTO Science Institute (Lucas Heights, Australia) using accelerator mass spectrometery (AMS). All AMS dates (new and pre-existing) were calibrated with the MARINE13 calibration curve using the OxCal 4.2 platform (Ramsey, 2009). References to the $\delta^{18}O$ records and the pre-existing age models used are compiled in Table 4.1.

4.2.2 Sediment digestion

Two hundred mg of freeze-dried and crushed sediments were spiked with ^{229}Th (0.32 Bq). The mixture was digested in a HCl, HNO_3 and HF cocktail using a pressure-assisted microwave (Milestone Ethos SK-12 microwave oven, Milestone, Shelton, CT, USA) following the protocol detailed in **chapter 2**. The digested solution was taken up in 4 mL of 7.5 M HNO_3 and separated into two aliquots. The first aliquot consisted of 400 µL, from the 4 mL solution, diluted into 15 mL of 12.5% HNO_3. The second aliquot consisted of the 3.6 mL left from the 4 mL solution. The first aliquot was used to measure ^{238}U, ^{232}Th, and ^{137}Ba while the second aliquot was used to measure ^{230}Th. Thorium was separated from the second aliquot using Dowex AG1-X8 anion exchange resin following Negre et al. (2009). Prior to measurement, the Th fraction was dried on a hotplate and taken into 2 mL of a 2% HNO_3, 0.1% HF solution.

4.2.3 Analysis of Uranium, Thorium and Barium

Analysis of ^{238}U, ^{232}Th, and ^{137}Ba were carried out using an Element 2 sector field ICP-MS from Thermo Fischer Scientific (Bremen, Germany) in low-resolution mode ($m/\Delta m \approx 400$). An external calibration method coupled with an internal standard (^{115}In) was used for the elemental quantification. The calibration solutions were prepared the day of the analysis from 100 µg/mL standard solutions (QCD Analysts, Spring Lake, NJ, USA). The sample handling procedure as well as the instrumental conditions have been detailed previously in **chapter 2**. Precision of the method was assessed across 19 analytical sequences carried out on an in-house reference sediment (D-178) over a three months period, deviations observed for ^{238}U, ^{232}Th, and ^{137}Ba were less than 10% (**chapter 2**).

230-Thorium concentrations from TAN0803-09, SO136GC-38 and Y9 were measured by isotopic dilution over ^{229}Th, on the same single collector ICP-MS instrument noted previously. Details on the method can be found in **chapter 3**.

230-Thorium concentrations from DSDP 593 were measured on a ThermoFisher Neptune Plus multi-collector inductively-coupled-plasma-mass spectrometer at the Research School of Earth Sciences, Australian National University. Sample was introduced using an Apex HF sample introduction system. Thorium fractions were analysed in peak jumping mode with the aide of a retarding potential quadrupole (RPQ) to minimise the tail of ^{232}Th. 229-Thorium/^{230}Th

was determined in a two-step process by determining 230/232 and 229/232. Intensities at 230.5 and 229.5 and 228.5 were monitored for tail corrections on ^{229}Th and ^{230}Th. Mass bias and secondary electron multiplier (SEM)/Faraday cup yield were corrected by standard bracketing using the uranium standard CRM-145.

4.2.4 Excess Barium calculation

Total Ba concentrations were corrected for detrital contributions as follows:

$$_{xs}Ba = Ba - (\frac{Ba}{Th})_{cc}.Th_{total} \tag{4.1}$$

The mean continental crust (cc) ratio used for $(Ba/Th)_{cc}$ was 81.43 (Rudnick and Gao, 2003). Mean continental crust ratios were compared to all records available for the New Zealand region (EarthChem database) and the averaged crust ratios were found representative for the lithogenic material deposited in the region. Overall, the detrital correction was approximately 30% of the total Ba for Y9 and DSDP 593 and SO136GC-38 and about 90% for TAN0803-09.

4.2.5 Opal, calcium carbonate, organic carbon and lithogenic fraction determination

Calcium carbonate was measured via vacuum-gasometric quantitative analysis with a precision of 2%, at NIWA, New Zealand, as per Jones and Kaiteris (1983). Organic carbon was estimated as the difference between total carbon and $CaCO_3$. Total carbon was measured using an ELTRA-C200 analyser with a precision of 0.05%, at the Centre of Excellence in Ore Deposits (CODES), University of Tasmania. The opal content of the sediment was measured by molybdite-blue spectrophotometry following alkaline leaching in 2 N Na_2CO_3, as described in Mortlock and Froelich (1989). The lithogenic fraction was estimated from the ^{232}Th measurements. 232-Thorium present in the sediments was assumed to be exclusively of detrital origin with an average ^{232}Th content of 10 ppm (Taylor and McLennan, 1985).

4.2.6 Flux calculations

Organic carbon, $_{xs}Ba$, opal, $CaCO_3$ and lithogenic rain rates were calculated using the Th-normalisation method to correct for post-depositional sediment redistribution (Francois et al., 2004). Excess initial ^{230}Th ($^{230}_{xs}Th_o$) was calculated using the XSAGE package (Bourne et al., 2012). The calculations were made using the ^{238}U and ^{232}Th concentrations measured by external calibration. The $^{230}_{xs}Th$ concentrations were calculated assuming $(^{230}Th/^{238}U)_{cc}$ as 0.96 ± 0.04. Additionally, the $^{234}U/^{238}U$ ratio of authigenic U was assumed to be the same as modern seawater (1.15 ± 0.02). The ^{230}Th concentrations were corrected for the ingrowth of ^{230}Th from the decay of lithogenic and authigenic U using ^{232}Th measurements and assuming detrital $^{238}U/^{232}Th$ activity ratio of 0.7 ± 0.1 (Henderson and Anderson, 2003). Overall the excess fraction represented about 80% of the total initial ^{230}Th measured for Y9, DSDP 593 and SO136GC-38, and 50% for TAN0803-09. The preserved vertical fluxes were calculated as:

$$F = 0.0256.\frac{z}{^{230}_{xs}Th_0} \tag{4.2}$$

Where z corresponds to the water depth at which sediment core was recovered and 0.0256 $dpm.m^{-3}.year^{-1}$ is the ^{230}Th production rate from ^{234}U decay. The sediment core depths was adjusted to account for sea-level change on the basis that glacial seawater level was 120 m shallower than present (Lambeck et al., 2002). To compare with Th-normalised fluxes, total MARs were calculated as follow:

$$MAR = LSR.\rho \tag{4.3}$$

Where LSR is the linear sedimentation rate ($cm.ka^{-1}$), and ρ is the dry bulk density ($g.cm^{-3}$). In the absence of dry bulk density data for TAN0803-09, SO136GC-38 and DSDP 593, ρ was estimated from the $CaCO_3$ concentrations, as per Carter et al. (2000).

Sediment focusing factors (ψ) were calculated as the ratio of ^{230}Th accumulation on the seafloor to ^{230}Th production in the water column (Table 4.2) (Suman and Bacon, 1989).

Table 4.2: Mean focussing factors of the different sediment cores presented in this study. The focusing factors (ψ) have been calculated for every sample point and then averaged between 18-21 ka for the LGM timeslice and 5-12 ka for the Holocene timeslice. $\psi > 1$ indicates sediment focussing, while $\psi < 1$ indicates sediment winnowing.

	Focussing factors (ψ)			
	Y9	TAN0803-09	SO138GC-38	DSDP 593
Holocene	4.1	1.3	1	3.5
LGM	0.8	3.9	1.1	2.7

4.3 Results

4.3.1 Sediment composition

DSDP 593, SO136GC-38 and Y9 are rich in $CaCO_3$ ($\geq$ 70%), while TAN0803-09 is rich in lithogenic material ($\geq$ 50%) (Figure 4.3). All four cores had lower $CaCO_3$ contents during the LGM compared to the Holocene, however the $CaCO_3$ changes were larger for Y9 and TAN0803-09 compared to DSDP 593 and SO136GC-38. Overall, opal and lithogenic contents were higher during the LGM compared to the Holocene for all cores. However, the opal content of the four cores remained low ($\leq$ 3%) across the LGM-Holocene transition.

4.3.2 230-Thorium normalised fluxes

Lithogenic fluxes were greater during the LGM and deglaciation at the four core sites (Figure 4.4a and 4.5b-c). Moreover, LGM lithogenic fluxes at TAN0803-09 were 10-30 times greater compared to the three other cores (Figures 4.4a and 4.5b-c). For TAN0803-08, Y9 and SO136GC-38 there was a gradual transition from high to low lithogenic fluxes around 12 ka (Figures 4.4a and 4.5b-c). This transition occurred 5 ka after the dust flux receded to background values in Antarctic ice cores (EDC, Antarctica) (Lambert et al., 2008). This offset was not observed at DSDP 593, where the lithogenic flux variations track with the dust flux from EDC. For the four cores, the opal fluxes correlate positively with the lithogenic fluxes, and were higher during the LGM compared to the Holocene (Figures 4.4a-b). Overall SO136GC-38, Y9 and 593 have similar C_{org}, $_{xs}Ba$ and $CaCO_3$ variation patterns, presenting no significant change since the LGM. In contrast, TAN0803-09 experienced a substantial increase in C_{org}, $_{xs}Ba$, and $CaCO_3$ flux during the deglaciation compared to the LGM.

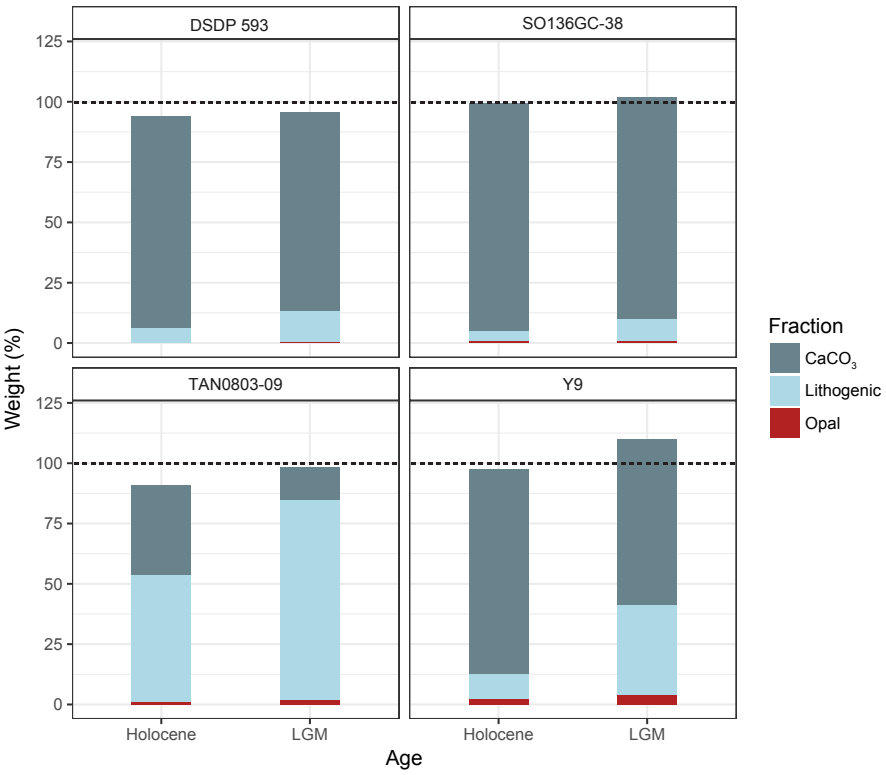

Figure 4.3: Mean composition of cores considered in this study during the LGM (18-21 ka) and the Holocene (5-12 ka). The lithogenic content was estimated from ^{232}Th as described in the text. The cumulative weight of opal, carbonate and lithogenic fractions is often less than 100%. This can be due to one or a combination of the following factors: (i) C_{org} contribution to the total weight (not represented) (ii) anomalous depletion in ^{232}Th of the lithogenic material (iii) analytical errors.

Large differences in sediment focusing were observed between the LGM and the Holocene at sites Y9 and TAN0803-09 (Table 4.2). Intense sediment focusing occurred at Y9 during the Holocene (ψ=4.1) compared to the LGM (ψ=0.8). However, at TAN0803-09 the focusing was larger during the LGM (ψ=3.9) compared to the Holocene (ψ=1.3). The focusing factor changed from 2.7 (LGM) to 3.5 (Holocene) at DSDP 593. No focusing occurred over SO136GC-38. Accordingly, for TAN0803-09, Y9 and DSDP 593, large differences were observed between the total MAR, calculated using sedimentation rates and sediment densities, and the ^{230}Th-normalised fluxes (Figure 4.6).

4.4 Discussion

The different EP proxies used in this study do not show a coherent temporal pattern of variations between the core sites. Consequently, findings here suggest that EP patterns in the New Zealand

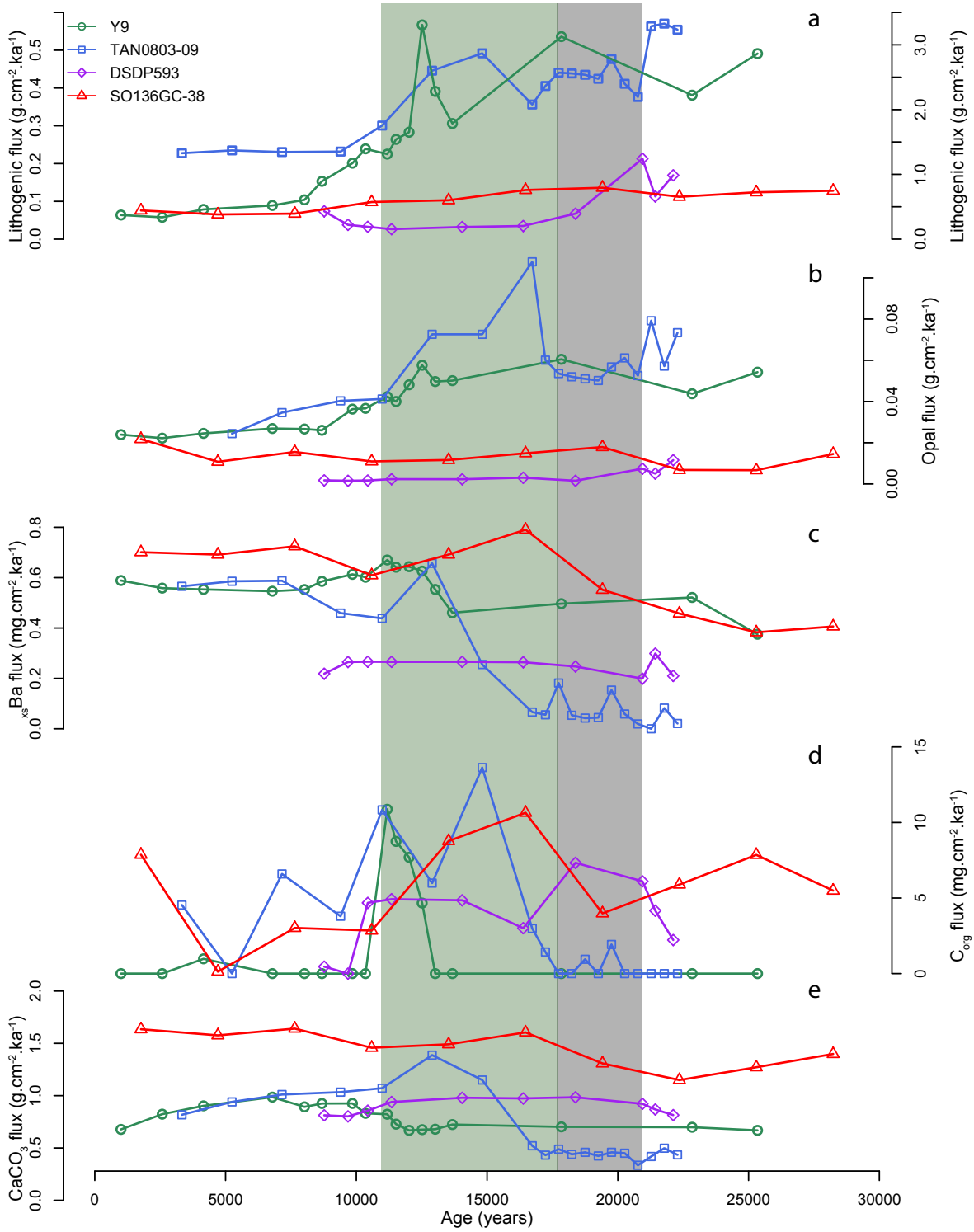

Figure 4.4: Th-normalised (a)Lithogenic, (b)Opal, (c)$_{xs}Ba$, (d)C_{org} and (e)$CaCO_3$ fluxes at Y9, TAN0803-09, DSDP 593, SO136GC-38. The lithogenic content was estimated from ^{232}Th as described in the text. As lithogenic fluxes at TAN0803-09 are 10-30 times greater than at the other sites, in the top panel (a), the axis representing TAN0803-09 is set on the right side. The grey and green panels represent the LGM and the deglaciation respectively.

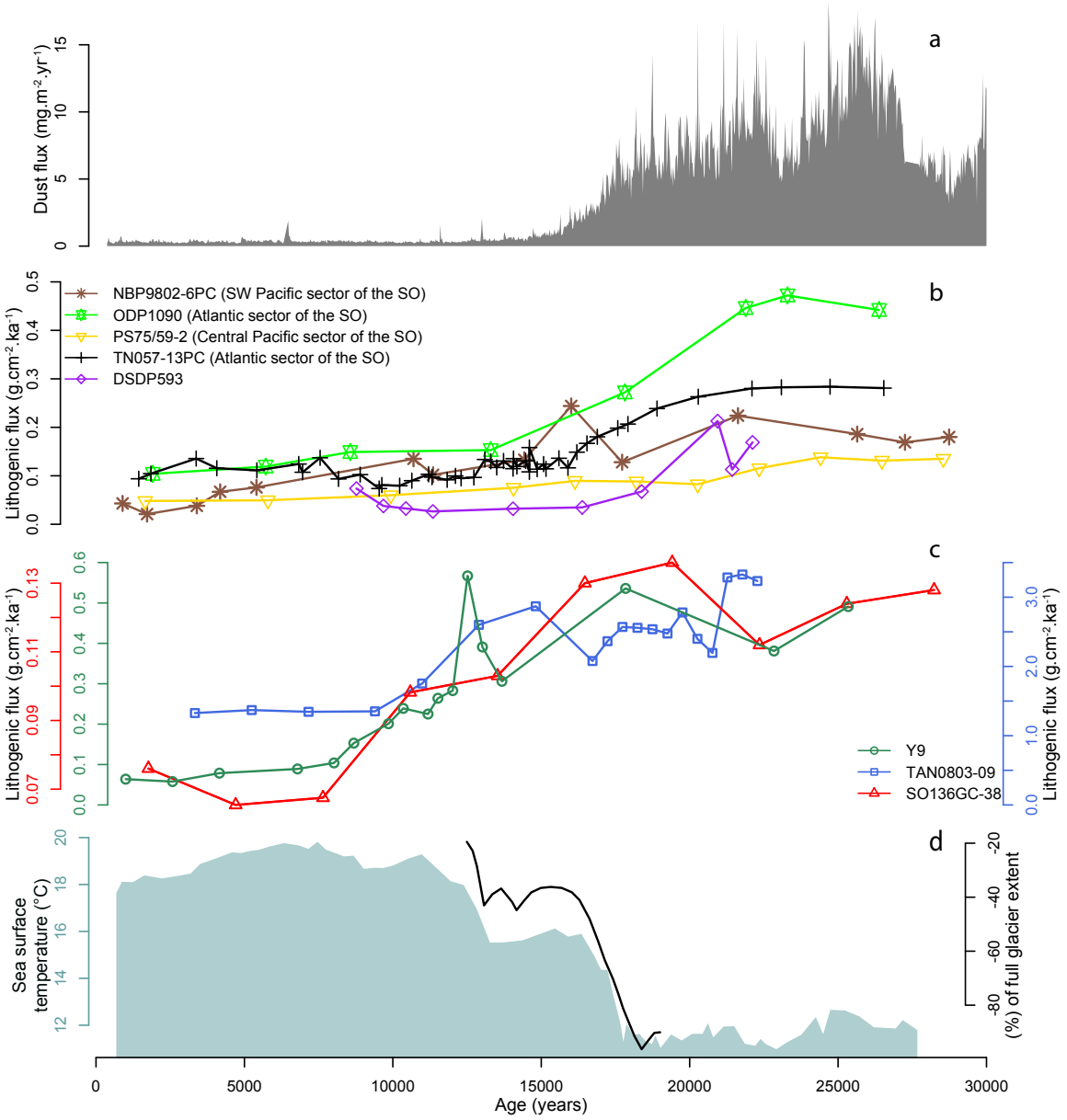

Figure 4.5: Lithogenic fluxes in the region and potential driving forces. (a) Dome C (EDC, Antarctica) dust flux (Lambert et al., 2008), (b)^{230}Th normalised lithogenic fluxes of sites in the Southern Ocean where the lithogenic deposition is driven by aeolian dust deposition: NBP9802-6PC and TN057-13PC (Anderson et al., 2009), ODP1090 (Martínez-Garcia et al., 2014), PS75/59-2 (Lamy et al., 2014), DSPD 593 (This study). SO stands for Southern Ocean and SW for southwest. (c) Lithogenic flux of the Campbell Plateau sites Y9, TAN0803-09 and SO136GC-38 (this study). The colour of the axis matches the colour of the site. (d) South Australian alkenone-derived SSTs from core MD03-2611 (blue shaded area, (Calvo et al., 2007)) and Southern Alps glacier extent relative to their maximum glacial extent (black line, (Putnam et al., 2010)).

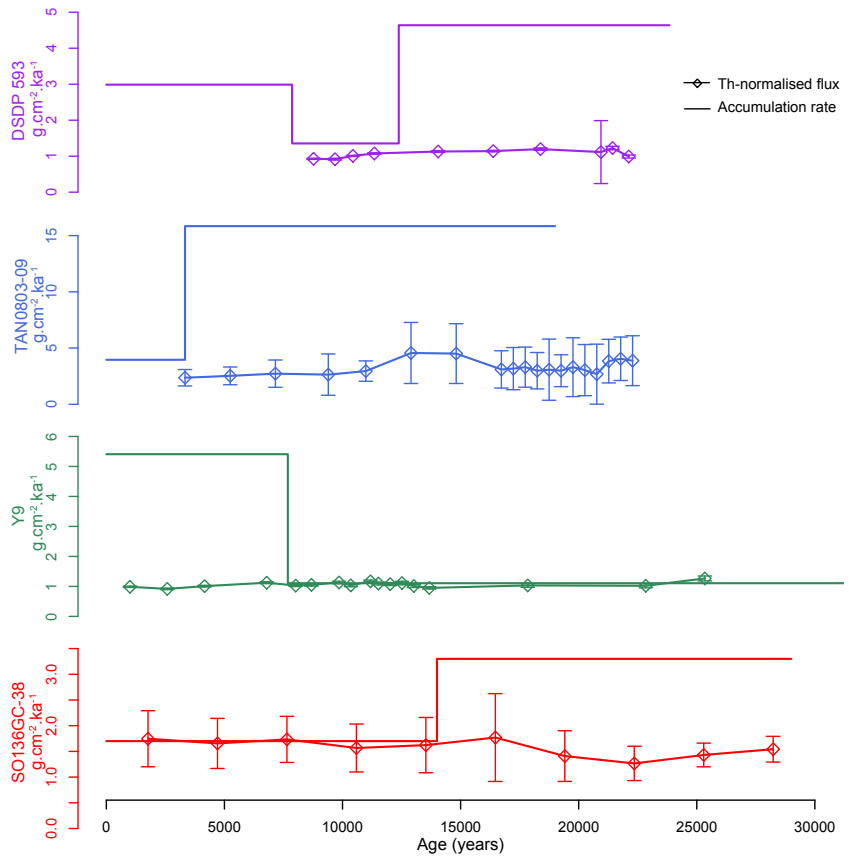

Figure 4.6: Comparison between the total mass accumulation rates (MAR) and Th-normalised total sediment fluxes, with propagated uncertainties, for the four sediment cores used in this study. Uncertainties are smaller than symbols for DSDP 593 and Y9.

region, since the LGM, have been characterised by a strong spatial variability, just as they are today. In the following sections, discussion will first revolve around the reliability of each proxy to assess EP changes. Next, EP variations that occurred in different parts of the New Zealand region and their drivers will be described. Finally, the changes in lithogenic material supply will be discussed to resolve the unusual lithogenic flux variations observed at Y9, SO136GC-38 and TAN0803-08, compared to other sites in the Southern Ocean.

4.4.1 Overview of the export production proxies

Each of the EP proxies used in this study has some limitations, which need to be considered before the records are interpreted. The opal contents in sediments considered in this work are very low, and in many cases are lower than the effective range of the leaching method ($\leq$ 3% opal, Figure 4.3) (Mortlock and Froelich, 1989). Moreover, the positive correlation between the opal and lithogenic fluxes at all sites (R^2=0.72) suggests that variations in opal content

could potentially be an artefact of partial dissolution of lithogenic Si and therefore be unrelated to variations in opal burial. However, the increased opal accumulation observed here during the LGM, and its correlation with lithogenic fluxes, is consistent with results from other sites in the SAZ of the Pacific (PS75/59-2, (Lamy et al., 2014)) and Atlantic (ODP1090, PS2498-1 (Anderson et al., 2009; Martínez-Garcia et al., 2014)) sectors of the Southern Ocean (Figure 4.7a). At these other sites, the correlation between opal and lithogenic flux is attributed to stimulation of opal export by Fe fertilisation from enhanced dust deposition associated with increased supply of dissolved Si (Anderson et al., 2014; Martínez-Garcia et al., 2014). While an iron-stimulated increase in opal export may well explain the opal flux pattern observed here, use of a more sensitive leaching procedure, able to distinguish between lithogenic and biogenic Si, at low Si concentrations, would be needed to determine whether the small increases in opal concentration observed here during the LGM are real or an artefact of the method used to measure opal.

Limitations are associated with the use of C_{org} flux as an EP proxy because C_{org} was not measured directly but estimated by difference between the total carbon and $CaCO_3$. Finally, dissolution and poor preservation conditions can result in erroneous opal, ${}_{xs}Ba$, $CaCO_3$, and C_{org} flux reconstructions. Overall, a wide range of limitations can compromise the use of opal, ${}_{xs}Ba$, $CaCO_3$ and C_{org} as EP proxies. However, because the factors compromising their use are different, we suggest that common variation patterns can be interpreted as reliable evidence of EP changes.

The low opal fluxes and the absence of correlation between the opal and other EP proxies supports the idea that the increased glacial opal export, if it did occur, did not significantly increase carbon export (Figure 4.4b-c-d-e). This absence of correlation could be explained by the dominance of phytoplankton species other than siliceous organisms to the total biogenic particle export. In other words, even if export by siliceous organism was higher during the LGM, it was too small to have a noticeable impact on the total export.

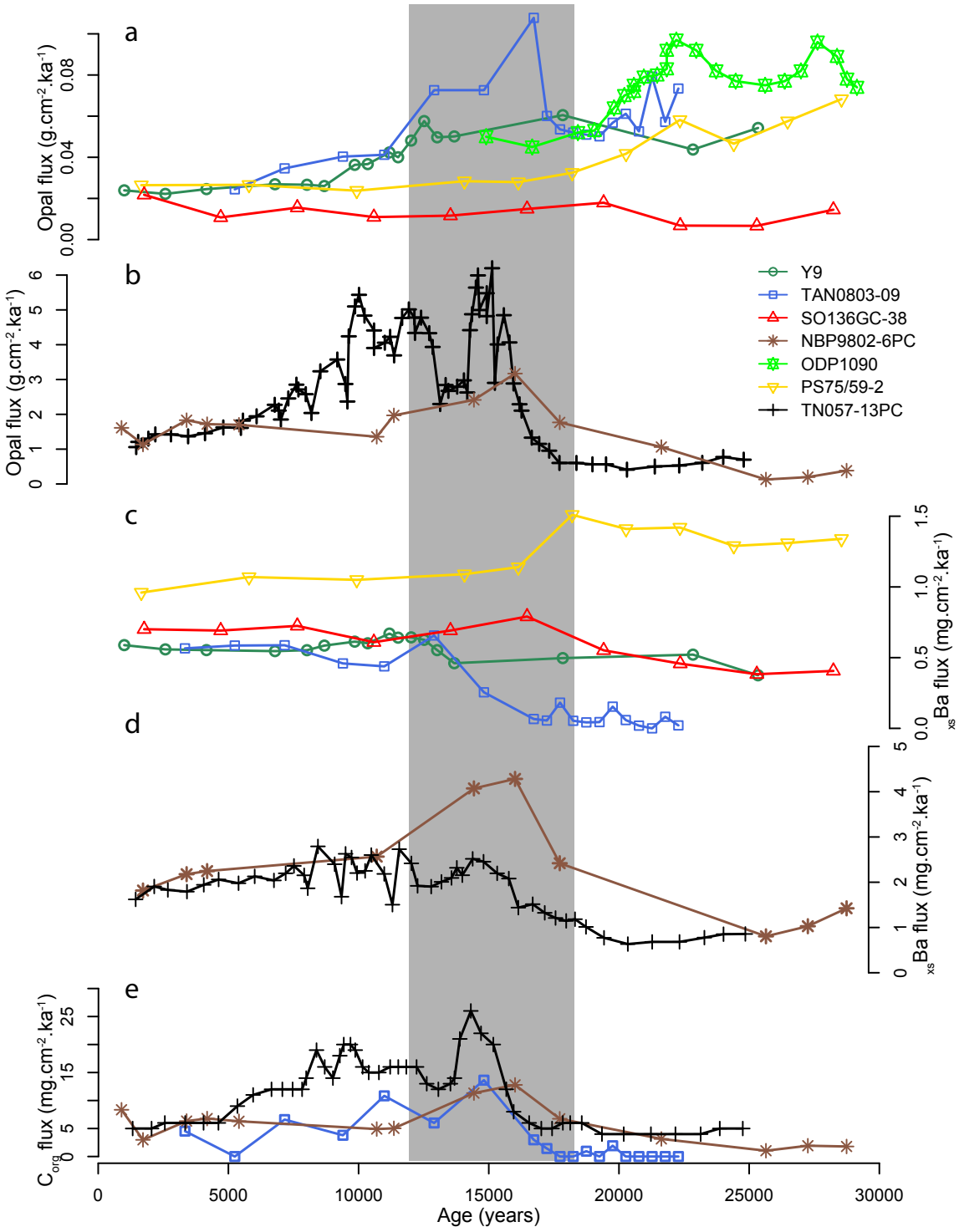

Figure 4.7: Th-normalised fluxes from this study in comparison to other sites in the Southern Ocean. (a) Opal fluxes at SO136GC-38, Y9 and TAN0803-09, together with SAZ sites ODP1090 (Atlantic, (Martínez-Garcia et al., 2014)) and PS75/59-2 (Central Pacific, (Lamy et al., 2014)). (b) Opal fluxes from polar front sites TN057-13PC (Atlantic) and NBP9802-6PC (Pacific) (Anderson et al., 2009). (c) $_{xs}Ba$ fluxes at SO136GC-38, Y9 and TAN0803-09 in comparison to PS75/59-2 (Central Pacific, (Lamy et al., 2014)). (d) $_{xs}Ba$ fluxes of TN057-13PC (Atlantic, (Jaccard et al., 2016)) and NBP9802-6PC (Pacific, (Chase et al., 2003)). (e) C_{org} flux at TAN0803-09 in comparison to TN057-13PC (Atlantic, (Jaccard et al., 2016; Wagner and Hendy, 2015)) and NBP9802-6PC (Pacific, Chase et al. (2003)). Grey shaded area shows the deglaciation (18-12 ka).

4.4.2 Export production changes and their drivers

Subantarctic zone

At sites SO136GC-38 and Y9, C_{org}, $_{xs}Ba$ and $CaCO_3$ fluxes have not noticeably changed since the LGM, suggesting that EP has not changed in the SAZ of the New Zealand region since the LGM. These findings are in agreement with Zn/Si results (Ellwood et al., 2005), and suggest that the EP in this region did not respond to the Fe fertilisation from increased glacial dust deposition (Albani et al., 2016; Lamy et al., 2014). In contrast, site PS75/59-2, in the SAZ of the central Pacific, shows increased $_{xs}Ba$, and opal fluxes during the LGM (Lamy et al., 2014), despite a smaller glacial lithogenic flux compared to our sites (Figure 4.5b). Therefore, the new data presented here suggest that either (i) the lithogenic glacial deposition in this region was dominated by sources other than dust (i.e. glacio-riverine runoff), or (ii) the Fe supplied by dust to the SAZ near New Zealand was not bioavailable, or (iii) other nutrients have been co-limiting any EP increase with Fe since the LGM.

We argue below for a contribution of glaciogenic sources to the higher lithogenic fluxes observed during the LGM on the Campbell plateau (see section 4.4.3 below). However, it is also likely that dust flux was greater at all sites during the LGM, as suggested by previous proxy (Hesse, 1994; Hesse and McTainsh, 1999) and modelling studies (Albani et al., 2016; Li et al., 2008). In particular, higher lithogenic fluxes are observed at DSDP 593 during the LGM compared to the Holocene, and this site has not been influenced by glaciogenic sources (see section 4.4.3 below). Furthermore, the higher lithogenic flux at DSDP 593 is accompanied by higher glacial fluxes of n-alkanes, a terrestrial plant biomarker (A. Rosel-Mele, pers. Comm 2015). This further strengthens the case for an aeolian source dominating the supply of lithogenic material at DSDP 593. Therefore, the greater lithogenic flux observed at DSDP 593 was likely driven by enhanced dust deposition. Moreover, the location of DSDP 593, west of New Zealand, coupled with the westerly wind pattern at this latitude suggests that Australia was a dominant dust source (Hesse, 1994; Hesse and McTainsh, 1999). This dust source would also have reached sites TAN0803-09, Y9 and SO136GC-38 in the SAZ, yet EP did not increase in response to this increased Fe delivery.

Although differences in bioavailability may have played a part in the observed lack of productivity response to dust in the SAZ around New Zealand, an alternative explanation to this

paradox might be found in observations of productivity today. Currently, the SAZ is nitrogen rich but Fe and $Si(OH)_4$ poor and characterised by low biological activity (Figure 4.8) (Boyd et al., 1999; Ellwood et al., 2008). Boyd et al. (1999) proposed that Fe limits phytoplankton growth and carbon export in these waters. However, during the SAGE Fe fertilisation experiment in the Bounty Trough region, no significant increase in primary productivity was detected while the area was fertilised (Peloquin et al., 2011). A similar outcome was observed during the LOHAFEX experiment in the SAZ of the Atlantic sector, where no change in carbon export fluxes were observed in the Fe fertilised area, even though higher chlorophyll-a concentrations were observed at the surface (Martin et al., 2013). Increased productivity was also observed during the SOFEX Fe fertilisation experiment in the Pacific sector of the Southern Ocean, however questions remain as to whether carbon was significantly exported at depth or remineralised in the euphotic zone (Coale et al., 2004). The absence of increased export when Fe limitation is relieved could be explained if $Si(OH)_4$ co-limits the carbon export with Fe, as suggested by Martin et al. (2013) and Boyd et al. (1999). In the absence of $Si(OH)_4$, Fe enrichment favours small phytoplankton species other than diatoms, which are strongly affected by remineralisation and reprocessing, and consequently have insignificant carbon export (Laurenceau-Cornec, 2015). Consequently, increased dust deposition during the LGM would not necessarily have increased carbon export in the SAZ if $Si(OH)_4$ limited the growth of diatoms. In this study, the small, and potentially artefactual, increase in opal export during the LGM, was clearly not associated with an increase in total export. This supports the idea that $Si(OH)_4$ depletion has been limiting diatom abundance and total carbon export in the SAZ since the LGM. This $Si(OH)_4 - Fe$ co-limitation has also been reported by earlier paleoceanographic studies (Anderson et al., 2014; Martínez-Garcia et al., 2014) and is also supported by new Th-normalised flux data from the SAZ in the south Tasman Sea, at site ODP1171, which show no EP change since the LGM (Figure 4.1; Kitchener et al., in.prep). The results of Kitchener et al. (in prep) are in opposition with those of Ikehara et al. (2000) who reported higher glacial EP in the Tasman Sea region. In this earlier study, sediment focusing and the absence of Th-normalisation might have erroneously induced higher MAR during the LGM. Therefore, we propose that the $Si(OH)_4 - Fe$ co-limitation described previously, might have applied to the SAZ of New Zealand and the Tasman Sea.

In summary, opal, C_{org}, $_{xs}Ba$ and $CaCO_3$ fluxes of Y9 and SO136GC-38 as well as the

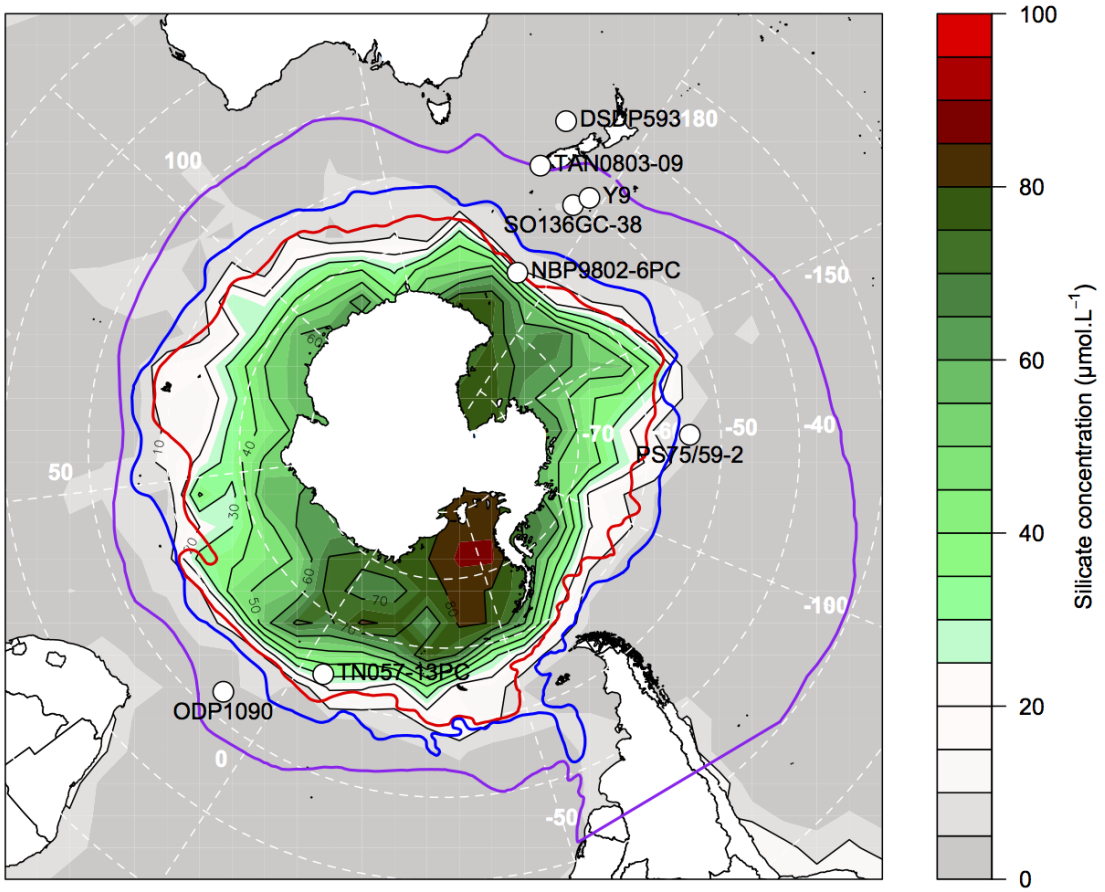

Figure 4.8: Present surface silicic acid concentration and core sites. Data from the World Ocean database). The positions of the Polar Front (red), Subantarctic Front (blue), and Subtropical Front (purple), are shown (Orsi et al., 1995).

results of other studies (Kitchener et al., in.prep; Ellwood et al., 2005) all suggest that the EP has remained steady in the SAZ of the southwest Pacific sector of the Southern Ocean since the LGM. This conflicts a previous study which reported higher EP above DSDP 594 in the Bounty Trough during the LGM compared to the Holocene (Figure 4.1) (Kowalski and A Meyers, 1997). However, in this study the absence of Th-normalised data could again be the issue. In particular, the large differences observed at Y9, TAN0803-09, and DSDP 593 between the MAR and Th-normalised fluxes show that sediment redistribution has likely compromised any non Th-normalised flux reconstructions in the New Zealand region (Figure 4.6).

Data reported here also differ from previous studies which suggest a slightly higher EP during

the LGM compared to the Holocene in the rest of the SAZ of the Pacific sector of the Southern Ocean (Bradtmiller et al., 2009; Chase et al., 2003; Lamy et al., 2014; Robinson et al., 2005). However, the sites that show signs of increased glacial EP are located approximately 5° further south compared Y9, SO136GC-38 and ODP1171 where the surface waters have higher $Si(OH)_4$ concentrations available (Figure 4.8). Accordingly, it is proposed that lower $Si(OH)_4$ supply at our sites may have inhibited any increase in LGM EP in comparison to other sites in the Pacific SAZ.

Subtropical waters

TAN0803-09 and DSPD 593 are currently located in STW. Biological activity above these two sites is currently not limited by Fe, like in the SAZ, but by the low nitrogen concentrations of STW (Boyd et al., 1999).

Changes in the position of the STF can explain the proxy records at TAN0803-09, which today sits just north of the STF. TAN0803-09 is the only core of this study that shows a significant EP change between the LGM and the Holocene. At TAN0803-09, C_{org}, $_{xs}Ba$ and $CaCO_3$ fluxes are positively correlated ($R^2 > 0.70$), and show an increase in EP during the deglaciation peaking between 14 and 15 ka (Figure 4.4c-d-e). The STF is today associated with high biological productivity fuelled by the mixing of nitrogen rich SAW and Fe rich STW (Boyd et al., 1999). Today, TAN0803-09 sits just north of the STF; however, Bostock et al. (2015) showed that the STF was located ≈5° further north during the LGM (Figure 4.1). Such a change in the position of the high EP area associated with the STF could explain the flux variations observed at the core site: during the deglaciation, when the front shifted southward toward its current position, higher nutrient availability fuelled higher biological activity over TAN0803-09.

A role for movement of the STF in driving productivity trends at TAN0803-09 is supported by comparison of the timing of changes with sites in the PF region of the Southern Ocean. The timing of the EP change at TAN0803-09 is similar to that observed at sites TN057-13PC and NBP9802-6PC in the PF region of the Atlantic and Pacific sectors of the Southern Ocean respectively (Anderson et al., 2009) (Figure 4.7b-c-d-e). A particularly strong correlation is observed between the C_{org} fluxes of TAN0803-09 and TN057-13PC (R^2=0.82; the two records were correlated by linearly interpolating between the dated samples to match both records). Anderson et al. (2009) proposed that the upwelling of Circumpolar Deep Water controls the

$Si(OH)_4$ supply and therefore the opal flux at TN057-13PC and NBP9802-6PC. This upwelling intensity is driven principally by the strength and position of the westerly winds. Consequently, during the deglaciation, a southward shift, and possible intensification of the westerlies, increased the supply of $Si(OH)_4$ and boosted opal flux at these PF sites (Anderson et al., 2009). The same southward shift of the westerlies drove the southward displacement of the STF from its LGM position (Bostock et al., 2015), and increased the EP at TAN0803-09. Therefore, the co-variations in biogenic flux between TAN0803-09, TN057-13PC and NBP9802-6PC strengthen the hypothesis that the STF shift drove the EP variations at TAN0803-09.

At DSDP 593, C_{org}, $_{xs}Ba$ and $CaCO_3$ fluxes show no noticeable change since the LGM. Therefore, EP above the Challenger Plateau has remained low and nutrient limited since the LGM and consequently free of SAW/STF influence. This finding is in agreement with results from Bostock et al. (2015), who showed that the STF was located south of the position of DSDP 593 during the LGM.

The absence of EP change at DSDP 593, west of New Zealand, contradicts previous work from STW north of the Chatham Rise, east of New Zealand (MD97-2121 and CHAT-1K), which showed higher EP during either the early deglaciation or the LGM (Figure 4.1) (Carter and Manighetti, 2006; Lean and McCave, 1998). Again the absence of Th-normalisation makes results from these earlier studies difficult to interpret in terms of EP. Alternatively, at MD97-2121, SST were 6 °C cooler during the LGM and the early deglaciation, relative to the Holocene, indicating the presence of SAW north of the Chatham Rise during the LGM (Marr et al., 2013; Nelson et al., 2000). Therefore, increased macro-nutrient availability under SAW influence may have increased EP over MD97-2121 (Carter and Manighetti, 2006). The same mechanism can also explain higher $CaCO_3$ MARs observed by Carter et al. (2000) north of the Chatham Rise during the LGM. Moreover, at CHAT-1K, mixing of SAW with STW, associated with northward displacement of the STF, potentially drove the increase in EP during the LGM (Lean and McCave, 1998). Consequently, east of New Zealand, SAW mixed into STW potentially increasing EP north of the modern STF during the LGM and early deglaciation, while west of New Zealand SAW did not mix into STW and EP remained low.

The smaller glacial northward extent of SAW west of New Zealand compared to east of New Zealand might have been driven by deeper bathymetry or by the lower flow of the STF west of New Zealand (no flow associated with the front) compared to east of New Zealand (strong

flow associated with the front) (Bostock et al., 2015). Carter et al. (2000) showed that both the shallow bathymetry of Chatham Rise and the Southland Current, associated with the lower glacial sea level, contributed to SAW leaking north of the Chatham Rise. Therefore, because EP at DSDP 593 has not changed significantly since the LGM, we suggest that the particular conditions for such a leak to occur have not been present west of New Zealand since the LGM.

4.4.3 Glaciogenic sources contributed to lithogenic fluxes on the Campbell Plateau

At all four sites, higher lithogenic fluxes were observed during the LGM and deglaciation compared to the Holocene. However, a 5 ka offset was observed between the maximum lithogenic deposition of TAN0803-09, SO136GC-38 and Y9 compared to DSDP 593 and other sites in the Southern Ocean and Antarctica (Figure 4.5a-b-c) (Anderson et al., 2014; Lambert et al., 2008; Lamy et al., 2014).

To explain this offset, we suggest that glaciogenic sources continued to supply lithogenic material to the eastern side of New Zealand, after dust deposition to the Southern Ocean had decreased to the very low present values. In the New Zealand region rivers and glaciers are an important source of lithogenic material (Carter et al., 2000). Furthermore, intense erosion during the LGM and deglaciation, driven by ice sheets, is believed to have caused an increased discharge of weathered and eroded material in the New Zealand region (Carter et al., 2000; Cogez et al., 2015; McGlone and Neall, 1994; Pillans et al., 1993). This increased glaciogenic discharge was limited to the eastern side of New Zealand, due to the larger volume of ice there compared to the western side (Cogez et al., 2015).

The timing of the lithogenic flux record is also consistent with a dominant glaciogenic source between 18 and 12 ka. While the aeolian supply of dust was almost insignificant by 18 ka (Lamy et al., 2014) (Figure 4.5a), the South Island erosion and associated lithogenic discharge was still high and only started substantially decreasing during the deglaciation under the influence of higher temperatures and higher sea level (Carter et al., 2000). Moreover the efficiency of this glaciogenic discharge was potentially enhanced by lower sea level during the early deglaciation, which allowed rivers to flow over emerged shelves and release sediments directly to the deep waters (Carter et al., 2000; Graham et al., 2015). Putnam et al. (2010, 2013) showed that the

majority of the melting of Southern Alps glaciers occurred during the deglaciation between 18 and 12 ka (Figure 4.5d). At Y9, SO136GC-38 and TAN0803-09 minimal lithogenic fluxes were reached around 9 ka, therefore it is proposed that a slow recession of the glacier extent after 12 ka continued to deliver lithogenic material at these sites. Alternatively, if the glacial retreat was complete by 12 ka, lithogenic material could have accumulated in sediment traps and diffused to Y9, SO136GC-38 and TAN0803-09 between 12 and 9 ka, as suggested by Carter et al. (2000).

The difference in magnitude of lithogenic fluxes at Y9, SO136GC-38 and TAN0803-09 can be explained by their proximity to sediment discharge zones. Lithogenic fluxes at TAN0803-09 during the LGM were 30 times greater compared to Y9, and LGM fluxes at Y9 were twice as large as at SO136GC-38 (Figure 4.5c). The greater lithogenic rain rates observed at TAN0803-09 can be explained by its greater proximity to the coast and river discharge zones compared to TAN0803-09 and SO136GC-38 (Figure 4.1). The different locations of Y9 and SO136GC-38 on the Campbell Plateau can also explain the twofold difference in lithogenic accumulation between the two sites. SO136GC-38 is located further away from the Bounty Trough sediment discharge zone and turbidity currents, and consequently might have received less riverine material compared to Y9 (Figure 4.1) (Carter et al., 2000).

As an alternative scenario, the possibility that dust is the dominant source of lithogenic material to this region was considered. In that case, increased dust deposition originating from New Zealand during the LGM and limited to a small area around the Campbell Plateau, could also explain the offset in timing between lithogenic flux at DSDP 593 and at SO136GC-38, TAN0803-09 and Y9. While most of the vegetation in Australia changed before 18 ka from grasslands to forest, the vegetation of New Zealand South Island only changed after 18 ka (McGlone et al., 1993). This later change is associated with the persistence of a cooler and dryer climate that might have enhanced the dust deposition east of New Zealand. Therefore, the persistence of high lithogenic flux on the Campbell Plateau after 18 ka might be associated with this increased dust deposition. In that case, the higher lithogenic flux observed at TAN0803-9, compared to the other sites, could be associated with the proximity between TAN0803-09 and the dust source. However, if dust from New Zealand is the only source of lithogenic material to the Campbell Plateau, this fails to explain why lithogenic deposition at Y9 is higher during the LGM compared to SO136GC-38. The two sites are located approximately at the same distance from the South Island and should receive similar amounts of dust. Consequently, lithogenic

discharge from glacier melts and erosion must have contributed to lithogenic fluxes on the Campbell Plateau; because only contribution from this source can explain the unique lithogenic accumulation pattern observed on the Campbell Plateau.

To assess the reliability of this interpretation, the LGM-present lithogenic flux changes observed at our core sites were compared to the overall LGM-present dust deposition change modelled by Albani et al. (2016) (Figure 4.9). While at DSDP 593 and SO136GC-38 there is a good agreement between observations and the modelled dust deposition change, at Y9 and TAN0803-09 lithogenic flux variations are significantly higher compared to modelled changes in dust deposition. This suggests that the enhanced lithogenic deposition at TAN0803-08 and Y9 was in part driven by glaciogenic inputs. However, at site SO136GC-38 the observed lithogenic flux change and modelled dust change agree, which suggests that the riverine discharge has been minor. Therefore, it is possible that the offset between the ice core dust deposition and the lithogenic flux at SO136GC-38 was driven by the South Island dust contribution, as mentioned earlier.

Finally, modern modelled dust deposition in the region (0.075-0.025 $g.cm^{-2}.ka^{-1}$; (Albani et al., 2016)) is consistent with Holocene lithogenic fluxes at Y9, SO136GC-38 and DSDP 593 (Figure 4.5). However, TAN0803-09 Holocene lithogenic fluxes ($\approx$1.5 $g.cm^{-2}.ka^{-1}$) are higher in comparison to present dust deposition. This suggests that even today sources of lithogenic material other than dust dominate lithogenic supply at TAN0803-09.

4.5 Conclusion

This work reconstructed strong spatial variability in EP changes in the New Zealand region since the LGM. In STW, out of any SAW influence, EP has not changed significantly since the LGM. Similarly, in the SAZ, EP has remained low and constant since the LGM. We suggest that $Si(OH)_4$ limited any increase in the total carbon export from enhanced Fe fertilisation during the LGM. This is different from other regions of the Southern Ocean that experienced significant increases in EP in the SAZ during the LGM due to Fe fertilisation from increased dust deposition. While lithogenic flux at DSDP 593 correlates with the dust deposition in Antarctica, an offset in timing was observed between the lithogenic fluxes of Campbell Plateau sites and DSDP 593. It is proposed that during the deglaciation intense erosion and glacier

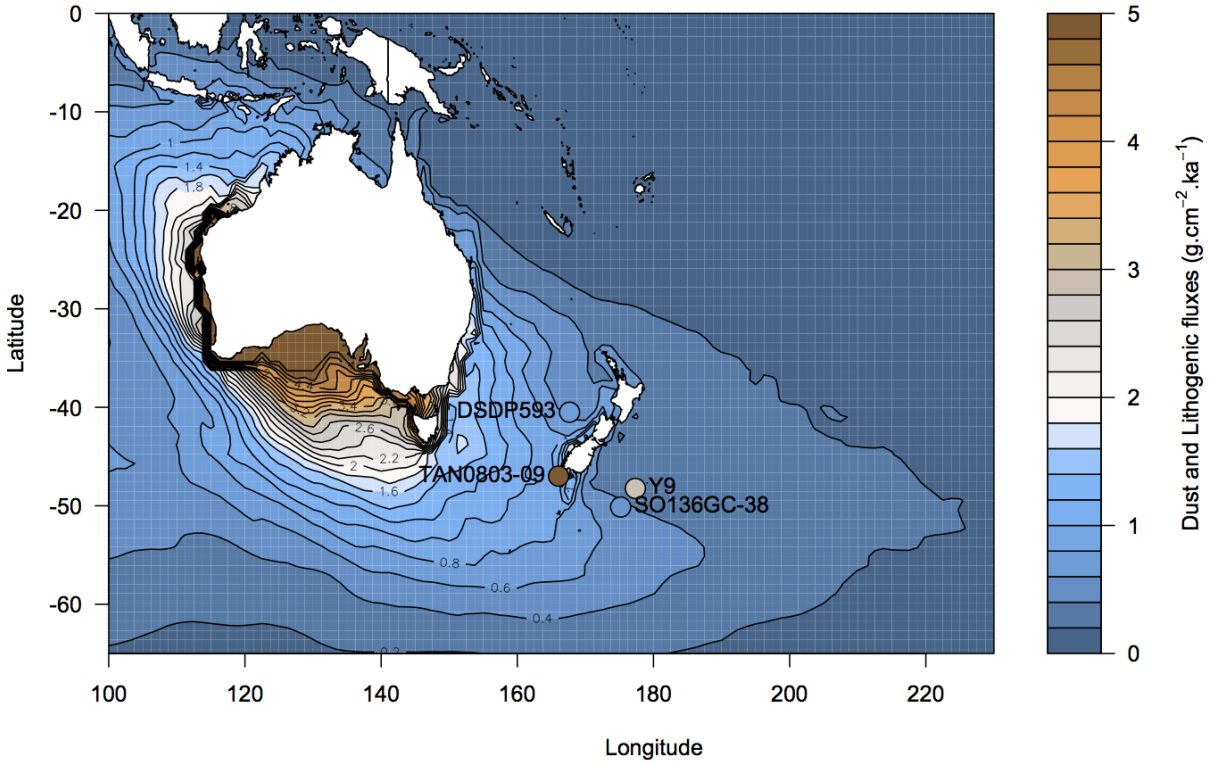

Figure 4.9: Comparison between the lithogenic flux changes from this study to the modelled dust deposition change between the LGM and present. Background: Modelled difference between the dust deposition during the LGM and present ($dust_{LGM}$ - $dust_{present}$) (Albani et al., 2016). Dots: lithogenic flux differences between the LGM (18-21 ka) and present ($\leq$ 8 ka). At DSDP 593 and SO136GC-38 observed and modelled changes in flux agree while at Y9 and TAN0803-09 observed changes in lithogenic flux are larger than modelled changes in dust deposition.

melting increased the sediment discharge to the Campbell Plateau and drove the observed offset in the timing of lithogenic flux. However, in agreement with previous studies, this sediment discharge from glacier melts and erosion was limited to sites east of New Zealand. Minor dust deposition from the South Island may have also contributed to this offset. Overall the multi-core, multi-proxy approach taken in this work allowed to resolve the EP history of the New Zealand region since LGM with a high degree of confidence. Since particular limitations are associated with each particular EP proxy, this work stresses the importance of a multi-proxy approach to estimate accurate EP changes.

4.6 Acknowledgements

This work was supported by the Australia/New Zealand IODP Consortium (ANZIC) and by an ARC Future Fellowship awarded to Zanna Chase [grant number FT120100759]. Radiocarbon analyses at ANSTO were supported by a AINSE grants ALNGRA11081 and ALNGRA14503. Access to ICP-MS instrumentation was supported through ARC LIEF funds [grant number LE0989539]. Samuel L. Jaccard was funded by the Swiss National Foundation (grant PP00P2-144811).

4.7 Supplementary material

Pangaea database compiling the new data created during this section of the PhD:

https://doi.pangaea.de/10.1594/PANGAEA.864678

Table 4.3: Summary of the sediment core locations, depths, proxies used and surface water masses overlaying sites. MAR refers to Mass Accumulation Rates without Th-normalisation.

Core	Latitude	Longitude	Depth (m)	Location	Overlaying water mass modern/LGM (interpreted)	Proxy used	Time of maximum productivity	References
MD97-2121	-40.38	177.99	3014	Chatham Rise	STW/STW mixing with SAW	Opal, $CaCO_3$ fluxes	deglacial	Carter et al. (2006)
DSDP 593	-40.5	167.67	1068	Challenger Plateau	STW/STW	Th normalised Opal, C_{org}, $_{xs}Ba$, $CaCO_3$, lithogenic fluxes	similar	This study
CHAT 1K	-41.58	188.5	3556	Chatham Rise	STW/STW mixing with SAW	C_{org} MAR, magnetite suceptibility	LGM	Lean et al. (1998)
ODP1090	-42.9	8.9	3700	Atlantic SAZ	SAW/SAW	Th normalised Opal, lithogenic fluxes	LGM	Martinez et al. (2014)
DSDP 594	-45.59	175.08	1204	Campbell Plateau	SAW/SAW	C_{org} MAR	LGM	Kowalski et al. (1997)
Y8	-46.58	178.39	1335	Campbell Plateau	SAW/SAW	Zn/Si	similar	Ellwood et al. (2005)
TAN0803-09	-47	166.06	1648	Solander Trough	STW/SAW	Th normalised Opal, C_{org}, $_{xs}Ba$, $CaCO_3$, lithogenic fluxes	deglacial	This study
TSP-2PC	-48.13	146.87	2321	Tasman Shelf	SAW/SAW	Biomarkers MAR	LGM	Ikehara et al. (2000)
Y9	-48.24	177.34	1267	Campbell Plateau	SAW/SAW	Th normalised Opal, C_{org}, $_{xs}Ba$, $CaCO_3$, lithogenic fluxes	similar	This study
1171B	-48.5	149.11	2150	Tasman Shelf	SAW/SAW	Th normalised Opal, C_{org}, $_{xs}Ba$, $CaCO_3$, lithogenic fluxes	LGM	Kitchener et al. (in prep)
Q585	-49.67	177.98	4354	Campbell Plateau	SAW/SAW	Zn/Si	similar	Ellwood et al. (2005)
SO136GC-38	-50.13	175.18	1359	Campbell Plateau	SAW/SAW	Th normalised Opal, C_{org}, $_{xs}Ba$, $CaCO_3$, lithogenic fluxes	similar	This study
Y16	-50.59	169.76	600	Campbell Plateau	SAW/SAW	Zn/Si	similar	Ellwood et al. (2005)
Y14	-51.34	171.9	523	Campbell Plateau	SAW/SAW	Zn/Si	similar	Ellwood et al. (2005)
TN057-13PC	-52.3	-5.1	2850	Atlantic PF region	AASW/AASW	Th normalised Opal, C_{org}, $_{xs}Ba$, lithogenic fluxes	deglacial	Anderson et al. (2009)
PS75/59-2	-54.21	-125.42	3613	Pacific SAZ	SAW/SAW or AASW	Th normalised Opal, $_{xs}Ba$, lithogenic fluxes	LGM	Lamy et al. (2014)
NBP9802-6PC	-61.9	170	3245	Pacific PF region	AASW/AASW	Th normalised Opal, C_{org}, $_{xs}Ba$, lithogenic fluxes	deglacial	Anderson et al. (2009)

References

Albani, S., Mahowald, N. M., Murphy, L. N., Raiswell, R., Moore, J. K., Anderson, R. F., McGee, D., Bradtmiller, L. I., Delmonte, B., Hesse, P. P., and Mayewski, P. A.: Paleodust variability since the Last Glacial Maximum and implications for iron inputs to the ocean, Geophysical Research Letters, 43, 3944–3954, 2016.

Anderson, R. F., Chase, Z., Fleisher, M. Q., and Sachs, J.: The Southern Ocean's biological pump during the last glacial maximum, Deep Sea Research Part II: Topical Studies in Oceanography, 49, 1909–1938, 2002.

Anderson, R. F., Ali, S., Bradtmiller, L. I., Nielsen, S. H. H., Fleisher, M. Q., Anderson, B. E., and Burckle, L. H.: Wind-driven upwelling in the Southern Ocean and the deglacial rise in atmospheric CO2., Science, 323, 1443–1448, 2009.

Anderson, R. F., Barker, S., Fleisher, M., Gersonde, R., Goldstein, S. L., Kuhn, G., Mortyn, P. G., Pahnke, K., and Sachs, J. P.: Biological response to millennial variability of dust and nutrient supply in the Subantarctic South Atlantic Ocean., Philosophical transactions. Series A, Mathematical, physical, and engineering sciences, 372, 20130 054–20130 054, 2014.

Bostock, H. C., Barrows, T. T., Carter, L., Chase, Z., Cortese, G., Dunbar, G. B., Ellwood, M., Hayward, B., Howard, W., Neil, H. L., Noble, T. L., Mackintosh, A., Moss, P. T., Moy, A. D., White, D., Williams, M. J. M., and Armand, L. K.: A review of the Australian-New Zealand sector of the Southern Ocean over the last 30 ka (Aus-INTIMATE project), Quaternary Science Reviews, 74, 35–57, 2013.

Bostock, H. C., Hayward, B. W., Neil, H. L., Sabaa, A. T., and Scott, G. H.: Changes in the position of the Subtropical Front south of New Zealand since the last glacial period, Paleoceanography, 30, 824–844, 2015.

Bourne, M. D., Thomas, A. L., Mac Niocaill, C., and Henderson, G. M.: Improved determination of marine sedimentation rates using 230Thxs, Geochemistry, Geophysics, Geosystems, 13, 2012.

Boyd, P., LaRoche, J., Gall, M., Frew, R., and McKay, R. M. L.: Role of iron, light, and silicate in controlling algal biomass in subantarctic waters SE of New Zealand, Journal of Geophysical Research, 104, 13 395–13 408, 1999.

Bradtmiller, L. I., Anderson, R. F., Fleisher, M. Q., and Burckle, L. H.: Comparing glacial and Holocene opal fluxes in the Pacific sector of the Southern Ocean, Paleoceanography, 24, 2009.

Calvo, E., Pelejero, C., De Deckker, P., and Logan, G. A.: Antarctic deglacial pattern in a 30 kyr record of sea surface temperature offshore South Australia, Geophysical Research Letters, 34, 2007.

Carter, L. and Manighetti, B.: Glacial/interglacial control of terrigenous and biogenic fluxes in the deep ocean off a high input, collisional margin: A 139 kyr-record from New Zealand, Marine Geology, 226, 307–322, 2006.

Carter, L., Neil, H. L., and McCave, I. N.: Glacial to interglacial changes in non-carbonate and carbonate accumulation in the SW Pacific Ocean, New Zealand, Palaeogeography, Palaeoclimatology, Palaeoecology, 162, 333–356, 2000.

Chase, Z., Anderson, R. F., and Fleisher, M. Q.: Evidence from authigenic uranium for increased productivity of the glacial Subantarctic Ocean, Paleoceanography, 16, 468–478, 2001.

Chase, Z., Anderson, R. F., Fleisher, M. Q., and Kubik, P. W.: Accumulation of biogenic and lithogenic material in the Pacific sector of the Southern Ocean during the past 40,000 years, Deep Sea Research Part II: Topical Studies in Oceanography, 50, 799–832, 2003.

Chiswell, S. M., Bradford-Grieve, J., Hadfield, M. G., and Kennan, S. C.: Climatology of surface chlorophyll a, autumn-winter and spring blooms in the southwest Pacific Ocean, Journal of Geophysical Research-Oceans, 118, 1003–1018, 2013.

Coale, K. H., Johnson, K. S., Chavez, F. P., Buesseler, K. O., Barber, R. T., Brzezinski, M. A., Cochlan, W. P., Millero, F. J., Falkowski, P. G., Bauer, J. E., Wanninkhof,

R. H., Kudela, R. M., Altabet, M. A., Hales, B. E., Takahashi, T., Landry, M. R., Bidigare, R. R., Wang, X., Chase, Z., Strutton, P. G., Friederich, G. E., Gorbunov, M. Y., Lance, V. P., Hilting, A. K., Hiscock, M. R., Demarest, M., Hiscock, W. T., Sullivan, K. F., Tanner, S. J., Gordon, R. M., Hunter, C. N., Elrod, V. A., Fitzwater, S. E., Jones, J. L., Tozzi, S., Koblizek, M., Roberts, A. E., Herndon, J., Brewster, J., Ladizinsky, N., Smith, G., Cooper, D., Timothy, D., Brown, S. L., Selph, K. E., Sheridan, C. C., Twining, B. S., and Johnson, Z. I.: Southern Ocean Iron Enrichment Experiment: Carbon Cycling in High- and Low-Si Waters, Science, 304, 408–414, doi:10.1126/science.1089778, URL `http://science.sciencemag.org/content/304/5669/408`, 2004.

Cogez, A., Meynadier, L., Allegre, C., Limmois, D., Herman, F., and Gaillardet, J.: Constraints on the role of tectonic and climate on erosion revealed by two time series analysis of marine cores around New Zealand, Earth and Planetary Science Letters, 410, 174–185, 2015.

Ellwood, M. J., Kelly, M., Neil, H., and Nodder, S. D.: Reconstruction of paleo–particulate organic carbon fluxes for the Campbell Plateau region of southern New Zealand using the zinc content of sponge spicules, Paleoceanography, 20, 2005.

Ellwood, M. J., Boyd, P. W., and Sutton, P.: Winter-time dissolved iron and nutrient distributions in the Subantarctic Zone from 40-52S; 155-160E, Geophysical Research Letters, 35, 2008.

Francois, R., Frank, M., Rutgers van der Loeff, M. M., and Bacon, M. P.: 230Th normalization: An essential tool for interpreting sedimentary fluxes during the late Quaternary, Paleoceanography, 19, 2004.

Genthon, C., Jouzel, J., Barnola, J. M., Raynaud, D., and Lorius, C.: Vostok ice core - Climatic response to CO2 and orbital forcing changes over the last climatic cycle, Nature, 329, 414–418, 1987.

Graham, R. M., De Boer, A. M., van Sebille, E., Kohfeld, K. E., and Schlosser, C.: Inferring source regions and supply mechanisms of iron in the Southern Ocean from satellite chlorophyll data, Deep Sea Research Part I: Oceanographic Research Papers, 104, 9–25, 2015.

Hain, M. P., Sigman, D. M., and Haug, G. H.: Carbon dioxide effects of Antarctic stratification, North Atlantic Intermediate Water formation, and subantarctic nutrient drawdown during

the last ice age: Diagnosis and synthesis in a geochemical box model, Global Biogeochemical Cycles, 24, 2010.

Henderson, G. M. and Anderson, R. F.: The U-series toolbox for paleoceanography, Uranium-Series Geochemistry, 52, 493–531, 2003.

Hernandez-Sanchez, M. T., Mills, R. A., Planquette, H., Pancost, R. D., Hepburn, L., Salter, I., and FitzGeorge-Balfour, T.: Quantifying export production in the Southern Ocean: Implications for the Baxs proxy, Paleoceanography, 26, n/a–n/a, doi:10.1029/2010PA002111, URL http://dx.doi.org/10.1029/2010PA002111, pA4222, 2011.

Hesse, P. P.: The Record of Continental Dust From Australia in Tasman Sea Sediments, Quaternary Science Reviews, 13, 257–272, 1994.

Hesse, P. P. and McTainsh, G. H.: Last glacial maximum to early holocene wind strength in the mid-latitudes of the Southern Hemisphere from aeolian dust in the Tasman Sea, Quaternary Research, 52, 343–349, 1999.

Ikehara, M., Kawamura, K., Ohkouchi, N., Murayama, M., Nakamura, T., and Taira, A.: Variations of terrestrial input and marine productivity in the Southern Ocean (48°S) during the last two deglaciations, Paleoceanography, 15, 170–180, 2000.

Jaccard, S. L., Hayes, C. T., Martínez-García, A., Hodell, D. A., Anderson, R. F., Sigman, D. M., and Haug, G. H.: Two modes of change in Southern Ocean productivity over the past million years, Science, 339, 1419–1423, 2013.

Jaccard, S. L., Galbraith, E. D., Martínez-Garcia, A., and Anderson, R. F.: Covariation of deep Southern Ocean oxygenation and atmospheric CO2 through the last ice age., Nature, 2016.

Jones, G. A. and Kaiteris, P.: A vacuum-gasometric technique for rapid and precise analysis of calcium-carbonate in sediments and soils, Journal of Sedimentary Petrology, 53, 655–660, 1983.

Kohfeld, K. E., Le Quere, C., Harrison, S. P., and Anderson, R. F.: Role of marine biology in glacial-interglacial CO2 cycles, Science, 308, 74–78, 2005.

Kowalski, E. A. and A Meyers, P.: Glacial–interglacial variations in Quaternary production of marine organic matter at DSDP Site 594, Chatham Rise, southeastern New Zealand margin, Marine Geology, 140, 249–263, 1997.

Kumar, N., Anderson, R. F., Mortlock, R. A., Froelich, P. N., Kubik, P., Dittrich-Hannen, B., and Suter, M.: Increased biological productivity and export production in the glacial Southern Ocean, Nature, 378, 675–680, 1995.

Lambeck, K., Esat, T. M., and Potter, E.-K.: Links between climate and sea levels for the past three million years., Nature, 419, 199–206, 2002.

Lambert, F., Delmonte, B., Petit, J. R., Bigler, M., Kaufmann, P. R., Hutterli, M. A., Stocker, T. F., Ruth, U., Steffensen, J. P., and Maggi, V.: Dust-climate couplings over the past 800,000 years from the EPICA Dome C ice core, Nature, 452, 616–619, 2008.

Lamy, F., Gersonde, R., Winckler, G., Esper, O., Jaeschke, A., Kuhn, G., Ullermann, J., Martínez-García, A., Lambert, F., and Kilian, R.: Increased dust deposition in the Pacific Southern Ocean during glacial periods, Science, 343, 403–407, 2014.

Laurenceau-Cornec, E.: Carbon export efficiency modulation by plankton communities in the Southern Ocean: results from a coupled physical-biogeochemical model , in: PhD thesis: Ecosystem controls on carbon export efficiency from the naturally iron-fertilised phytoplankton bloom over the Kerguelen Plateau, University of Tasmania, 2015.

Lean, C. M. B. and McCave, I. N.: Glacial to interglacial mineral magnetic and palaeoceanographic changes at Chatham Rise, SW Pacific Ocean, Earth and Planetary Science Letters, 163, 247–260, 1998.

Li, F., Ginoux, P., and Ramaswamy, V.: Distribution, transport, and deposition of mineral dust in the Southern Ocean and Antarctica: Contribution of major sources, Journal of Geophysical Research-Atmospheres, 113, 2008.

Lisiecki, L. E. and Raymo, M. E.: A Pliocene-Pleistocene stack of 57 globally distributed benthic δ18O records, Paleoceanography, 20, 2005.

Marr, J. P., Carter, L., Bostock, H. C., Bolton, A., and Smith, E.: Southwest Pacific Ocean response to a warming world: Using Mg/Ca, Zn/Ca, and Mn/Ca in foraminifera to track surface ocean water masses during the last deglaciation, Paleoceanography, 28, 347–362, 2013.

Martin, P., Loeff, M. R., Cassar, N., Vandromme, P., d'Ovidio, F., Stemmann, L., Rengarajan, R., Soares, M., González, H. E., Ebersbach, F., Lampitt, R. S., Sanders, R., Barnett, B. A., Smetacek, V., and Naqvi, S. W. A.: Iron fertilization enhanced net community production but not downward particle flux during the Southern Ocean iron fertilization experiment LOHAFEX, Global Biogeochemical Cycles, 27, 871–881, 2013.

Martínez-Garcia, A., Sigman, D. M., Ren, H., Anderson, R. F., Straub, M., Hodell, D. A., Jaccard, S. L., Eglinton, T. I., and Haug, G. H.: Iron fertilization of the Subantarctic Ocean during the last ice age, Science, 343, 1347–1350, 2014.

McGlone, M. S. and Neall, V. E.: The Late Pleistocene and Holocene Vegetation History of Taranaki, North-Island, New-Zealand, New Zealand Journal of Botany, 32, 251–269, 1994.

McGlone, M. S., Salinger, M. J., and Moar, N. T.: Paleovegetation studies of New Zealand's climate since the last glacial maximum, Global climates since the Last Glacial Maximum, pp. 294–317, 1993.

Mortlock, R. A. and Froelich, P. N.: A Simple Method for the Rapid-Determination of Biogenic Opal in Pelagic Marine-Sediments, Deep Sea Research Part A. Oceanographic Research Papers, 36, 1415–1426, 1989.

Murphy, R. J., Pinkerton, M. H., Richardson, K. M., Bradford Grieve, J. M., and Boyd, P. W.: Phytoplankton distributions around New Zealand derived from SeaWiFS remotely-sensed ocean colour data, New Zealand Journal of Marine and Freshwater Research, 35, 343–362, 2001.

Neftel, A., Oeschger, H., Staffelbach, T., and Stauffer, B.: CO2 record in the Byrd ice core 50, 000–5, 000 years bp, Nature, 331, 609–611, 1988.

Negre, C., Thomas, A. L., Mas, J. L., Garcia-Orellana, J., Henderson, G. M., Masqué, P., and Zahn, R.: Separation and measurement of Pa, Th, and U isotopes in marine sediments by

microwave-assisted digestion and multiple collector inductively coupled plasma mass spectrometry, Analytical Chemistry, 81, 1914–1919, 2009.

Neil, H. L., Carter, L., and Morris, M. Y.: Thermal isolation of Campbell Plateau, New Zealand, by the Antarctic Circumpolar Current over the past 130 kyr, Paleoceanography, 19, 2004.

Nelson, C. S., Hendy, I. L., Neil, H. L., Hendy, C. H., and Weaver, P.: Last glacial jetting of cold waters through the Subtropical Convergence zone in the Southwest Pacific off eastern New Zealand, and some geological implications, Palaeogeography, Palaeoclimatology, Palaeoecology, 156, 103–121, 2000.

Nodder, S. D., Chiswell, S. M., and Northcote, L. C.: Annual cycles of deep-ocean biogeochemical export fluxes in subtropical and subantarctic waters, southwest Pacific Ocean, Journal of Geophysical Research: Oceans, 121, 2405–2424, doi:10.1002/2015JC011243, URL `http://dx.doi.org/10.1002/2015JC011243`, 2016.

Orsi, A. H., Whitworth, T., and Nowlin, W. D.: On the Meridional Extent and Fronts of the Antarctic Circumpolar Current, Deep Sea Research Part I: Oceanographic Research Papers, 42, 641–673, 1995.

Paillard, D., Labeyrie, L., and Yiou, P.: Macintosh program performs time-series analysis, Eos, Transactions American Geophysical Union, 77, 379–379, 1996.

Paytan, A., Kastner, M., and Chavez, F. P.: Glacial to interglacial fluctuations in productivity in the equatorial Pacific as indicated by marine barite, Science, 274, 1355–1357, 1996.

Peloquin, J., Hall, J., Safi, K., Smith, W. O. J., Wright, S., and van den Enden, R.: The response of phytoplankton to iron enrichment in Sub-Antarctic HNLCLSi waters: Results from the SAGE experiment, Deep Sea Research Part II: Topical Studies in Oceanography, 58, 808–823, 2011.

Pillans, B., McGlone, M., Palmer, A., Mildenhall, D., Alloway, B., and Berger, G.: The Last Glacial Maximum in Central and Southern North Island, New-Zealand - a apleoenvironmental reconstruction using the Kawakawa tephra formation as a chronostratigraphic marker, Palaeogeography, Palaeoclimatology, Palaeoecology, 101, 283–304, 1993.

Putnam, A. E., Denton, G. H., Schaefer, J. M., Barrell, D. J. A., Andersen, B. G., Finkel, R. C., Schwartz, R., Doughty, A. M., Kaplan, M. R., and Schluechter, C.: Glacier advance in southern middle-latitudes during the Antarctic Cold Reversal, Nature Geoscience, 3, 700–704, 2010.

Putnam, A. E., Schaefer, J. M., Denton, G. H., Barrell, D. J. A., Andersen, B. G., Koffman, T. N. B., Rowan, A. V., Finkel, R. C., Rood, D. H., Schwartz, R., Vandergoes, M. J., Plummer, M. A., Brocklehurst, S. H., Kelley, S. E., and Ladig, K. L.: Warming and glacier recession in the Rakaia valley, Southern Alps of New Zealand, during Heinrich Stadial 1, Earth and Planetary Science Letters, 382, 98–110, 2013.

Ragueneau, O., Leynaert, A., Tréguer, P., Demaster, D. J., and Anderson, R. F.: Opal studied as a marker of paleoproductivity, Eos, Transactions American Geophysical Union, 77, 491–491, 1996.

Ramsey, C. B.: Bayesian analysis of radiocarbon dates, Radiocarbon, 51, 337–360, 2009.

Robin, E., Rabouille, C., Martinez, G., Lefevre, I., Reyss, J., van Beek, P., and Jeandel, C.: Direct barite determination using SEM/EDS-ACC system: implication for constraining barium carriers and barite preservation in marine sediments, Marine Chemistry, 82, 289 – 306, doi:http://dx.doi.org/10.1016/S0304-4203(03)00075-6, URL `//www.sciencedirect.com/science/article/pii/S0304420303000756`, 2003.

Robinson, R. S., Sigman, D. M., DiFiore, P. J., Rohde, M. M., Mashiotta, T. A., and Lea, D. W.: Diatom-bound 15N/14N: New support for enhanced nutrient consumption in the ice age subantarctic, Paleoceanography, 20, 2005.

Rudnick, R. L. and Gao, S.: Composition of the Continental Crust, Treatise on Geochemistry, 3, 1–64, 2003.

Sigman, D. M. and Boyle, E. A.: Glacial/interglacial variations in atmospheric carbon dioxide, Nature, 407, 859–869, 2000.

Sigman, D. M., Hain, M. P., and Haug, G. H.: The polar ocean and glacial cycles in atmospheric CO2 concentration., Nature, 466, 47–55, 2010.

Suman, D. O. and Bacon, M. P.: Variations in Holocene sedimentation in the North American Basin determined from 230Th measurements, Deep Sea Research Part A. Oceanographic Research Papers, 36, 869–878, 1989.

Taylor, S. R. and McLennan, S. M.: The continental crust: Its composition and evolution, Blackwell Scientific Publications, 1985.

Wagner, M. and Hendy, I. L.: Trace metal evidence for a poorly ventilated glacial Southern Ocean, Climate of the Past Discussions, 11, 637–670, 2015.

Chapter 5

Sediment cores reveal a deoxygenated Southern Ocean surrounding New Zealand during the last glacial maximum

This chapter has been prepared for submission as an article in Earth and Planetary Science Letters.

Axel Durand[1], Zanna Chase[1], Taryn L. Noble[1], Helen Bostock[2], Samuel Jaccard[3], Ashley T. Townsend[4], Nathan Bindoff[1, 5, 6, 7, 8], Helen Neil[2], Geraldine Jacobsen[9]

[1]Institute for Marine and Antarctic Studies, University of Tasmania, Hobart, Australia
[2]NIWA, Wellington, New Zealand
[3]Institute of Geological Sciences and Oeschger Centre for Climate Change Research, University of Bern, Switzerland
[4]Central Science Laboratory, University of Tasmania, Hobart, Australia
[5]Australian Research Council Centre of Excellence for Climate System Science, Sydney, New South Wales, Australia
[6]CSIRO Marine Atmospheric Research, Hobart, Tasmania, Australia
[7]ACE CRC, Hobart, Tasmania, Australia
[8]CAWCR, Melbourne, Victoria, Australia
[9]Australian Nuclear Science and Technology Organisation (ANSTO), Lucas Heights, New South Wales, Australia

Abstract

To investigate changes in oxygenation between the Last Glacial Maximum (LGM) and the Holocene, redox sensitive elements were measured in 12 sediment cores located on the Campbell and Challenger Plateaux surrounding New Zealand. Subantarctic Mode Water (SAMW), Antarctic Intermediate Water (AAIW) and Upper Circumpolar Deep Water (UCDW) currently bathe the core sites. The sedimentary distributions of authigenic uranium and rhenium reveal that intermediate depths (800-1500 m) of the southwest Pacific were depleted in oxygen during the LGM compared to the Holocene. Additionally, data from deeper waters ($\geq$ 1500 m) indicate higher oxygen content during the LGM compared to the Holocene. These data, together with variations in benthic foraminiferal $\delta^{13}C$ and carbonate mass accumulation rates, are consistent with a shallower AAIW-UCDW boundary over the Campbell Plateau during the LGM (800 m vs 1200 m today). Delta ^{13}C data indicate that AAIW continued to bathe the shallower core sites on the Campbell Plateau ($\leq$ 800 m depth) as well as the intermediate depths of the Challenger Plateau ($\leq$ 1500 m) during the LGM and Holocene; however redox sensitive elements in these cores also reveal that glacial AAIW contained less oxygen compared to the Holocene. These results are at odds with the general notion that AAIW was better oxygenated and expanded deeper during the LGM due to stronger westerlies and colder temperatures. It is suggested that these findings may be explained by a significant change in the mode of AAIW circulation.

5.1 Introduction

The loss of dissolved oxygen from the oceans, referred to as ocean deoxygenation, is a global phenomenon threatening all aerobic marine organisms (Diaz and Rosenberg, 2008; Keeling et al., 2010; Stramma et al., 2010). The Southern Ocean is particularly affected and accounts for 25% of the total oxygen losses reported since 1970 (Helm et al., 2011; Matear et al., 2000). However, although ocean deoxygenation consequences are potentially far reaching, future trends remain unclear and more work needs to be done in order to understand deoxygenation drivers.

The oxygen content in the ocean interior is determined by the balance between the supply of oxygen by ventilation (the process whereby surface mixed layer water is transported into the ocean interior) on one hand and its removal by bacterial respiration of labile organic matter, associated with remineralisation, on the other (Helm et al., 2011). This study focuses on

the southwest Pacific sector of the Southern Ocean. Today, the oceanic productivity there is relatively low (Murphy et al., 2001), thus ventilation constitutes the primary factor controlling dissolved oxygen levels. The ventilation in this region occurs through the formation of Subantarctic Mode Waters (SAMW) and Antarctic Intermediate Waters (AAIW) (Figure 5.1, 5.2). Antarctic Intermediate Water and SAMW are two oxygen rich water masses present at intermediate depths in the Southern Ocean (600-1200 m and 500-600 m, respectively). They are formed by subduction of Antarctic surface waters below buoyant subtropical waters (Talley, 2013). Prior to their subduction, their pre-formation is controlled by the Ekman driven upwelling of oxygen-depleted Upper Circumpolar Deep Water (UCDW, 1500-2500 m) and Lower Circumpolar Deep Water (LCDW, 2500-3000 m) by the Westerly winds (Figure 5.2) (Sloyan and Rintoul, 2001). Upper Circumpolar Deep Water and LCDW become oxygenated through atmospheric interactions when they reach the surface. Then, they are advected and subducted northward, feeding the AAIW and SAMW (Talley, 2013). Of the two water masses, AAIW is volumetrically the largest and dominates the oxygen supply to the ocean interior at low latitudes (Piola and Georgi, 1982).

Because AAIW has an essential role in ventilating the ocean interior, modelling studies have focused on AAIW to predict future oxygen variations (Downes et al., 2009; Rintoul and Bullister, 1999; Sallee et al., 2010). However, large uncertainties remain about the mechanisms driving AAIW formation in the modern ocean (Bostock et al., 2013). Hence, the reconstruction of past variations in oxygenation may be key to better predict future oxygen changes in the Southern Ocean. Previous studies provided conflicting results regarding the AAIW geometry in the Pacific sector of the Southern Ocean between glacial and interglacial periods. Using benthic foraminiferal $\delta^{18}O$, $\delta^{30}Si$ and $\delta^{13}C$, several authors reported AAIW contraction during glacial periods in the southwest Pacific sector of the Southern Ocean (Elmore et al., 2015; Pahnke and Zahn, 2005; Ronge et al., 2015; Rousseau et al., 2016). They proposed that this AAIW contraction decreased the ventilation at intermediate depths. However, other authors reported increased ventilation at intermediate depths in the southeast Pacific sector of the Southern Ocean (along the Chilean margin) during the last ice age (Muratli et al., 2009). They attributed this increased ventilation to greater AAIW formation. Based on a large scale data compilation, Jaccard and Galbraith (2012) and Jaccard et al. (2014) showed that intermediate depths of the Pacific Ocean were generally better oxygenated during the Last Glacial Maximum (LGM)

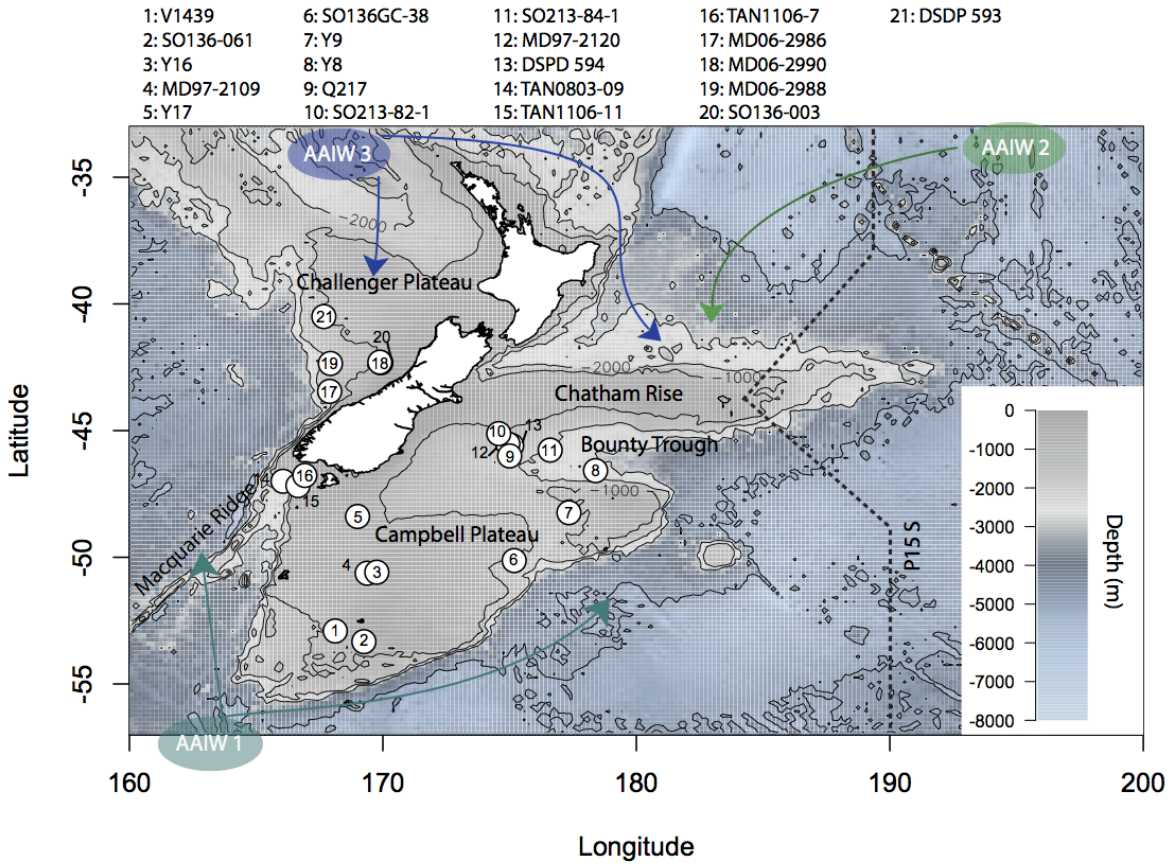

Figure 5.1: Map representing the bathymetry of the New Zealand region as well as the sediment core locations. The present AAIW circulation is also represented (Chiswell et al., 2015). Three different AAIW types are present in the New Zealand region. The position of the P15S section used in the Figure 5.2 is also represented.

compared to the Holocene, while abyssal waters remained poorly ventilated. However, a general lack of data from the Southern Ocean limits interpretations for this region. Consequently, uncertainties remain about past oxygen variations in the Pacific sector of the Southern Ocean. In particular, redox-sensitive metal proxies of bottom water oxygen have not been applied in the southwest Pacific.

In this study we aim to reconstruct the variations in the oxygen content of the intermediate waters of the southwest Pacific sector of the Southern Ocean, between the LGM and the Holocene. To this end, the Uranium (U) and Rhenium (Re) contents of 12 sediment cores from the New Zealand region were analysed (Campbell Plateau, Challenger Plateau, Bounty Trough) (Figure 5.1, 5.2, Table 5.1). This region is of particular interest because the shallow plateaux surrounding New Zealand are partially bathed by AAIW (Figure 5.1 and 5.2) (Bostock et al., 2013; Chiswell et al., 2015; Forcén-Vàzquez, 2014). The solubility of U and Re in seawater is

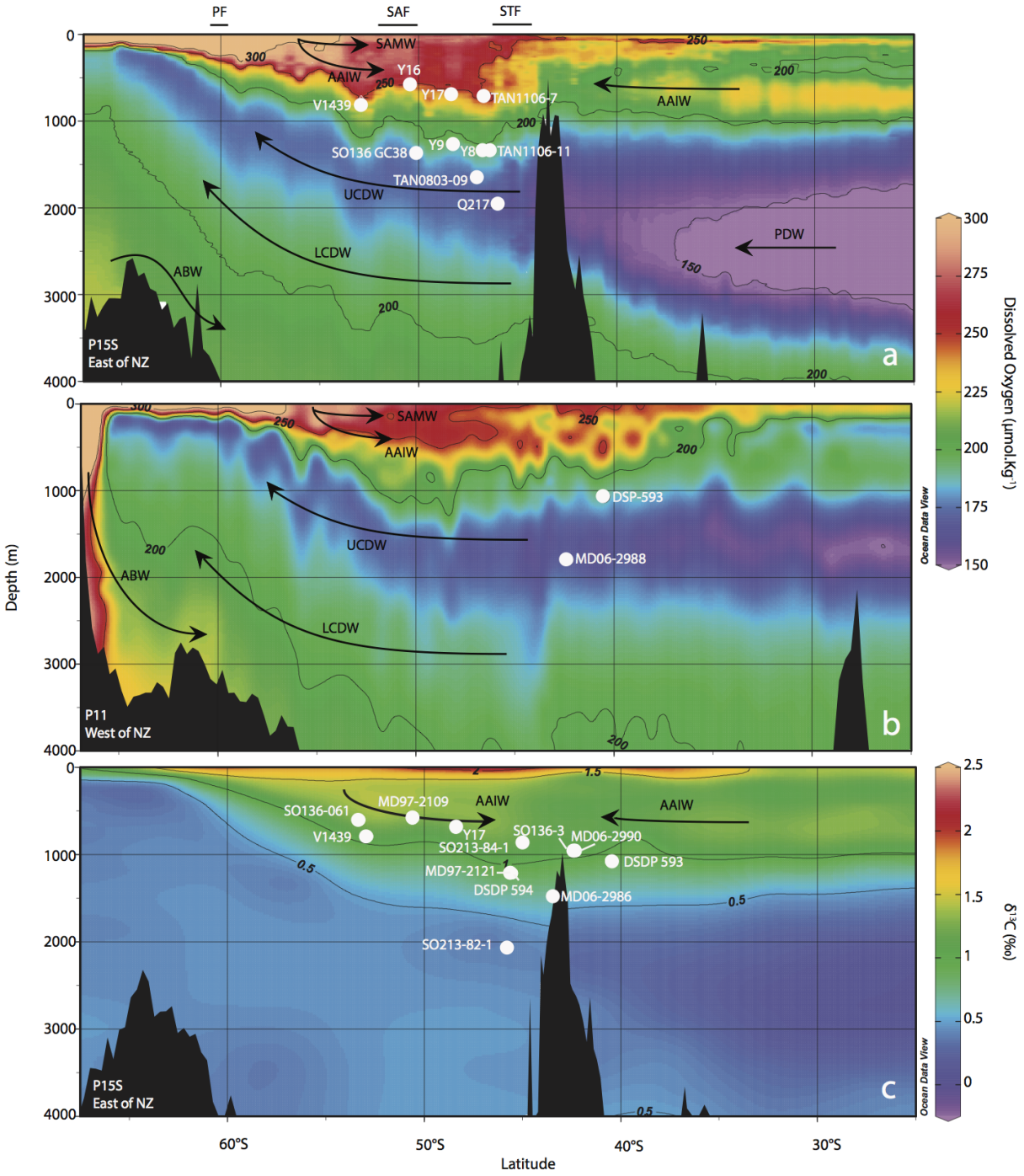

Figure 5.2: Oceanographic settings of the New Zealand region. Dissolved oxygen concentrations from the P15S (a) and P11 (b) sections (WOCE). The positions of the sediment cores analysed (aU, aRe) on the Campbell and Challenger Plateaux are represented on the top and bottom panels respectively. (c) Carbon isotope composition of Dissolved Inorganic Carbon ($\delta^{13}DIC$) from the P15S section of the World Ocean Data Base (WOCE). The positions of the sediment cores from which foraminifera $\delta^{13}C$ were used in this study were added. A simplified Southern Ocean circulation was adapted from Talley (2013). The southern source AAIW corresponds to the AAIW 1 while the northern source corresponds to the AAIW 2 and 3.

dependent on the seawater oxygen concentration. When the dissolved oxygen concentration decreases, U and Re are reduced from their soluble forms ($(UO_2(CO_3)_3)^{4-}$, $U(OH)_4$ and ReO_4^-) to insoluble forms ($UO_{2(s)}$ and $ReO_2.2H_2O$). This causes U and Re solid phases to accumulate in the sediments (Colodner et al., 1993; Crusius et al., 1996; Morford and Emerson, 1999; Tribovillard et al., 2006). This relationship between U, Re sediment enrichments and oxygen concentration is not linear and closer to a threshold. Consequently, U and Re concentration variations in sediment are a semi-quantitative proxy for oxygenation changes. In order to identify potential drivers of oxygen variations, circulation changes were also reconstructed using published stable carbon isotopes from benthic foraminifera ($\delta^{13}C$ benthic) from 12 sediment cores and determined $CaCO_3$ Mass Accumulation Rate (MAR) variations from 6 sediment cores in the studied region (Figure 5.1, 5.2, Table 5.1 and supplementary material see section 5.7.3).

Table 5.1: Summary of the sediment core locations, depths, proxies used and age models. Delta^{13}C data all correspond to benthic foraminifera $\delta^{13}C$. An indication of the water masses, bathing the core sites is included, based on the densities of the P15S section from the World Ocean database (WOCE). When the core is at the interface of two water masses, both are reported. (*)Previously published age models were used without modifications (**) New radiocarbon dates were used to update previously published age models

Core	Latitude	Longitude	Depth (m)	Location	Present water Mass bathing core site	Proxy used	References	Age model
DSDP 593	-40.5	167.67	1068	Challenger P.	AAIW	aU, aRe, $\delta^{13}C$	aU and aRe: This study; $\delta^{13}C$: Elmore et al. (2015)	Radio carbon (this study) + $\delta^{18}O$ alignment with LR04 stack (Martinez et al. 1994)
DSDP 594	-45.59	175.08	1204	Campbell P.	AAIW	$\delta^{13}C$ $CaCO_3$ MAR	$\delta^{13}C$: Nelson et al. (1993); $CaCO_3$ MAR: Carter et al. (2000)	(*) Nelson et al. (1993)
MD06-2986	-43.45	167.9	1477	Challenger P.	UCDW	$\delta^{13}C$	Ronge et al. (2015)	(*) Ronge et al. (2015)
MD06-2988	-42.35	167.93	1792	Challenger P.	UCDW	aU, aRe	This study	(*) Neil, NIWA (unpublished)
MD06-2990	-42.32	169.92	943	Challenger P.	AAIW	$\delta^{13}C$	Ronge et al. (2015)	(*) Ronge et al. (2015)
MD97-2109	-50.63	169.38	585	Campbell P.	AAIW-SAMW	$\delta^{13}C$	Sturm (2003)	(*) Sturm (2004)
MD97-2120	-45.53	174.93	1210	Campbell P.	AAIW	$\delta^{13}C$	Pahnke et al. (2005)	(*) Pahnke et al. (2005)
Q217	-46	175	1936	Campbell P.	UCDW	aU, aRe, $CaCO_3$ MAR	aU and aRe: This study; $CaCO_3$ MAR: Carter et al. (2000)	Radio carbon (this study)
SO136 GC38	-50.13	175.18	1359	Campbell P.	AAIW-UCDW	aU, aRe, $CaCO_3$ MAR	This study	(*) Neil et al. (2004)
SO136-003	-42.3	169.88	958	Challenger P.	AAIW	$\delta^{13}C$	Sturm (2003)	(*) Sturm (2003)
SO136-061	-53.33	169.25	602	Campbell P.	AAIW	$\delta^{13}C$	Sturm (2003)	(*) Sturm (2003)
SO213-82-1	-45.77	176.6	2066	Campbell P.	UCDW	$\delta^{13}C$	Ronge et al. (2015)	(*) Ronge et al. (2015)
SO213-84-1	-45.12	174.57	972	Campbell P.	AAIW	$\delta^{13}C$	Ronge et al. (2015)	(*) Ronge et al. (2015)
TAN0803-09	-47	166.06	1648	Campbell P.	UCDW	aU, aRe, $CaCO_3$ MAR	This study	Radio carbon (this study) + $\delta^{18}O$ alignment with LR04 stack (Neil, NIWA; unpublished)
TAN1106-11	-47.17	166.65	1349	Campbell P.	AAIW-UCDW	aU, aRe	This study	Radio carbon (this study) + $\delta^{18}O$ alignment with LR04 stack) (Neil, NIWA; unpublished)
TAN1106-7	-46.77	166.92	743	Campbell P.	AAIW	aU, aRe	This study	Radio carbon (this study) + $\delta^{18}O$ alignment with LR04 stack (Neil, NIWA; unpublished)
V1439	-52.91	168.12	791	Campbell P.	AAIW	aU, aRe, $\delta^{13}C$ (benthic foram.), $CaCO_3$ MAR	aU and aRe: This study; $CaCO_3$ MAR: This study, $\delta^{13}C$: Neil, NIWA (unpublished)	Radio carbon (Neil et al. 2004) + $\delta^{18}O$ alignment with LR04 stack (Neil et al. 2004)
Y16	-50.59	169.76	600	Campbell P.	AAIW	aU, aRe	This study	Radio carbon (**) + $\delta^{18}O$ alignment with LR04 stack (Neil et al. 2004)
Y17	-48.39	169	691	Campbell P.	AAIW	aU, aRe, $\delta^{13}C$	aU and aRe: This study; $\delta^{13}C$: Neil, NIWA (unpublished)	Radio carbon (**) + $\delta^{18}O$ alignment with LR04 stack (Neil et al. 2004)
Y8	-46.58	178.39	1335	Campbell P.	AAIW-UCDW	aU, aRe, $CaCO_3$ MAR	This study	(*) Ellwood et al. (2005)
Y9	-48.24	177.34	1267	Campbell P.	AAIW-UCDW	aU, aRe $CaCO_3$ MAR	aU and aRe: This study; $CaCO_3$ MAR: Carter et al. (2000), $\delta^{13}C$: Neil, NIWA (unpublished)	Radio carbon (Neil et al. 2004) + $\delta^{18}O$ alignment with LR04 stack (Neil et al. 2004)

5.2 Methods

5.2.1 Age models

Previously published age models were used without modifications for several sediment cores in this study (Table 5.1). For the other cores, mixed planktonic foraminiferal radiocarbon data were used to update or to construct new age models. The new radiocarbon measurements were conducted by the ANSTO Science Institute (Lucas Heights, Australia) using an accelerator mass spectrometer (AMS). All AMS dates (new and pre-existing) were calibrated with the MARINE13 calibration curve (Reimer et al., 2013) using the OxCal 4.2 platform (Ramsey, 2009). When foraminiferal $\delta^{18}O$ were available (Table 5.1), the radiocarbon and foraminiferal $\delta^{18}O$ were combined to construct/update the age models. The radiocarbon dates were used as tie points, and correlated the $\delta^{18}O$ records to the LR04 stack using the Analyseries software (Paillard et al., 1996).

5.2.2 Sediment preparation and digestion

Sixty mg of freeze-dried and homogenized sediments were digested in a mix of HCl, HNO_3 and HF using a pressure-assisted microwave (Milestone Ethos SK-12 microwave oven, Milestone, Shelton, CT, USA). The sample preparation has been described in detail previously in **chapter 2**.

5.2.3 Thorium, Uranium and Rhenium Analysis

The day prior to analysis, samples were heated on a hot plate at 60 °C for 24 hours and then diluted by a factor of 10 with milli-Q water. At this stage Indium (^{115}In) was added as an internal standard. An ELEMENT 2 sector field Inductively Coupled Plasma-Mass spectrometer (ICP-MS) from Thermo Fischer Scientific (Bremen, Germany) was used in low resolution ($m/\Delta m \approx 400$) to measure Re, Thorium (Th) and U concentrations, with isotopes ^{115}In, ^{185}Re, ^{232}Th and ^{238}U monitored. An external calibration method was used for the elemental quantification. The calibration solutions were prepared daily from 100 µg/mL standard solutions (QCD Analysts, Spring Lake, NJ, USA). Further details concerning sample handling procedures, as well as the instrument operating conditions can be found in **chapter 2**. The long-term reproducibility

of the method was tested over multiple digestions and analysis of D-178, a surface sediment from the Campbell Plateau. Across the 19 measurements over a three month period, standard deviations observed for Re, Th and U were less than 10% **chapter 2**.

5.2.4 Calculation of authigenic Uranium and Rhenium concentrations

The total U and Re concentrations in the sediments represent input from both the land (detrital U and Re) and the water (authigenic U and Re). Authigenic U, and Re (aU and aRe) concentrations were estimated as follows (M indicates Metal):

$$M_{authigenic} = M - (\frac{M}{Th})_{cc}.Th_{total} \tag{5.1}$$

The mean continental crust (cc) ratios $(U/Th)_{cc}$ and $(Re/Th)_{cc}$ used were 0.23 and $33e^{-6}$ respectively (Rudnick and Gao, 2003). Mean continental crust ratios were compared to the records available in the New Zealand region (EarthChem database) and the averaged crust ratios were found to be representative for the New Zealand region. Overall, the detrital fraction represented approximately 10 to 25% of the total U for the cores located on the Campbell Plateau, and 60 to 70% of the total U for the cores located in the Macquarie Ridge region. The detrital Re corrections were less than 1% of the total Re for the cores located on the Campbell Plateau and up to 8% for the cores in the Macquarie Ridge region.

5.3 Results

In the following sections the LGM and Holocene time slices have been defined as intervals ranging between 18 to 25 ka and 5 to 12 ka, respectively.

5.3.1 Authigenic Uranium and Rhenium

The sedimentary aU and aRe concentrations were higher during the LGM compared to the Holocene in the cores located on the Campbell and Challenger Plateaux (Figure 5.3). On the Campbell Plateau, the aU concentrations in V1439 were 4.5 mg/kg higher during the LGM

compared to the Holocene. However, for the other sites on the Campbell Plateau (Y16, Y17, SO136GC-38, Y9), the aU concentrations were only 3 mg/kg higher during the LGM. For the same cores aRe concentrations were generally 10 to 20 µg/kg higher during the LGM. On the Challenger Plateau (cores MD06-2988 and DSDP 593) the aU and aRe concentrations were on average 2 mg/kg and 7.5 µg/kg higher respectively, during the LGM relative to the Holocene. Overall, larger aU and aRe concentration differences are observed between the LGM and the Holocene on the Campbell Plateau compared to the Challenger Plateau.

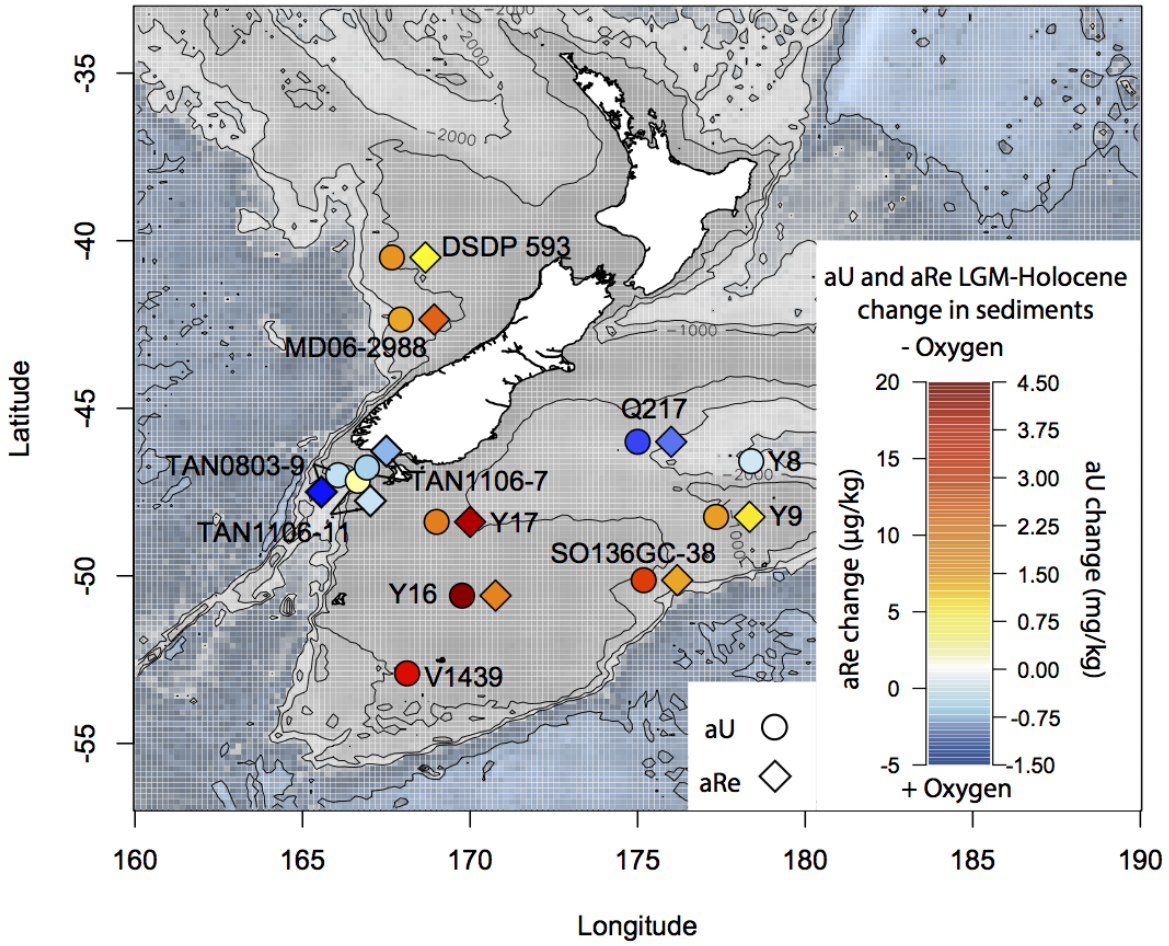

Figure 5.3: Difference in authigenic U and Re (aU: dots and aRe: diamonds) between the LGM (18-25 ka) and the Holocene (5-12 ka). Positive values indicate higher aU and aRe concentrations in the sediment during the LGM, and lower inferred bottom water oxygen concentrations.

The sediment cores located in the Bounty Trough area (Y8 and Q217) as well as the cores located in the Solander Trough, which sits between the Macquarie ridge and the Campbell

Plateau (TAN1106-11, TAN1106-07, TAN0803-09) had slightly lower aU and aRe concentrations during the LGM compared to the Holocene. However, the differences for these five cores were modest: aU and aRe differences between the LGM and the Holocene never exceeded 1.5 mg/kg and 5 µg/kg respectively.

5.3.2 Benthic $\delta^{13}C$

To determine whether the oxygen concentrations were primarily controlled by changes in ocean circulation the existing benthic carbon isotope data for this region were compiled (both published and unpublished). The benthic foraminifera $\delta^{13}C$ values observed for the Challenger and Campbell Plateaux during the Holocene agree well with the modern Dissolved Inorganic Carbon (DIC) values (Figure 5.1 and 5.4).

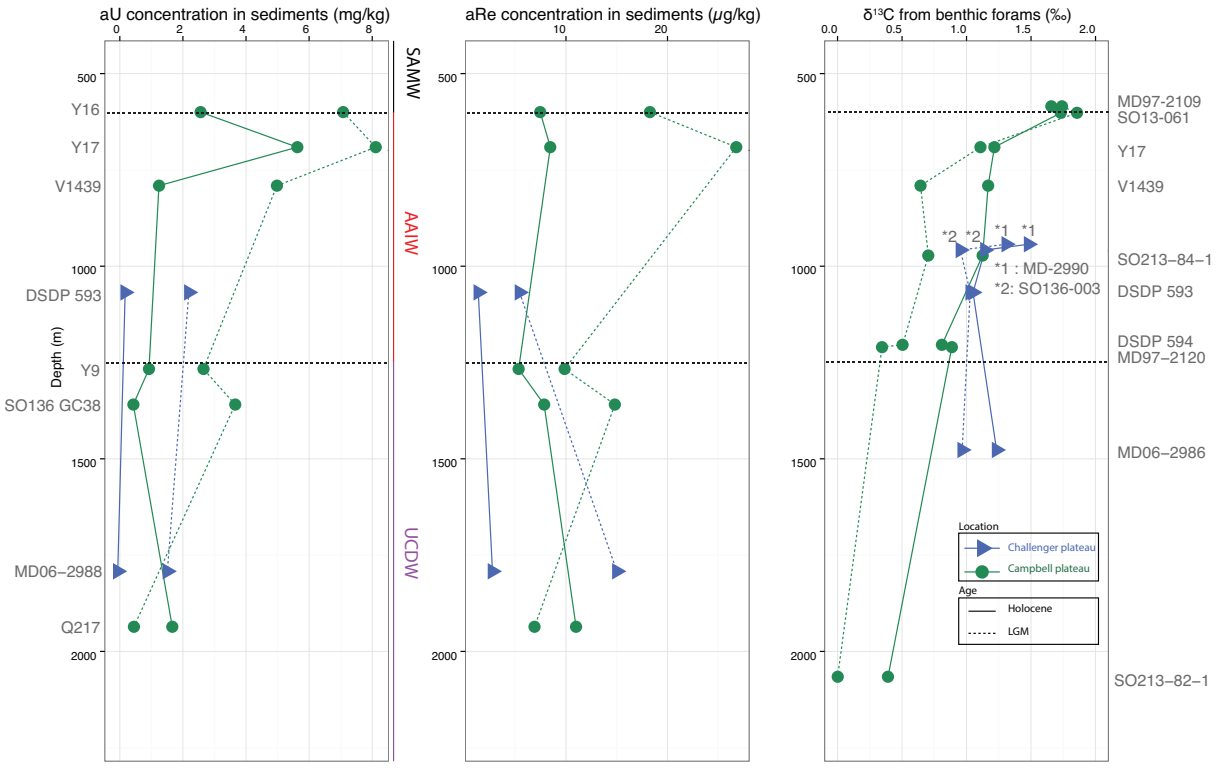

Figure 5.4: Authigenic U and Re (aU and aRe) and benthic foraminifera $\delta^{13}C$ as a function of core depth for LGM (dashed; 18-25 ka) and Holocene (plain; 5-12 ka) time slices on the Challenger (blue triangles) and Campbell (green circles) Plateaux.

The benthic foraminifera $\delta^{13}C$ variations with depth show a dramatic regional difference between the Campbell and Challenger Plateaux (Figure 5.4). On the Challenger Plateau, similar $\delta^{13}C$ values are observed during the LGM and the Holocene at all depths. However, on the

Campbell Plateau, below 600 m, cores show large $\delta^{13}C$ increases (0.4-0.85‰) between the LGM and the Holocene, increases that are larger than the whole-ocean glacial-interglacial $\delta^{13}C$ change produced from the difference in the terrestrial carbon reservoir (0.34‰, Figure 5.4) (Peterson et al., 2014). The $\delta^{13}C$ values of V1439, SO213-84-1, DSDP 594, and MD97-2120, representing the AAIW during the Holocene, were typical of the UCDW during the LGM (Figure 5.4). Cores on the Campbell Plateau above 600m (MD97-2109, SO13-061 and Y17) show no $\delta^{13}C$ change between the LGM and the Holocene (Figure 5.4).

5.4 Discussion

In this work, changes in redox sensitive metal concentrations were interpreted in terms of oxygenation changes at the water-sediment interface. By this interpretation the data presented here suggest that the intermediate depths of the southwest Pacific sector of the Southern Ocean, where AAIW flows presently, were depleted in oxygen during the LGM compared to the Holocene. During the LGM, at typical AAIW depths (500-1200 m), the aU and aRe concentrations were higher than in sediments presently bathed by UCDW (1500-2500 m). In contrast, waters of the Solander Trough region (where TAN1106-07, TAN1106-11 and TAN0803-9 were retrieved) were depleted in aU and aRe during the LGM compared to the Holocene. As several other factors may drive changes in aM concentrations, we address each of these in turn.

Sedimentation rates can influence the incorporation of aM in the sediments independently of any bottom water oxygenation changes (Tribovillard et al., 2006). However, no relationship was found between sedimentation rates and aM concentration variations, suggesting sedimentation rate changes are not the main driver of aM changes (Supplementary material, see section 5.7.2.

As much as sedimentation rate changes, post-deposition remobilisation of U and Re in the sediments by oxygen rich waters during the Holocene can interfere with the use of aU and aRe as proxies for oxygen changes (Crusius and Thomson, 2000, 2003). Particularly, because most sites in this study have slow sedimentation rates they can be extremely affected by remobilisation (see discussion in supplementary material section 5.7.2). To limit the impact of remobilisation on aU and aRe time slices were defined across large time intervals. Moreover, the large number of sites presented here and the coherent spatial and temporal aM variations between these sites, show that remobilisation is not a dominant driver of aM variations in the sediments of this study.

Finally, the strong correlation between aU and $\delta^{13}C$ as well as the similar behaviour between aU and aRe enrichments, increase the confidence that oxygen changes drove the aM concentration variations (Figure 5.3, 5.4 and 5.5).

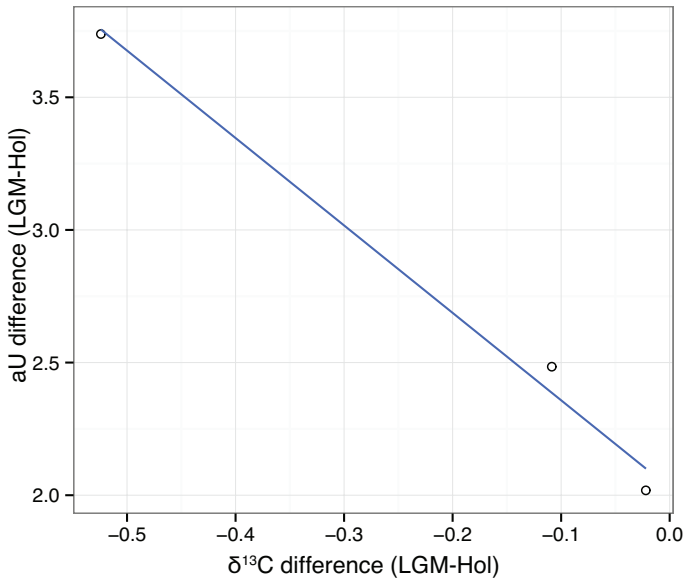

Figure 5.5: Comparison between the LGM (18-25 ka) - Holocene (5-12 ka) difference in benthic foraminifera $\delta^{13}C$ and aU for the three sediment cores in this study where both parameters were measured. From left to right, V1439, Y17 and DSDP 593.

The following sections discuss the mechanisms that could possibly have driven the substantial oxygen changes inferred from aU and aRe variations between the LGM and the Holocene.

5.4.1 Export production as a dissolved oxygen driver

Since labile organic matter is supplied by export production (EP), an increase in EP leads to oxygen depletion in the ocean interior. As a consequence, increased EP in the New Zealand region during the LGM could potentially explain aU and aRe enrichments in the sediments of the Challenger and Campbell Plateaux. In **chapter 4** it is shown that EP stayed low and rather constant over the Campbell and Challenger Plateaux since the LGM. This result is in agreement with previous findings (Ellwood et al., 2005) and rules out increased organic matter remineralisation as a major driver for oxygen changes between the LGM and the Holocene over the Campbell and Challenger Plateaux. However, at site TAN0803-09, the reconstructions showed increased EP during the deglaciation and Holocene compared to the LGM. This was likely caused by a southward shift of the highly productive subtropical front over the core location

during the deglaciation (12-18 ka) (Bostock et al., 2015). Therefore, we suggest that the high aU and aRe values observed during the Holocene for the three Solander Trough cores may have been influenced by increased EP due to changes in ocean circulation during the Holocene.

5.4.2 Shallower and deoxygenated glacial AAIW above the Campbell Plateau

By plotting the temporal aU and aRe variations along depth, it is apparent that depth and thus the water mass geometry has been the primary driver of change on the Campbell Plateau between the LGM and the Holocene (Figure 5.4). The higher oxygen concentrations observed at intermediate depths over the Campbell Plateau during the Holocene compared to the LGM could be partly explained by a deepening of the AAIW-UCDW boundary between the LGM and the Holocene. During the Holocene, this deepening would have brought oxygenated AAIW to sites that were bathed by oxygen-depleted UCDW during the LGM. Such a change could help explain the aU and aRe variations at core sites V1439, Y16, Y17, SO136G-C38 and Y9. Similarly, deepening the UCDW-LCDW boundary between the LGM and the Holocene could explain the higher aM concentrations observed during the Holocene at deeper sites (Q217 and Y8) because UCDW has a lower oxygen concentration than LCDW (Figure 5.2).

Several studies using benthic foraminifera $\delta^{13}C$ variations in sediment cores found that the AAIW-UCDW boundary deepened between the LGM and the Holocene in the Pacific sector of the Southern Ocean (Pahnke and Zahn, 2005; Ronge et al., 2015). Even though several factors such as differences in biological productivity or air-sea gas exchange can compromise the use of $\delta^{13}C$ as a circulation proxy (Schmittner et al., 2013), in this region, circulation is the main driver of $\delta^{13}C$ changes (Pahnke and Zahn, 2005; Ronge et al., 2015). The benthic $\delta^{13}C$ data from the Campbell Plateau compiled here agree with these findings (Figure 5.3 and 5.4). On the Campbell Plateau the large $\delta^{13}C$ variations observed ($\approx 0.5‰$) cannot only be driven by the glacial-interglacial reservoir change (0.34‰). Therefore, these variations show that the AAIW-UCDW boundary, presently around 1200 m, resided above 790 m during the LGM. Due to a lack of deeper cores, we cannot constrain how deep the UCDW extended during the LGM. A mix of LCDW and UCDW bathed the deepest core site (SO213-82-81, 2066 m) during the LGM (Figure 5.4). Consequently the glacial boundary between the UCDW and LCDW was

shallower compared to the Holocene and must have resided between 1210 m and 2066 m. On the Campbell Plateau, above 600 m, the data do not display lower glacial $\delta^{13}C$. This result is in agreement with a recent study which suggests that the glacial-interglacial terrestrial carbon reservoir change was only manifested as a 0.018‰ change above 500 m (Peterson et al., 2014). Therefore, we suggest that AAIW continued to bathe core sites above 600 m on the Campbell Plateau during the LGM.

Redox metal variations between the LGM and the Holocene were the largest where there were the greatest changes in benthic $\delta^{13}C$ (Figure 5.5). This suggests change in the water column geometry (AAIW-UCDW boundary deepening) as a major driver of oxygen change at intermediate depths. Moreover, a shallower AAIW during the LGM compared to the Holocene could also explain the significantly reduced $CaCO_3$ MARs on the northern edge of the Campbell Plateau and in the Bounty Trough during the LGM (see details in supplementary material section 5.7.3). These lower glacial $CaCO_3$ MARs could partially result from increased dissolution associated with the intrusion of corrosive PDW (Pacific Deep Water) at intermediate depths (Ronge et al., 2016). A shallower AAIW during the LGM would have allowed this PDW intrusion at depths presently occupied by AAIW.

A shallower AAIW during the LGM above the Campbell Plateau can be explained by a decrease in the AAIW formation rate, or a northward displacement of AAIW formation region (Figure 5.6). A decrease in the AAIW production could have resulted from a shift of the westerlies towards lower latitudes (Downes et al., 2011; Voigt et al., 2015). Some authors also suggested that during the LGM, increased sea-ice cover would have increased buoyancy forcing (Pahnke and Zahn, 2005), thereby decreasing AAIW density, limiting its subduction depth (Ronge et al., 2015). Finally, Watson et al. (2015) suggested that during the LGM, increased sea-ice extent influenced the slopes of the Southern Ocean isopycnals, which influence the upwelling in the Southern Ocean. This study suggested that AAIW and Antarctic Bottom Water (AABW) are competing for a common water source and that during the LGM, AABW formation was potentially increased, consequently decreasing AAIW formation.

Alternatively to a decrease in the AAIW formation, the shallower AAIW during the LGM above the Campbell Plateau could be explained by a northward displacement of the AAIW production area. Antarctic Intermediate Water extends deeper as it flows northward. Presently, the well-oxygenated core of AAIW extends to 500 m deep at 60 °S and extends to 1500 m at 50

°S (Figure 5.2). Therefore, a northward displacement of the AAIW formation area during the LGM could have resulted in an AAIW shoaling above the Campbell Plateau. Such a northward displacement of the AAIW formation region could have been driven by a northward displacement of the westerly wind belt, as well as a northward displacement of the Subantarctic front (SAF) (Downes et al., 2011).

On the Campbell Plateau a shallower AAIW during the LGM can explain the aM and $\delta^{13}C$ variations of V1439, Y9, SO136GC-38, Y8 and Q217. However, although AAIW continued bathing the shallow sites Y16 and Y17 since the LGM, as inferred by unchanging $\delta^{13}C$ at these depths, higher glacial aU and aRe concentrations, relative to the Holocene, are observed in their sediments (Figure 5.4). This suggests lower oxygen content of AAIW during the LGM compared to the Holocene. Winds influence the AAIW oxygen content by controlling the duration and rate of exchange with the atmosphere (Russell and Dickson, 2003). Therefore, decreased westerly winds could have decreased the AAIW oxygen content. During the LGM, even if the westerlies intensity was not lower, their mean position was located further north (Kohfeld et al., 2013). Moreover, the northward advection of the westerlies is thought to have been greater than that of the fronts (Ronge et al., 2015). Because the AAIW formation region is constricted south of the SAF, the greater northward advection of the westerlies compared to the SAF would lead to a reduction of the wind stress in the subantarctic regions, where AAIW is formed. This could have decreased the oxygen content of AAIW during the LGM and countered the influence of colder temperatures. Alternatively, reduced wind stress in the AAIW formation region could also have decreased AAIW formation rate and circulation velocity. This would have given more time for remineralisation processes to consume oxygen along the path, before reaching the core sites. All the potential drivers of AAIW deoxygenation mentioned above are consistent with a decrease in AAIW formation. However, in the case of the northward advection of the formation region, lower glacial AAIW content can be explained by greater carbon export in the formation, which would have increased oxygen consumption.

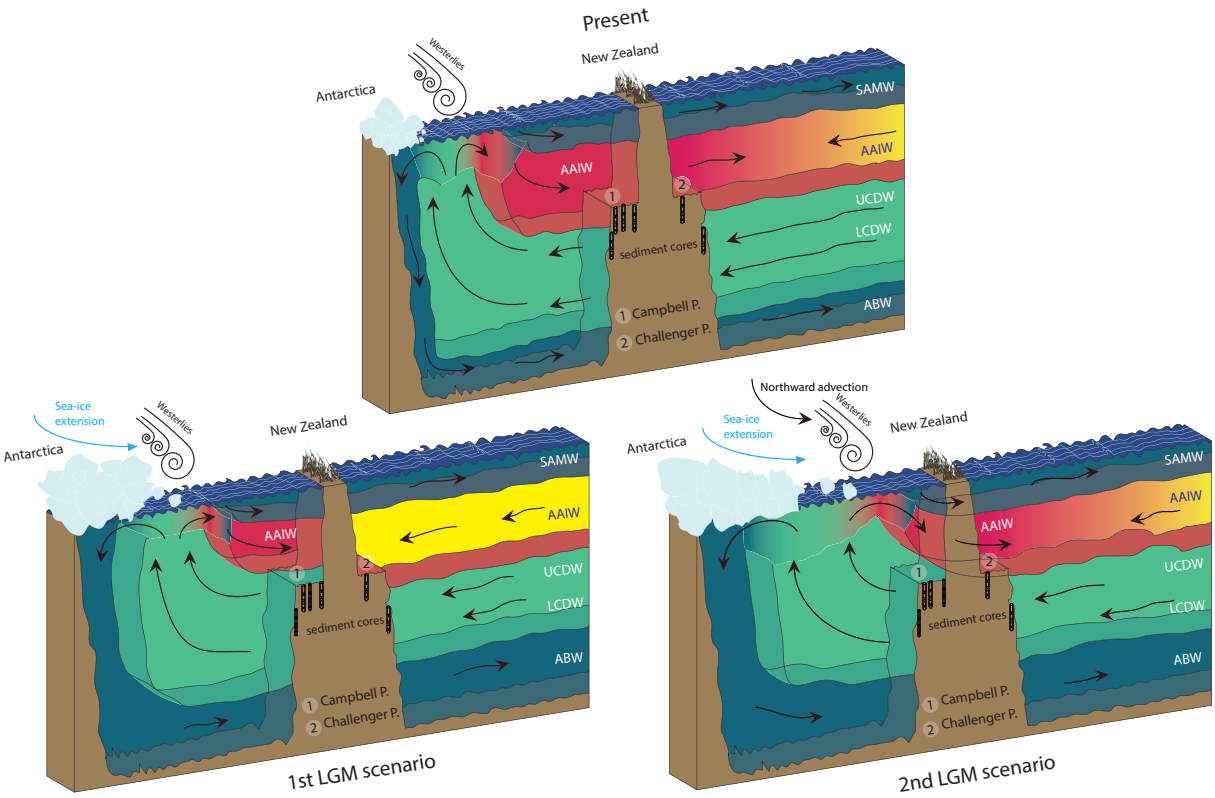

Figure 5.6: Schematics of the two different scenarios that can explain the differences between the Campbell and Challenger Plateaux $\delta^{13}C$ and redox-sensitive metal data. On the top panel, modern circulation. On the bottom left panel the southern source AAIW (red) shoaled and left the Campbell Plateau partly bathed by oxygen depleted UCDW, while the deoxygenated northern source AAIW (yellow) intensified and bathed the Challenger Plateau, with no $\delta^{13}C$ change. On the bottom right panel, the AAIW subducting region was shifted northward. As a consequence the southern source AAIW did not reach the Campbell Plateau. However, the Challenger Plateau continued to be bathed by AAIW because it is located 10° further north compared to the Campbell Plateau.

5.4.3 Reconciling differences between Campbell and Challenger Plateaux

On the Campbell Plateau both redox-sensitive metals and $\delta^{13}C$ suggest that AAIW was shallower during the LGM compared to the Holocene. In contrast, on the Challenger Plateau, at DSDP 593, un-changing $\delta^{13}C$ values, typical of AAIW, suggest this site has been bathed by AAIW during both the LGM and the Holocene (Figure 5.4 and 5.5). Together, these data indicate that, during the LGM, AAIW was significantly shallower above the Campbell Plateau compared to the Challenger Plateau, even though the two plateaux span similar depths. In the following sections it is shown that two scenarios are consistent with the aM and $\delta^{13}C$ variations

observed on both plateaux (Figure 5.6).

The northward displacement of the AAIW production area, mentioned previously, could explain why the Challenger Plateau continued to be bathed by AAIW while the Campbell Plateau was partly bathed by UCDW (Figure 5.6). The Challenger Plateau is located 10° further north compared to the Campbell Plateau; therefore, northward displacement of the AAIW formation area during the LGM could have maintained AAIW flowing on the Challenger Plateau while being too far north to reach the intermediate depths of the Campbell Plateau (Figure 5.6). Moreover, the aU and aRe data at DSDP 593 are consistent with the ones at Y16 and Y17, on the Campbell Plateau, and also suggest a lower AAIW oxygen content during the LGM compared to the Holocene (Figure 5.4).

Alternatively, a change in the AAIW source bathing the Challenger Plateau could also explain the oxygen changes and also why the Challenger Plateau continued to be bathed by AAIW while the Campbell Plateau was partly bathed by UCDW (Figure 5.4 and 5.6). Bostock et al. (2013) showed that there are three types of AAIW present around New Zealand (Figure 5.1). The first type is a southern source AAIW, formed locally in the southwest Pacific sector of the Southern Ocean (AAIW 1). The second type comes from the southeast Pacific via the South Pacific gyre (AAIW 2). Finally, AAIW 3, which is present in the Tasman Sea, is a mixture between the AAIW from the southeast Pacific source and surface waters from the Tasman Sea. In terms of oxygen concentrations, AAIW 1 is younger and has higher oxygen content than AAIW 2 and 3 (Chiswell et al., 2015). Presently the southern source AAIW (AAIW 1) is bathing the Challenger and Campbell Plateaux (Chiswell et al., 2015). However, it is possible that during the LGM a transition of the AAIW type bathing the Challenger Plateau occurred between the southern source AAIW (AAIW 1) and a northern source (AAIW 3). This change may not have modified the $\delta^{13}C$ of the Challenger Plateau cores because today northern and southern AAIW sources have similar $\delta^{13}C$ signatures (Figure 5.2). However, because AAIW 3 is poorer in oxygen compared to AAIW 1, it may have decreased the oxygen concentrations above the Challenger Plateau, consistent with the aU and aRe variations. Muratli et al. (2009) revealed that the southeast Pacific AAIW production during the LGM was higher. The southeast Pacific AAIW is the source of the AAIW types 2 and 3, both present around New Zealand (Figure 5.1). Therefore, increased AAIW production in the southeast Pacific during the LGM could have resulted in the expansion of the AAIW type 3 in the New Zealand region. In this case, expanded AAIW type 3

could have bathed the Challenger Plateau without reaching the Campbell Plateau (Figure 5.6). This phenomenon would have allowed the Challenger Plateau to be constantly bathed by AAIW during the LGM-Holocene transition; while a shallower, deoxygenated glacial AAIW type 1 did not reach the Campbell Plateau intermediate depths. The shallow AAIW 1 above the Campbell Plateau was likely driven by a decrease in the AAIW 1 production rate, as mentioned earlier.

In summary two scenarios are consistent with the aM and $\delta^{13}C$ data of the Campbell and Challenger Plateaux (Figure 5.6). Future work investigating Neodymium isotopic composition (ε_{Nd}) change between the LGM and the Holocene has the potential to reveal which of these two scenarios occurred. In the Pacific sector of the Southern Ocean, AAIW ε_{Nd} signature changes from around -8 close to its formation region to around -6.5 at 32°S (Molina-Kescher et al., 2014). Consequently, the AAIW 2 and 3 have a more radiogenic ε_{Nd} signature compared to AAIW 1 and therefore northern and southern AAIW sources can be differentiated in the New Zealand region. Accordingly, ε_{Nd} determination from foraminifera preserved in sediments at sites bathed by AAIW on the Challenger Plateau could resolve if a change of AAIW source occurred between the LGM and the Holocene (Noble et al., 2013).

5.5 Conclusion

This study shows that the intermediate depths of the southwest Pacific sector of the Southern Ocean were less oxygenated during the LGM compared to the Holocene.

In the Solander Trough this was likely partially explained by an increase in EP from the shifting of the subtropical front over the region during the deglaciation.

On the Campbell Plateau, such a change was likely associated with shallower southern AAIW (AAIW 1), leaving deeper parts of the plateau bathed by UCDW. Such a shallower glacial AAIW overlaying the Campbell Plateau was associated with either a decrease in AAIW formation or a northward shift in the AAIW formation region. However, this change in geometry can only explain part of the glacial oxygen depletion observed. Therefore, we also suggest that the AAIW 1 oxygen content was lower during the LGM.

Even though the Challenger Plateau spans similar depths to the Campbell Plateau, $\delta^{13}C$ variations show that AAIW continued overlaying the Challenger Plateau. Therefore, we hypothesise that two different scenarios could explain the lower glacial oxygen levels observed there

and why the Challenger Plateau continued to be bathed by AAIW while the Campbell Plateau was partly bathed by UCDW. First a change in the dominant AAIW source, from a southern source AAIW (AAIW 1) to an oxygen poorer, northern source AAIW (AAIW 3) can explain these results. Alternatively, lower glacial oxygen content of AAIW 1 coupled with the northward displacement of the AAIW 1 formation area, could also explain this trend.

5.6 Acknowledgements

This work was supported by the Australia/New Zealand IODP Consortium (ANZIC), and by an ARC Future Fellowship awarded to Zanna Chase [grant number FT120100759]. Access to ICP-MS instrumentation was supported through ARC LIEF funds [grant number LE0989539]. Samuel L. Jaccard was funded by the Swiss National Foundation (grant PP00P2-144811). Radiocarbon analyses at ANSTO were supported by a AINSE grants ALNGRA11081 and ALNGRA14503.

5.7 Supplementary material

5.7.1 Pangaea database compiling the new data created during this section of the PhD

https://doi.pangaea.de/10.1594/PANGAEA.864666

5.7.2 Sedimentation rates do not drive authigenic Uranium and Rhenium variations

In this study aU and aRe sediment concentrations were used as proxies for oxygen changes. At most sites, aU and aRe enrichments were observed in the sediments during the LGM compared to the Holocene, which was interpreted as a glacial deoxygenation. However, changes in the sedimentation rates can influence the amount of U and Re precipitated in the sediment independently of any redox-condition changes (Crusius and Thomson, 2000, 2003; McManus et al., 2005; Tribovillard et al., 2006). Therefore, sedimentation rate changes can interfere with the use of aU and aRe as oxygenation proxies. Table 5.2 compiles sedimentation rates at different sites

during the Holocene and the LGM. Overall, no coherent pattern of sedimentation rate changes between the LGM and the Holocene can explain the aU and aRe glacial enrichments observed in the New Zealand region. Three cores had moderately higher sedimentation rates during the LGM compared to the Holocene. Three cores had lower sedimentation rates during the LGM compared to the Holocene and three cores had no change. Only TAN0803-09 and TAN1106-11 had noticeably higher sedimentation rates during the LGM compared to the Holocene. However, these two cores had higher aU and aRe concentrations during the Holocene compared to the LGM. Therefore, we conclude that the aU and aRe variations observed in this study are not simply the product of sedimentation rate changes.

Table 5.2: Sedimentation rates during the Holocene and the LGM at different core sites

Core	Holocene sed.rate (cm/ka)	LGM sed.rate (cm/ka)
DSDP 593	3.3	3.3
Q217	2.2	2.2
SO136GC-38	1.7	3.3
TAN0803-09	4.9	19.8
TAN1106-07	7.4	8.7
TAN1106-11	5.7	16.2
V1439	2.9	3.9
Y8	3.9	3.9
Y9	6	1.2
Y16	7.2	1
Y17	7.5	1.5

5.7.3 Calcium carbonate mass accumulation rate variations in the New Zealand region

On the Campbell Plateau, V1439 and SO136GC-38 had similar CaCO3 MARs between the LGM and the Holocene (Figure 5.7). However, in the Bounty Trough periphery a significant increase in $CaCO_3$ deposition was observed 14 ka ago. This increase was particularly intense at site DSDP 594, where the $CaCO_3$ deposition increased from 0.5 $g.cm^{-2}.ka^{-1}$ during the LGM to over 4 $g.cm^{-2}.ka^{-1}$ during the late Holocene. At Y9, similar $CaCO_3$ MAR variations were observed here compared to the Th-normalised $CaCO_3$ reported in **chapter 4**, which suggests that the trends observed here are not related to sediment focussing. Therefore, the lower $CaCO_3$ accumulation during the LGM compared to the Holocene could be explained by decreased $CaCO_3$

production during the LGM or increased glacial dissolution. Several authors reported increased $CaCO_3$ dissolution at intermediate depths north of the Chatham Rise (1200-3290 m) during the glacial periods (Cobianchi et al., 2015; Pahnke and Zahn, 2005). They suggested that the increased dissolution observed was associated with the presence of old and corrosive PDW overlaying their core sites. Bostock et al. (2011) published a detailed study of the lysocline in the New Zealand region. They found that today the lysocline of the New Zealand region is around 4800 m deep with some minor local variations. They also studied the corrosivity of the different water masses, and showed that PDW is the most corrosive water mass of the region. It is unlikely that the lysocline deepened by more 2500 m throughout the New Zealand region between the LGM and the Holocene; however a glacial local intrusion of PDW limited to the Bounty Trough would explain the large decrease of the $CaCO_3$ MARs in the sediment cores located in this vicinity during the LGM. This possible intrusion of PDW at intermediate depths is in agreement with recent studies, suggesting glacial PDW expansion at shallower depths (Ronge et al., 2016). It also adds support to the idea of a shallower AAIW during the LGM compared to the Holocene. A shallower AAIW during the LGM would have allowed PDW intrusion at intermediate depths, presently occupied by AAIW.

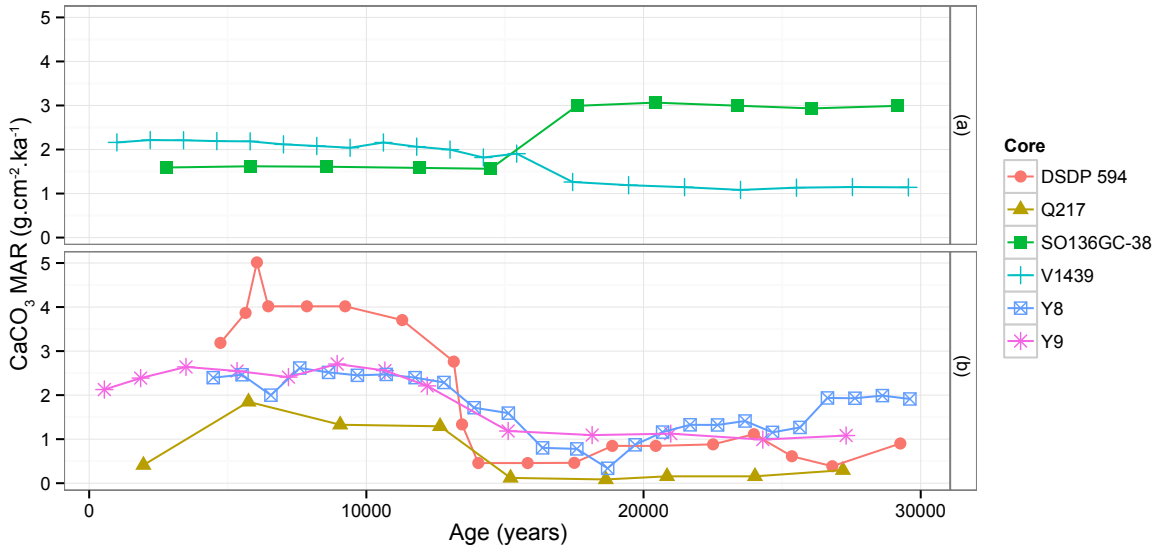

Figure 5.7: $CaCO_3$ MAR variations. The top panel (a) represents the small $CaCO_3$ MAR variations of two sediment cores located on the Campbell Plateau, while the bottom panel (b) represents the larger $CaCO_3$ MAR variations of four sediment cores in the Bounty Trough vicinity.

Method

Previously published $CaCO_3$ MARs were used in this study without any modifications for Y9, DSDP 594 and Q217 (Carter et al., 2000). Calcium carbonate MARs ($g.cm^{-2}.ka^{-1}$) for V1439, SO136GC-38 and Y8 were calculated as: $MAR = W_f.LSR.\rho$; where W_f is the $CaCO_3$ weight fraction, LSR is the linear sedimentation rate ($cm.ka^{-1}$), and ρ is the dry bulk density ($g.cm^{-3}$). In the absence of dry bulk density data for V1439, SO136GC-38 and Y8, ρ was estimated from the $CaCO_3$ concentrations, as per Carter et al. (2000). Calcium carbonate concentrations previously published by Neil et al. (2004) were used to calculated V1439 and SO136GC-38 $CaCO_3$ MARs, while $CaCO_3$ concentrations from Ellwood et al. (2005) were used to calculate Y8 $CaCO_3$ MARs.

5.7.4 Radiocarbon ages and uncertainties

Table 5.3: Radiocarbon ages and incertitudes used to develop new age models.

Cores	Calibrated age BP (years)
DSDP 593	7864±274 at 0.5 cm
	12381.5±427 at 15.5 cm
	20533±451 at 27.5 cm
	23846±538 at 45.5 cm
Q217	9430±254 at 24.5 cm
TAN0803-09	3332±200 at 5.5 cm
	16474±459 at 70.5 cm
TAN1106-11	2499±259 at 1.5 cm
	12962±310 at 61.5 cm
	13690±519 at 121.5 cm
TAN1106-7	6316±110 at 1.5 cm
	11709±631 at 41 cm
	19728±510 at 111 cm
Y16	4905±255 at 0.5 cm
	8273±274 at 24.5 cm
	41004±1254 at 48.5 cm
Y17	3802±189 at 0.5 cm
	8582±164 at 36.5 cm
	22262±472 at 56.5 cm

References

Bostock, H. C., Hayward, B. W., Neil, H. L., Currie, K. I., and Dunbar, G. B.: Deep-water carbonate concentrations in the southwest Pacific, Deep Sea Research Part I: Oceanographic Research Papers, 58, 72–85, 2011.

Bostock, H. C., Barrows, T. T., Carter, L., Chase, Z., Cortese, G., Dunbar, G. B., Ellwood, M., Hayward, B., Howard, W., Neil, H. L., Noble, T. L., Mackintosh, A., Moss, P. T., Moy, A. D., White, D., Williams, M. J. M., and Armand, L. K.: A review of the Australian-New Zealand sector of the Southern Ocean over the last 30 ka (Aus-INTIMATE project), Quaternary Science Reviews, 74, 35–57, 2013.

Bostock, H. C., Hayward, B. W., Neil, H. L., Sabaa, A. T., and Scott, G. H.: Changes in the position of the Subtropical Front south of New Zealand since the last glacial period, Paleoceanography, 30, 824–844, 2015.

Carter, L., Neil, H. L., and McCave, I. N.: Glacial to interglacial changes in non-carbonate and carbonate accumulation in the SW Pacific Ocean, New Zealand, Palaeogeography, Palaeoclimatology, Palaeoecology, 162, 333–356, 2000.

Chiswell, S. M., Bostock, H. C., Sutton, P. J., and Williams, M. J.: Physical oceanography of the deep seas around New Zealand: a review, New Zealand Journal of Marine and Freshwater Research, 49, 1–32, 2015.

Cobianchi, M., Mancin, N., Lupi, C., Bordiga, M., and Bostock, H. C.: Effects of oceanic circulation and volcanic ash-fall on calcite dissolution in bathyal sediments from the SW Pacific Ocean over the last 550ka, Palaeogeography, Palaeoclimatology, Palaeoecology, 429, 72–82, 2015.

Colodner, D. C., Boyle, E. A., and Edmond, J. M.: Determination of rhenium and platinum

in natural waters and sediments, and iridium in sediments by flow injection isotope dilution inductively coupled plasma mass spectrometry, Analytical Chemistry, 65, 1419–1425, 1993.

Crusius, J. and Thomson, J.: Comparative behavior of authigenic Re, U, and Mo during reoxidation and subsequent long-term burial in marine sediments, Geochimica et Cosmochimica Acta, 64, 2233–2242, 2000.

Crusius, J. and Thomson, J.: Mobility of authigenic rhenium, silver, and selenium during postdepositional oxidation in marine sediments, Geochimica et Cosmochimica Acta, 67, 265–273, 2003.

Crusius, J., Calvert, S., Pedersen, T., and Sage, D.: Rhenium and molybdenum enrichments in sediments as indicators of oxic, suboxic and sulfidic conditions of deposition, Earth and Planetary Science Letters, 145, 65–78, 1996.

Diaz, R. J. and Rosenberg, R.: Spreading dead zones and consequences for marine ecosystems, Science, 321, 926–929, 2008.

Downes, S. M., Bindoff, N. L., and Rintoul, S. R.: Impacts of climate change on the subduction of mode and intermediate water masses in the Southern Ocean, Journal of Climate, 22, 3289–3302, 2009.

Downes, S. M., Budnick, A. S., Sarmiento, J. L., and Farneti, R.: Impacts of wind stress on the Antarctic Circumpolar Current fronts and associated subduction, Geophysical Research Letters, 38, 2011.

Ellwood, M. J., Kelly, M., Neil, H., and Nodder, S. D.: Reconstruction of paleo–particulate organic carbon fluxes for the Campbell Plateau region of southern New Zealand using the zinc content of sponge spicules, Paleoceanography, 20, 2005.

Elmore, A. C., McClymont, E. L., Elderfield, H., Kender, S., Cook, M. R., Leng, M. J., Greaves, M., and Misra, S.: Antarctic Intermediate Water properties since 400 ka recorded in infaunal (Uvigerina peregrina) and epifaunal (Planulina wuellerstorfi) benthic foraminifera, Earth and Planetary Science Letters, 428, 193–203, 2015.

Forcén-Vàzquez, A.: PhD thesis: Oceanography of the New Zealand subantarctic region, University of Wellington, 2014.

Helm, K. P., Bindoff, N. L., and Church, J. A.: Observed decreases in oxygen content of the global ocean, Geophysical Research Letters, 38, 2011.

Jaccard, S. L. and Galbraith, E. D.: Large climate-driven changes of oceanic oxygen concentrations during the last deglaciation, Nature Geoscience, 5, 151–156, 2012.

Jaccard, S. L., Galbraith, E. D., Froelicher, T. L., and Gruber, N.: Ocean (De)Oxygenation across the last deglaciation, insights for the future, Oceanography, 27, 26–35, 2014.

Keeling, R. F., Körtzinger, A., and Gruber, N.: Ocean deoxygenation in a warming world, Annual Review of Marine Science, 2, 199–229, 2010.

Kohfeld, K., Graham, R., de Boer, A., Sime, L., Wolff, E., Le Quéré, C., and Bopp, L.: Southern Hemisphere westerly wind changes during the Last Glacial Maximum: paleo-data synthesis, Quaternary Science Reviews, 68, 76–95, 2013.

Matear, R., Hirst, A., and McNeil, B.: Changes in dissolved oxygen in the Southern Ocean with climate change, Geochemistry, Geophysics, Geosystems, 1, 1050, 2000.

McManus, J., Berelson, W. M., Klinkhammer, G. P., Hammond, D. E., and Holm, C.: Authigenic uranium: relationship to oxygen penetration depth and organic carbon rain, Geochimica et Cosmochimica Acta, 69, 95–108, 2005.

Molina-Kescher, M., Frank, M., and Hathorne, E.: South Pacific dissolved Nd isotope compositions and rare earth element distributions: Water mass mixing versus biogeochemical cycling, Geochimica et Cosmochimica Acta, 127, 171–189, 2014.

Morford, J. L. and Emerson, S.: The geochemistry of redox sensitive trace metals in sediments, Geochimica et Cosmochimica Acta, 63, 1735–1750, 1999.

Muratli, J., Chase, Z., Mix, A., and McManus, J.: Increased glacial-age ventilation of the Chilean margin by Antarctic Intermediate Water, Nature Geoscience, 3, 23–26, 2009.

Murphy, R. J., Pinkerton, M. H., Richardson, K. M., Bradford Grieve, J. M., and Boyd, P. W.: Phytoplankton distributions around New Zealand derived from SeaWiFS remotely-sensed ocean colour data, New Zealand Journal of Marine and Freshwater Research, 35, 343–362, 2001.

Neil, H. L., Carter, L., and Morris, M. Y.: Thermal isolation of Campbell Plateau, New Zealand, by the Antarctic Circumpolar Current over the past 130 kyr, Paleoceanography, 19, 2004.

Noble, T. L., Piotrowski, A. M., and McCave, I. N.: Neodymium isotopic composition of intermediate and deep waters in the glacial southwest Pacific, Earth and Planetary Science Letters, 384, 27–36, 2013.

Pahnke, K. and Zahn, R.: Southern Hemisphere water mass conversion linked with North Atlantic climate variability, Science, 307, 1741–1746, 2005.

Paillard, D., Labeyrie, L., and Yiou, P.: Macintosh program performs time-series analysis, Eos, Transactions American Geophysical Union, 77, 379–379, 1996.

Peterson, C. D., Lisiecki, L. E., and Stern, J. V.: Deglacial whole-ocean δ13C change estimated from 480 benthic foraminiferal records, Paleoceanography, 29, 549–563, 2014.

Piola, A. R. and Georgi, D. T.: Circumpolar properties of Antarctic intermediate water and Subantarctic Mode Water, Deep Sea Research Part A. Oceanographic Research Papers, 29, 687–711, 1982.

Ramsey, C. B.: Bayesian analysis of radiocarbon dates, Radiocarbon, 51, 337–360, 2009.

Rintoul, S. R. and Bullister, J. L.: A late winter hydrographic section from Tasmania to Antarctica, Deep Sea Research Part I: Oceanographic Research Papers, 46, 1417–1454, 1999.

Ronge, T. A., Steph, S., Tiedemann, R., Prange, M., Merkel, U., Nürnberg, D., and Kuhn, G.: Pushing the boundaries: Glacial/Interglacial variability of intermediate- and deep-waters in the southwest Pacific over the last 350,000 years, Paleoceanography, 30, 23–38, 2015.

Ronge, T. A., Tiedemann, R., Lamy, F., Köhler, P., Alloway, B. V., De Pol-Holz, R., Pahnke, K., Southon, J., and Wacker, L.: Radiocarbon constraints on the extent and evolution of the South Pacific glacial carbon pool., Nature Communications, 7, 11 487, 2016.

Rousseau, J., Ellwood, M. J., Bostock, H. C., and Neil, H.: Estimates of late Quaternary mode and intermediate water silicic acid concentration in the Pacific Southern Ocean, Earth and Planetary Science Letters, 439, 101–108, 2016.

Rudnick, R. L. and Gao, S.: Composition of the Continental Crust, Treatise on Geochemistry, 3, 1–64, 2003.

Russell, J. L. and Dickson, A. G.: Variability in oxygen and nutrients in South Pacific Antarctic Intermediate Water, Global Biogeochemical Cycles, 17, 2003.

Sallee, J.-B., Speer, K., Rintoul, S., and Wijffels, S.: Southern Ocean Thermocline Ventilation, Journal of Physical Oceanography, 40, 509–529, 2010.

Schmittner, A., Gruber, N., Mix, A. C., Key, R. M., Tagliabue, A., and Westberry, T. K.: Biology and air-sea gas exchange controls on the distribution of carbon isotope ratios ($\delta^{13}C$) in the ocean, Biogeosciences, 10, 5793–5816, 2013.

Sloyan, B. M. and Rintoul, S. R.: Circulation, Renewal, and Modification of Antarctic Mode and Intermediate Water, Journal of Physical Oceanography, 31, 1005–1030, 2001.

Stramma, L., Schmidtko, S., Levin, L. A., and Johnson, G. C.: Ocean oxygen minima expansions and their biological impacts, Deep Sea Research Part I: Oceanographic Research Papers, 57, 587–595, 2010.

Talley, L. D.: Closure of the Global Overturning Circulation Through the Indian, Pacific, and Southern Oceans: Schematics and Transports, Oceanography, 26, 80–97, 2013.

Tribovillard, N., Algeo, T. J., Lyons, T., and Riboulleau, A.: Trace metals as paleoredox and paleoproductivity proxies: An update, Chemical Geology, 232, 12–32, 2006.

Voigt, I., Chiessi, C. M., Prange, M., Mulitza, S., Groeneveld, J., Varma, V., and Henrich, R.: Holocene shifts of the Southern Westerlies across the South Atlantic, Paleoceanography, 2015.

Watson, A. J., Vallis, G. K., and Nikurashin, M.: Southern Ocean buoyancy forcing of ocean ventilation and glacial atmospheric CO2, Nature Geoscience, 8, 861–864, 2015.

Chapter 6

Conclusions

Potential collapse of fisheries and enhancement of global warming in response to worldwide increasing marine deoxygenation pushed the scientific community to focus on understanding the marine oxygen cycle (Bograd et al., 2008; Diaz and Rosenberg, 2008; Helm et al., 2011; Keeling et al., 2010; Matear et al., 2000; Nevison et al., 1995). Despite this greater attention over the last decade, the complex consequences of climatic forcing on oceanic oxygenation prevent future oxygenation projections from being made accurately (Emerson and Bushinsky, 2014). By reconstructing past oxygenation variations and their drivers, paleoceanographic studies have great potential to help better understand how oxygenation varies in response to climatic changes.

The aims of this project were (i) to develop methodology to measure 230-Thorium (^{230}Th) and redox sensitive metals in carbonate-rich marine sediments; (ii) to examine oxygenation changes that occurred in the southwest Pacific sector of the Southern Ocean since the last glacial maximum (LGM); and (iii) to understand the exact combination of factors driving these changes. This section will outline the completion of these aims by briefly describing the main findings of this thesis in relation to past oceanic oxygenation, including new methodological developments introduced to reveal them. It will also detail the importance of this work and its implication for future research in the Southern Ocean.

The precise quantification of elemental proxies used in this thesis to reveal the oxygenation history requires the complete digestion of sediments prior to analysis. As the sediments from the New Zealand region are carbonate-rich in composition, previously published methods were found to be unsuccessful for complete digestion of these sediments. This problem was addressed by pre-digesting sediments in concentrated hydrochloric acid on a hot-plate prior to microwave assisted digestion in a mixture of nitric and hydrofluoric acids. This new method development allowed easy digestion of not only sediments from the New Zealand region, but also a wide range of

carbonate-rich materials, which had remained challenging to dissolve prior to this advancement (Durand et al., 2016; Kemp and Brown, 1990; Muratli et al., 2012). Even though this new method uses less acid, particularly HF, compared to most digestion methods, more progress needs to be done to keep minimising the amount of acid used and decrease the environmental impact. In a context of green chemistry, future technological developments have the potential to minimise the impact of sediment analysis on the environment. Wet digestion systems such as microwave might require less acid in the future, by producing higher temperature and pressure conditions in digestion vessels. Moreover, the ongoing improvements of laser ablation ICP-MS might allow trace isotopes to be measured precisely with limited impact on the environment.

In addition to this new digestion method, a special analytical methodology was also developed for the first time in our laboratories to measure ^{230}Th in sediment digests by isotopic dilution on a single collector Inductively Coupled Plasma-Mass Spectrometer (ICP-MS). To do so the insufficient sensitivity of our instrument was increased through the use of the instrumental guard electrode coupled with a micro-concentric desolvating nebuliser. In this optimised mode, the instrumental sensitivity was increased by a factor 100 compared to classic wet aerosol introduction with the guard electrode off. This approach allowed measurement of desired isotopes (238-Uranium, ^{232}Th, and ^{230}Th) to a precision of 5%. Future work will need to further investigate the accuracy and detection limits of this method.

The main contribution of this thesis was the successful characterisation, at high-spatial resolution, of oxygenation changes that occurred in the southwest Pacific sector of the Southern Ocean since the LGM. Previous work in this region focused on the geometry of the water masses without directly investigating oxygenation changes (Pahnke and Zahn, 2005; Ronge et al., 2015). Glacial authigenic Uranium and Rhenium (aU and aRe) enrichments in sediments relative to the Holocene show that the intermediate depths of the southwest Pacific sector of the Southern Ocean were depleted in oxygen during the LGM. Based on multi-proxy evidence, this thesis also proposes a complete and realistic description of the mechanisms driving the changes observed.

In order to understand the precise combination of drivers of this glacial deoxygenation, characterising the influence of export production (EP) changes as a deoxygenation driver was essential. So far results from previous studies are difficult to compare to each other because of the inconsistent use of EP proxies amongst them (Carter and Manighetti, 2006; Ellwood et al., 2005; Ikehara et al., 2000; Kowalski and A Meyers, 1997; Lean and McCave, 1998). In partic-

ular, many previous studies have used biogenic fluxes as EP proxies without Th-normalisation, which can result in erroneous flux reconstructions from lateral advection of the sediments on the seafloor (Francois et al., 2004). A strength of this work was to consistently use several Th-normalised biogenic fluxes, across four sites, to reconstruct EP changes in the New Zealand region since the LGM. This work shows that the position of the biologically productive zone associated with the Subtropical Front (STF) has been a major driver of EP changes in the New Zealand region. Around the Solander Trough a shift of the STF above the core sites during the deglaciation likely drove increased aU and aRe deposition in the sediments of this region. Away from the influence of changes in the STF position, EP has not changed significantly since the LGM in the southwest Pacific, and therefore has not driven oxygenation changes. In Subtropical Waters (STW), this thesis proposes that EP remained limited by nitrogen availability. To understand the invariable EP in the Subantarctic Zone (SAZ), the influence of iron (Fe) fertilisation from dust was investigated by measuring changes in lithogenic supply at the core sites. The higher lithogenic supply observed during the LGM at all sites was used to infer greater Fe fertilisation from enhanced dust deposition during the LGM for the whole region. However, at sites east of New Zealand an unusual lithogenic deposition pattern offset from other sites in the rest of the Southern Ocean was observed. This thesis proposes that erosion and glacier melt during the deglaciation (12-18 ka) increased the sediment discharge and can explain this offset. Additionally to these glaciogenic inputs, dust from the South Island may have contributed to enhance lithogenic deposition during the deglaciation. To explain why in the SAZ enhanced glacial Fe fertilisation from dust did not enhance EP, it is proposed that silicic acid ($Si(OH)_4$) limited any potential increase of total carbon export. This differs from other regions of the Southern Ocean that experienced significant EP increases in the SAZ during the LGM due to Fe fertilisation from increased dust deposition (Bradtmiller et al., 2009; Chase et al., 2003; Lamy et al., 2014; Robinson et al., 2005). However, sites from other studies that showed higher glacial EP are located further south, where the surface waters today have higher $Si(OH)_4$ concentrations. Therefore, this thesis shows that both $Si(OH)_4$ and Fe have been co-limiting EP in the SAZ since the LGM, which is consistent with modern process studies (Boyd et al., 1999). To our knowledge it is the first time that a study suggests that $Si(OH)_4$ limited EP in the SAZ during the LGM. Future work will have to investigate if this $Si(OH)_4$ limitation was generalised everywhere in the northern section of the SAZ or if it was a localised phenomenon.

This can be achieved through new mutli-proxy EP reconstructions in this region. Moreover, this work suggests that dust from the South Island may have contributed to the lithogenic flux offset observed at sites east of New Zealand. Future work investigating the grain size spectrum of the lithogenic fraction applying geochemical provenance tracers such as lead, strontium and neodymium isotopes has the potential to determine whether this suggestion is correct. Finally, in this study uncertainties remain as to whether opal fluxes are representative of changes in opal export or if they are an artefact of dissolution of lithogenic silicon. Remeasuring the opal content of the sediment using a less aggressive leaching method or by Fourier transform-infrared spectroscopy could address this uncertainty.

Since EP has remained steady in most of the New Zealand region since the LGM, other factors must have driven the glacial deoxygenation demonstrated here. This thesis suggests that modifications in Antarctic Intermediate Water (AAIW) ventilation and circulation could have driven these changes. Previous work in the New Zealand region proposed that a shallower southern source AAIW during the LGM left parts of the region bathed by UCDW (Pahnke and Zahn, 2005; Ronge et al., 2015). However, the new compilation of $\delta^{13}C$ data presented here shows that this mechanism is only valid on the Campbell Plateau. The absence of $\delta^{13}C$ changes in sediments from the Challenger Plateau suggests that AAIW has overlayed the Challenger Plateau uninterruptedly since the LGM, even though it spans similar depths as the Campbell Plateau. To explain the lower glacial oxygen content observed on Campbell Plateau, this thesis proposes that a shallower southern source AAIW left deeper parts of the plateau bathed by oxygen depleted UCDW, as suggested by earlier studies. However, on the Challenger Plateau a change in the dominant AAIW source, from a southern source AAIW to an oxygen-poorer, northern source AAIW can explain the glacial deoxygenation. Alternatively, lower glacial oxygen content of southern source AAIW coupled with a northward displacement of its production area, could also explain this trend. Future work investigating Neodymium isotopic composition (ε_{Nd}) change between the LGM and the Holocene has the potential to elucidate the true scenario.

The glacial deoxygenation observed here is at odds with the general notion that AAIW ventilation at intermediate depths was greater during the LGM in the Southern Ocean (Jaccard et al., 2014). This increased ventilation is thought to have resulted from colder temperatures, which increase the oxygen content of AAIW, and stronger westerly winds that are thought to enhance AAIW formation (Downes et al., 2009, 2010). Moreover, the results from this thesis

are also in opposition to those of Muratli et al. (2009) who, using redox sensitive proxies, reported higher oxygen content at intermediate depths in the southeast Pacific sector of the Southern Ocean (along the Chilean Margin). Therefore, these opposing patterns stress the complex responses of AAIW ventilation to climate forcing. In particular, the results presented here highlight an asymmetry of oxygenation at intermediate depths between the eastern and western sides of the Pacific sector of the Southern Ocean. Future work will need to address this discrepancy and determine why the response of AAIW to the climatic changes that occurred since the LGM differed between the eastern and western Pacific sectors. New redox-metal measurements from multiple sediment cores from the southeast Pacific, spanning a wider range of depths, could help to solve this question. So far AAIW oxygenation reconstruction in this region is based on a limited record (three sites) spanning a small depth range ($\approx$ 500 m) (Muratli et al., 2009). Being able to reconstruct AAIW ventilation and circulation is critical because AAIW plays an important role in sequestering greenhouse gas in the ocean interior (Sabine et al., 2004). Therefore, the reliability of future climate change scenarios depends on our ability to resolve how AAIW responds to climatic forcing.

In this thesis, a multi-proxy, high spatial resolution approach was taken to study past oxygenation and their drivers. Seven new proxy data measured on 12 sediment cores from the New Zealand region, as well as $\delta^{13}C$ data from 12 sediment cores (previously published) allowed to resolve oxygenation, EP and circulation changes since the LGM at the regional scale. By resolving previously unappreciated small-scale processes with global implication, this thesis highlights the necessity for more high-spatial resolution paleo-studies. Moreover, this thesis stresses that a multi-proxy approach increases the power to reveal the exact combination of drivers of change.

References

Bograd, S. J., Castro, C. G., Di Lorenzo, E., Palacios, D. M., Bailey, H., Gilly, W., and Chavez, F. P.: Oxygen declines and the shoaling of the hypoxic boundary in the California Current, Geophysical Research Letters, 35, 2008.

Boyd, P., LaRoche, J., Gall, M., Frew, R., and McKay, R. M. L.: Role of iron, light, and silicate in controlling algal biomass in subantarctic waters SE of New Zealand, Journal of Geophysical Research, 104, 13 395–13 408, 1999.

Bradtmiller, L. I., Anderson, R. F., Fleisher, M. Q., and Burckle, L. H.: Comparing glacial and Holocene opal fluxes in the Pacific sector of the Southern Ocean, Paleoceanography, 24, 2009.

Carter, L. and Manighetti, B.: Glacial/interglacial control of terrigenous and biogenic fluxes in the deep ocean off a high input, collisional margin: A 139 kyr-record from New Zealand, Marine Geology, 226, 307–322, 2006.

Chase, Z., Anderson, R. F., Fleisher, M. Q., and Kubik, P. W.: Accumulation of biogenic and lithogenic material in the Pacific sector of the Southern Ocean during the past 40,000 years, Deep Sea Research Part II: Topical Studies in Oceanography, 50, 799–832, 2003.

Diaz, R. J. and Rosenberg, R.: Spreading dead zones and consequences for marine ecosystems, Science, 321, 926–929, 2008.

Downes, S. M., Bindoff, N. L., and Rintoul, S. R.: Impacts of climate change on the subduction of mode and intermediate water masses in the Southern Ocean, Journal of Climate, 22, 3289–3302, 2009.

Downes, S. M., Bindoff, N. L., and Rintoul, S. R.: Changes in the subduction of Southern Ocean water masses at the end of the twenty-first century in eight IPCC models, Journal of Climate, 23, 6526–6541, 2010.

Durand, A., Chase, Z., Townsend, A. T., Noble, T., Panietz, E., and Goemann, K.: Improved methodology for the microwave digestion of carbonate-rich environmental samples, International Journal of Environmental Analytical Chemistry, 96, 119–136, 2016.

Ellwood, M. J., Kelly, M., Neil, H., and Nodder, S. D.: Reconstruction of paleo–particulate organic carbon fluxes for the Campbell Plateau region of southern New Zealand using the zinc content of sponge spicules, Paleoceanography, 20, 2005.

Emerson, S. R. and Bushinsky, S.: Oxygen Concentrations and Biological Fluxes in the Open Ocean, Oceanography, 27, 168–171, 2014.

Francois, R., Frank, M., Rutgers van der Loeff, M. M., and Bacon, M. P.: 230Th normalization: An essential tool for interpreting sedimentary fluxes during the late Quaternary, Paleoceanography, 19, 2004.

Helm, K. P., Bindoff, N. L., and Church, J. A.: Observed decreases in oxygen content of the global ocean, Geophysical Research Letters, 38, 2011.

Ikehara, M., Kawamura, K., Ohkouchi, N., Murayama, M., Nakamura, T., and Taira, A.: Variations of terrestrial input and marine productivity in the Southern Ocean (48°S) during the last two deglaciations, Paleoceanography, 15, 170–180, 2000.

Jaccard, S. L., Galbraith, E. D., Froelicher, T. L., and Gruber, N.: Ocean (De)Oxygenation across the last deglaciation, insights for the future, Oceanography, 27, 26–35, 2014.

Keeling, R. F., Körtzinger, A., and Gruber, N.: Ocean deoxygenation in a warming world, Annual Review of Marine Science, 2, 199–229, 2010.

Kemp, A. J. and Brown, C. J.: Microwave digestion of carbonate rock samples for chemical analysis, Analyst, 115, 1197–1199, 1990.

Kowalski, E. A. and A Meyers, P.: Glacial–interglacial variations in Quaternary production of marine organic matter at DSDP Site 594, Chatham Rise, southeastern New Zealand margin, Marine Geology, 140, 249–263, 1997.

Lamy, F., Gersonde, R., Winckler, G., Esper, O., Jaeschke, A., Kuhn, G., Ullermann, J., Martínez-García, A., Lambert, F., and Kilian, R.: Increased dust deposition in the Pacific Southern Ocean during glacial periods, Science, 343, 403–407, 2014.

Lean, C. M. B. and McCave, I. N.: Glacial to interglacial mineral magnetic and palaeoceanographic changes at Chatham Rise, SW Pacific Ocean, Earth and Planetary Science Letters, 163, 247–260, 1998.

Matear, R., Hirst, A., and McNeil, B.: Changes in dissolved oxygen in the Southern Ocean with climate change, Geochemistry, Geophysics, Geosystems, 1, 1050, 2000.

Muratli, J., Chase, Z., Mix, A., and McManus, J.: Increased glacial-age ventilation of the Chilean margin by Antarctic Intermediate Water, Nature Geoscience, 3, 23–26, 2009.

Muratli, J. M., McManus, J., Mix, A., and Chase, Z.: Dissolution of fluoride complexes following microwave-assisted hydrofluoric acid digestion of marine sediments, Talanta, 89, 195–200, 2012.

Nevison, C. D., Weiss, R. F., and Erickson, D. J.: Global oceanic emissions of nitrous oxide, Journal of Geophysical Research, 100, 15 809–15 820, 1995.

Pahnke, K. and Zahn, R.: Southern Hemisphere water mass conversion linked with North Atlantic climate variability, Science, 307, 1741–1746, 2005.

Robinson, R. S., Sigman, D. M., DiFiore, P. J., Rohde, M. M., Mashiotta, T. A., and Lea, D. W.: Diatom-bound 15N/14N: New support for enhanced nutrient consumption in the ice age subantarctic, Paleoceanography, 20, 2005.

Ronge, T. A., Steph, S., Tiedemann, R., Prange, M., Merkel, U., Nürnberg, D., and Kuhn, G.: Pushing the boundaries: Glacial/Interglacial variability of intermediate- and deep-waters in the southwest Pacific over the last 350,000 years, Paleoceanography, 30, 23–38, 2015.

Sabine, C. L., Feely, R. A., Gruber, N., Key, R. M., Lee, K., Bullister, J. L., Wanninkhof, R., Wong, C. S., Wallace, D. W. R., Tilbrook, B., Millero, F. J., Peng, T.-H., Kozyr, A., Ono, T., and Rios, A. F.: The oceanic sink for anthropogenic CO2, Science, 305, 367–371, 2004.